

UNCLASSIFIED

AD NUMBER

AD881488

LIMITATION CHANGES

TO:

Approved for public release; distribution is unlimited.

FROM:

Distribution authorized to U.S. Gov't. agencies and their contractors; Critical Technology; JAN 1971. Other requests shall be referred to Air Force Materials Laboratory, Attn: AFML/LN, Wright-Patterson AFB, OH 45433. This document contains export-controlled technical data.

AUTHORITY

AFML ltr, 7 Dec 1972

THIS PAGE IS UNCLASSIFIED

AD881488

AFML - TR - 66 - 310  
PART V  
VOLUME I

20  
23

# INTEGRATED RESEARCH ON CARBON COMPOSITE MATERIALS

## VOLUME I MATERIALS RESEARCH

UNION CARBIDE CORPORATION  
CARBON PRODUCTS DIVISION  
- IN ASSOCIATION WITH -  
CASE WESTERN RESERVE UNIVERSITY  
BELL AEROSPACE COMPANY, DIVISION OF TEXTRON

### PROGRAM SUPERVISORS

H.F. VOLK  
H.R. NARA  
D.P. HANLEY

TECHNICAL REPORT AFML-TR-66-310, PART V, VOLUME I

JANUARY 1971

AIR FORCE MATERIALS LABORATORY  
AIR FORCE SYSTEMS COMMAND  
WRIGHT-PATTERSON AIR FORCE BASE, OHIO

THIS DOCUMENT IS SUBJECT TO SPECIAL EXPORT CONTROLS AND EACH  
TRANSMITTAL TO FOREIGN GOVERNMENTS OR FOREIGN NATIONALS  
MAY BE MADE ONLY WITH PRIOR APPROVAL OF THE NONMETALLIC  
MATERIALS DIVISION, AFML/LN, AIR FORCE MATERIALS LABORATORY,  
WRIGHT-PATTERSON AIR FORCE BASE, OHIO 45433

14A

## NOTICES

When Government drawings, specifications, or other data are used for any purpose other than in connection with a definitely related Government procurement operation, the United States Government thereby incurs no responsibility nor any obligation whatsoever; and the fact that the Government may have formulated, furnished, or in any way supplied the said drawings, specifications or other data, is not to be regarded by implication or otherwise as in any manner licensing the holder or any other person or corporation, or conveying any rights or permission to manufacture, use, or sell any patented invention that may in any way be related thereto.

This document is subject to special export controls and each transmittal to foreign Governments or foreign Nationals may be made only with prior approval of the Nonmetallic Materials Laboratory, Wright-Patterson Air Force Base, Ohio 45433.

APPROVED BY	
OFFICE	WHITE SECTION <input type="checkbox"/>
DOB	BLUE SECTION <input type="checkbox"/>
UNCLASS.	SEC. <input type="checkbox"/>
RECLASSIFICATION	
BY	
DISTRIBUTION/AVAILABILITY CODE	
DISC.	AVAIL. and/or SPECIAL
2	

Copies of this report should not be returned unless return is required by security considerations, contractual obligation or notice on a specific document.

INTEGRATED RESEARCH ON  
CARBON COMPOSITE MATERIALS

Summary Technical Report

AFML-TR-66-310, Part V

Volume I

Materials Research

Program Supervisors

H. F. Volk  
H. R. Nara  
D. P. Hanley

January 1971

This document is subject to special export controls and each transmittal to foreign Governments or foreign Nationals may be made only with prior approval of the Nonmetallic Materials Division, AFML/LN, Air Force Materials Laboratory, Wright-Patterson Air Force Base, Ohio 45433.



## FOREWORD

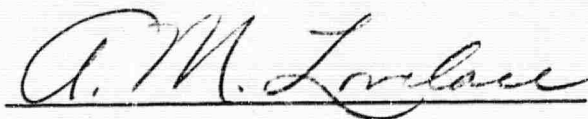
The work reported herein was performed under the sponsorship of the Advanced Research Projects Agency, Department of Defense, through Contract F33615-68-C-1077, ARPA Order No. 719, Program Code 7D10, with the Air Force Materials Laboratory, LN, Wright-Patterson Air Force Base, Ohio. Mr. H. S. Schwartz is the Air Force Program Manager.

This work is a continuation of the effort under Contract AF 33(615)-3110 which had covered the period May 17, 1965 to June 17, 1969, and which was reported in Parts I through IV of this series.

The prime contractor is Union Carbide Corporation, Carbon Products Division with Dr. H. F. Volk (Phone 216-433-8600) as program supervisor. The subcontractors are the Case Western Reserve University with Dr. H. R. Nara (Phone 216-368-4192) as program supervisor and Prof. T. P. Kicher as associate program supervisor and Bell Aerospace Company, a Division of Textron, with Mr. D. P. Hanley (Phone 716-297-1000) as program supervisor.

This is part V of the report and covers work performed from July 1969 to September 1970. Part V is issued in three volumes. Volume I covers materials research; Volume II, structural mechanics; and Volume III, structural component development.

This technical report was submitted by the authors on December 31, 1970 and has been reviewed and approved.



A. M. Lovelace  
Director  
Air Force Materials Laboratory

## ABSTRACT

The work presented in Volume I is concerned with materials research on graphite fiber reinforced composites. Graphite fiber surfaces were characterized by gas phase and solution adsorption experiments and by Raman spectroscopy. The latter technique allows a differentiation between fibers of different origins and heat-treatment temperatures. The fabrication of "Thornel" fiber, polyamide-imide and polysulfone composites was investigated. Fabrication of polyamide-imide composites was very tedious and evaluation was limited to determinations of torsion shear strength. Several plates of polysulfone matrix composites were fabricated; the evaluation of these plates is presented in Volume II of this report. "Thornel" fiber composites were further prepared by in situ polymerization of nylon. The epitaxial crystallization of nylon monomer on graphite fiber surfaces has been investigated. Graphite fiber, nickel matrix composites were further characterized at room and at elevated temperatures. Measurements of Young's moduli, tensile strength, stress rupture, thermal expansion, and thermal fatigue are presented. Graphite filament degradation resulting from fabrication (hot-pressing) of nickel matrix composites was also determined.

This abstract is subject to special export controls and each transmittal to foreign Governments or foreign Nationals may be made only with prior approval of the Nonmetallic Materials Division, AFML/LN, Air Force Materials Laboratory, Wright-Patterson Air Force Base, Ohio 45433.

## TABLE OF CONTENTS

<u>Section</u>	<u>Page</u>
I INTRODUCTION . . . . .	I
II SUMMARY . . . . .	5
III CHARACTERIZATION OF GRAPHITE FIBER SURFACES . .	6
A. Adsorption Wettability and Adhesion in Fiber Reinforced Composites (Prof. Fort, Mr. J. J. Moller, and Mr. S. C. Sharma (Case). . . . .	6
B. Characterization of Graphite Fiber Surfaces with Raman Spectroscopy (Prof. Koenig and Dr. F. Tuinstra, Case). . . . .	17
IV RESEARCH ON GRAPHITE-FIBER, RESIN-MATRIX COMPOSITES. . . . .	28
A. In Situ Polymerization of Nylon Matrix Composites (Prof. Litt and Dr. J. B. Shortall, Case). . . . .	28
B. Crystallization and Reaction on Graphite Fiber Surfaces (Prof. Lando and Mr. P. Frayer, Case) . . . .	40
C. Polyamide-imide and Polysulfone Composites (Dr. I. C. Lewis and Dr. B. H. Eckstein, Union Carbide) . . . . .	42
V RESEARCH ON GRAPHITE-FIBER, METAL-MATRIX COMPOSITES (R. V. Sara, Union Carbide). . . . .	65
A. Fabrication Studies . . . . .	65
B. Filament and Strand Tests . . . . .	76
C. Composite Behavior-Room Temperature . . . . .	78
D. Properties of Composites Fabricated From Tapes . . . .	94
E. Composite Behavior - Elevated Temperature. . . . .	97
REFERENCES . . . . .	128

**BLANK PAGE**

# LIST OF ILLUSTRATIONS

Figure		Page
1	Gravimetric Gas Adsorption Apparatus . . . . .	7
2	Microbalance Cryostat . . . . .	9
3	Sorption Isotherms for Nitrogen Gas at 77.3°K on "Thornel" 50 . . . . .	10
4	Liquid Chromatograph . . . . .	12
5	Adsorption Isotherms for Stearic Acid on Carbon . . . . .	13
6	Isosteric Heats of Adsorption for Stearic Acid on "Thornel" 50 . . . . .	16
7	Geometry of the Microsampler . . . . .	19
8	Plot of Relative Intensity versus Crystallite Size for Samples of Different Origin . . . . .	20
9	Comparison of the Raman Spectra of Morganite I and Morganite II . . . . .	22
10	Relation Between Composite Shear Strength and the $L_a$ found through the Raman Spectrum of the Graphite Fiber . . . .	24
11	Direct Transmission Electron Microphotograph of a Section of Composite I, . . . . .	29
12	Direct Transmission Electron Microphotograph of a Sheath from Composite I . . . . .	30
13	Electron Diffraction Photograph of Figure 11 Orientation not Specified . . . . .	31
14	Electron Microphotographs of a Section of Composite II . . . .	33
15	Electron Diffraction of Lower Section of Figure 14, only Oriented Graphite Visible . . . . .	34
16	X-Ray Photographs of Thin Section of Composite 12 . . . . .	35
17	Cross-Section of Single Strands of "Thornel" Yarn Coated with Epoxy, Polysulfone, and Amide-Imide Resins . . . . .	46
18	Torque versus Angular Displacement Curve for "Thornel" 25 P-1700 Composite . . . . .	48
19	Cross-Section Photomicrographs of "Thornel" 25 P-1700 Composites . . . . .	49
20	Cross-Section Photomicrograph of Low Shear Strength Polyamide-Imide "Thornel" 25 Composite Showing Voids . . . .	50
21	Torque versus Angular Displacement Curves for Composites of "Thornel" 50S with ERLA-4617 and P-1700 Resins . . . . .	53
22	Torque versus Angular Displacement Curves Obtained for a Repetitively Tested "Thornel" 50S P-1700 Composite . . . . .	54

# LIST OF ILLUSTRATIONS (Cont'd.)

<u>Figure</u>		<u>Page</u>
23	Cross-Section Photograph of "Thornel" P-1700 Composite Rods . . . . .	55
24	Photomicrographs of "Thornel" P-1700 Composites . . . . .	56
25	Photomicrographs of a Shear Tested "Thornel" 50S-P-1700 Composite Showing Cracks . . . . .	57
26	"Thornel" 50 AI-11 Cured Composites . . . . .	59
27	"Thornel" 50 AI-11 Cured Composites . . . . .	60
28	"Thornel" 50S AI-11 Composite - Uncured . . . . .	61
29	"Thornel" 50S AI-11 Composites - Cured . . . . .	62
30	Thermogravimetric Analysis Curves for AI-11 Polymer in Argon and Air . . . . .	63
31	Electrodeposited Nickel on "Thornel" Fibers . . . . .	66
32	Nickel-Coated Fibers Annealed at 1050°C for One Hour . . . . .	67
33	Nickel-Coated Fibers Annealed at 1050°C for One Hour . . . . .	68
34	Young's Modulus of Graphite Fibers After Electrodeposition and After Fabrication of Composite . . . . .	69
35	Tensile Strength of Graphite Fibers After Electrodeposition and After Fabrication of Composite . . . . .	70
36	Young's Modulus of "Thornel" 75 Graphite Fibers After Electrodeposition and After Fabrication of Composite . . . . .	71
37	Tensile Strength of "Thornel" 75 Graphite Fibers After Electrodeposition and After Fabrication of Composite . . . . .	72
38(a)	Graphite Fibers After Electrodeposition; Nickel Removed by Dissolution . . . . .	73
38(b)	Graphite Fibers After Fabrication of Composite; Nickel Removed by Dissolution . . . . .	74
39	Strand Tensile Strength Values of Nickel-Coated "Thornel" 75 Graphite Fibers . . . . .	77
40	Stress-Strain Behavior of "Thornel" 50 and "Thornel" 75 Fibers in Nickel Matrix . . . . .	79
41	Fracture Edge of a Graphite-Fiber, Nickel-Matrix Compression Specimen . . . . .	80
42	Etched Fracture Edge of a Graphite-Fiber, Nickel-Matrix Compression Specimen . . . . .	80
43	Microhardness Indentations in the Nickel-Matrix and in the Grain Boundary . . . . .	81
44	Microstructure of Graphite-Fiber, Nickel-Matrix Compression Specimen . . . . .	81

# LIST OF ILLUSTRATIONS (Cont'd.)

<u>Figure</u>		<u>Page</u>
45	Fracture Edge of a Graphite-Fiber, Nickel-Matrix Tensile Specimen . . . . .	81
46	Compression Stress-Strain Behavior of Graphite-Fiber, Nickel-Matrix Composites Fabricated from As-Plated and Hydrogen Treated Nickel Coated Fibers . . . . .	83
47	Strand Tensile Strength Values of Nickel-Coated "Thornel" 75 Graphite-Fibers Compared with Composite Tensile Strengths . . . . .	84
48	Strand Tensile Strength Values of Nickel-Coated "Thornel" 50 Graphite-Fibers Compared with Composite Tensile Strengths . . . . .	85
49	Young's and Shear Modulus of Graphite Particulate, Nickel-Matrix Composites . . . . .	87
50	Variation of Young's and Shear Modulus with Porosity . . . . .	88
51	Comparison Between Experimental and Calculated Young's Modulus for Bands of Equivalent Strain and Equivalent Stress . . . . .	90
52	Agreement Between Experimental and Predicted Young's Modulus Values in Graphite-Fiber, Nickel-Matrix Composites Assuming Perfect and Partial Interfacial Bonding . . . . .	92
53	Experimental and Predicted Shear Modulus ( $G$ ) Values for Graphite-Fiber, Nickel-Matrix Composites . . . . .	93
54	Torque vs. Angular Displacement Curves for Nickel and Graphite-Fiber, Nickel and Resin-Matrix Composites . . . . .	95
55	Microstructure of Graphite-Fiber, Nickel-Matrix Composite Fabricated from Tapes . . . . .	96
56	Longitudinal Thermal Expansion of Graphite-Fiber, Nickel-Matrix Composite . . . . .	98
57	Thermal Expansion Coefficient of Graphite-Fiber, Nickel-Matrix Composite . . . . .	99
58	Linear Thermal Expansion of Nickel and of a Graphite-Fiber, Nickel-Matrix Composite in the Transverse Direction . . . . .	100
59	Properties of Composite Specimens Utilized in Thermal Cycle Experiments . . . . .	101
60	Schematic of Thermal Fatigue Apparatus . . . . .	102
61	Thermal Fatigue Cycle Between 100° and 500°C . . . . .	103
62	Change in Specimen Width as a Result of Elapsed Cycles Between 100° and 500°C . . . . .	104
63	Specimen Width After Cycling 500 Times Between 125°C and the Indicated Temperatures . . . . .	104

# LIST OF ILLUSTRATIONS (Cont'd.)

<u>Figure</u>		<u>Page</u>
64	Surface Crazing in a Graphite-Fiber, Nickel-Matrix Composite After 1000 Cycles Between 100° and 500°C . . . . .	105
65	Fibers Devoid of Nickel After Cycling 1000 Times Between 100° and 500°C . . . . .	105
66	Redistribution of Matrix as a Result of Thermal Cycling . . .	106
67	Specimen Cross-Sectional Area After Cycling 500 Times to Various Peak Temperatures . . . . .	108
68	Specimen Cross-Sectional Area in Relation to Elapsed Cycles Between 100° and 500°C . . . . .	108
69	Effect of Peak Temperature in Cycle Band on Composite Density . . . . .	109
70	Effect of Peak Temperature in Cycle Band on Composite Young's and Shear Modulus . . . . .	109
71	Effect of Peak Temperature in Cycle Band on Composite Flexural Strength . . . . .	110
72	Effect of Elapsed Cycles on Composite Density . . . . .	111
73	Effect of Elapsed Cycles on Composite Young's and Shear Modulus . . . . .	111
74	Effect of Elapsed Cycles on Composite Flexural Strength . . .	112
75	Effect of Elapsed Cycles on Composite Thermal Expansion . .	113
76	Effect of Cycle Band on Thermal Expansion Hysteresis in a Unidirectional Composite . . . . .	113
77(a)	Graphite-Fiber, Nickel-Matrix Composite Prior to Cycling . . . . .	114
77(b)	Graphite-Fiber, Nickel-Matrix Composite After 200 Cycles Between 125° and 500°C . . . . .	115
78	Graphite-Fiber, Nickel-Matrix Composite After 350 Cycles Between 125° and 500°C . . . . .	116
79	Graphite-Fiber, Nickel-Matrix Composite After 350 Cycles Between 125° and 500°C . . . . .	116
80	Graphite-Fiber, Nickel-Matrix Composite After 1000 Cycles Between 125° and 500°C . . . . .	117
81	Distance Between Fiber Ends and Matrix Surface After Cycling in the Internal 125°-500°C . . . . .	118
82	Initial Stage of a Discontinuity in the Nickel-Coating After Cycling Between 125° and 500°C . . . . .	119



# LIST OF ILLUSTRATIONS (Cont'd.)

<u>Figure</u>		<u>Page</u>
83	Multiple Discontinuities in the Nickel Coating on "Thornel" Yarn After 500 Cycles Between 125° and 500° C . . . . .	119
84	Longitudinal Thermal Expansion Behavior of SiO <sub>2</sub> -Fiber, Aluminum-Matrix Composite . . . . .	120
85	Delamination of a 5-Ply Orthogonal Specimen After 525 Cycles Between 125° and 500° C . . . . .	121
86	Young's Modulus of Nickel-Metal and "Thornel" 50 and "Thornel" 75 Graphite-Fiber, Nickel-Matrix Composites . . .	122
87	Tensile Strength of "Thornel" 50 and "Thornel" 75 Graphite-Fiber, Nickel-Matrix Composites . . . . .	124
88	Ultimate Flexure Strength of "Thornel" 75 Graphite-Fiber, Nickel-Matrix Composite . . . . .	125
89	Flexure Specimens After Testing at the Indicated Temperatures . . . . .	126
90	Stress-Rupture at 500° C for "Thornel" 75 Graphite-Fiber, Nickel-Matrix Composites . . . . .	127

## LIST OF TABLES

<u>Table</u>		<u>Page</u>
I	MEASUREMENT OF DEAD-VOLUME . . . . .	14
II	RAMAN SPECTROSCOPY RESULTS FOR CARBON AND GRAPHITE FIBERS . . . . .	25
III	NYLON COMPOSITE TEST DATA . . . . .	36
IV	EVALUATION OF POTENTIAL CATALYSTS . . . . .	40
V	PROPERTIES OF EPOXY, POLYSULFONE, AND POLYAMIDE-IMIDE RESINS . . . . .	44
VI	PROPERTIES OF RESIN-GLASS FILLED LAMINATES FOR EPOXY, POLYSULFONE AND POLYAMIDE-IMIDE . .	44
VII	TORSION SHEAR TEST RESULTS FOR "THORNEL" 25 P-1700 COMPOSITES . . . . .	47
VIII	SHEAR STRENGTH VALUES FOR P-1700 "THORNEL" 50 COMPOSITES . . . . .	52
IX	SHEAR STRENGTH VALUES FOR "THORNEL" 50S COMPOSITES WITH ERLA-4617 AND P-1700 . . . . .	52
X	PROPERTIES OF "THORNEL" 50 AND "THORNEL" 75 GRAPHITE FIBERS . . . . .	65
XI	STRUCTURAL PARAMETERS OF GRAPHITE FIBERS BEFORE AND AFTER COMPOSITE FABRICATION . . . . .	75
XII	"THORNEL" 75 FIBER PROPERTIES BEFORE AND AFTER PRESSING IN A PARAFFIN MATRIX AT 3000 PSI . . . . .	75
XIII	PROPERTIES OF NICKEL-COATED AND AS- RECEIVED FIBERS BASED ON FILAMENT AND STRAND TESTS . . . . .	76

## SECTION I

### INTRODUCTION

The present program is a continuation of the work performed under Contract AF 33(615)-31110 (see References 1 through 6). This report covers the fifth (and final) year's work of a program which represented a novel approach designed to fulfill three different, but clearly interdependent, needs of the Department of Defense: a materials need, a structural design capability need, and a need for more scientists and engineers trained in applied materials problems and advanced design methods. The Carbon Products Division of Union Carbide Corporation, Case Western Reserve University, and Bell Aerospace Company have formed an Association to meet these needs.

The Association has formulated a broad program which includes the development of new materials, generation of advanced analyses and design methods, and education of graduate students. In brief, the major objectives are (1) to develop high modulus graphite fiber composites, (2) to extend the methods of structural mechanics, (3) to identify DOD applications toward which the program efforts should be directed, (4) to educate engineers capable of developing and using modern materials, and (5) to integrate materials research with the needs of the design by extending the technique of structural synthesis to include material variables.

The primary responsibilities of Union Carbide Corporation, Carbon Products Division, are the development and production of composite materials and the measurement of those mechanical and thermal properties needed for the structural design work within the Association. The technical program at Union Carbide consists of: (1) materials research, a basic research program to develop new, improved composites of high modulus graphite fibers in both resin and metal matrices; (2) materials fabrication, an applied research program to produce materials for the joint research programs of the Association and to seek new ways of fabricating components which better utilize the superior properties of composite materials; (3) properties evaluation, the measurement of the mechanical and thermal properties of certain composites to provide data for the joint research programs of the Association; and (4) failure criteria, a basic research program to determine experimentally adequate failure criteria for anisotropic materials under multiaxial stress states and to find ways of representing the failure surface which can be used by the designer in practical calculation.

The work at Case Western Reserve University has two major objectives. The first objective is to advance the basic structural mechanics technology required for rational design with composite materials. Composite materials offer the structural design engineer the prospect of being able ultimately to carry on simultaneously the design of the structural configuration and the material. Achieving this capability will require fundamental advances in structural synthesis as well as a substantially improved understanding of the behavior of composite materials. The goals of the structural mechanics

research program at Case are (1) the quantitative formulation and efficient solution of the structural synthesis problem, including material variables, for elementary, but representative components fabricated from composite materials; (2) experimental stress analysis studies and theoretical investigations in micromechanics with the objective of improving the measurement and calculation of stiffness properties and failure mode criteria for composite materials; and (3) the development of improved analysis methods for anisotropic, nonlinear, and nonconservative materials. The second objective of the work at Case Western Reserve University is to develop new or improved graphite fiber-resin composites through materials research. At present, the knowledge of fiber surface morphology and the relation between fiber surface characteristics and interfacial adhesion to the resin system(s) is incomplete. A better understanding of these interfacial interactions will lead to improvements in presently used fiber resin composites and will ultimately permit the judicious selection of new resins and new fabrication methods, thus leading to a second generation of advanced composites.

The primary purposes of Bell Aerospace Company's participation in this program are to interject user requirements into the applied materials research efforts; to apply at the prototype design level, the advanced analytical procedures and improved understanding of material behavior which will result from the research; and to establish application-related property specifications for materials research activities. To attain these objectives, a six-part technical program is being performed by Bell: (1) application selection, the objective of which is to define representative configurations and environmental conditions which reflect DOD requirements; (2) recognition of failure modes, a task which involves the overall structural behavior such as elastic instability, deformation limits, and fracture and the material failure modes; (3) determination of the nature of and methods for the application of analytical tools needed to cope with the anisotropic, anelastic, and nonconservative material property behavior and the multiaxial stress distributions anticipated in structural configuration associated with the use of the subject materials; (4) structural synthesis, a task which involves the application of structural synthesis techniques at the practical level to define the most desirable material compositions within a particular class of composites; (5) study of creative design concepts which will be required because of the complex material behavior of composites; (6) testing to verify the value of analysis procedures used to design composite materials and the components made from composite materials.

Although this report of the Association's fifth year activities is the last report of the Association, the Case Western Reserve University will be continuing research on composite materials during the sixth year under sponsorship of the Advanced Research Projects Agency.

This report is divided into three volumes. Volume I covers the effort on materials research; Volume II covers the work on structural mechanics, analysis, and optimization; and Volume III covers the testing, stress analysis and evaluation of a representative subscale fuselage component. This division was made because particular projects might be of interest to a particular audience; this arrangement also made possible the reduction of the physical size of each volume. However, the following Summary (Section II) also contains a brief outline of the contents of the other two volumes.

## SECTION II

### SUMMARY

#### Volume I: Materials Research

Gas phase and solution adsorption experiments indicated a surface area of from 0.6 to 1.4 m<sup>2</sup>/g for "Thornel" 50 graphite filaments with no surface finish. The exact value obtained depends on the technique of measurement and the history of the filaments. Outgassing in vacuum at elevated temperatures appears to decrease both the surface area and the surface energy of these filaments.

Raman spectroscopy was used to characterize the fiber surface of graphite and carbon fibers. A correlation exists between the Raman spectrum of the fiber surface and the shear strength of the composite. Effects of surface treatments are reflected in the Raman spectrum as well as the shear strength of the composite. Many graphite fibers have a weak surface layer where the graphite planes are oriented parallel to the surface.

"Thornel" fiber nylon matrix composites have been fabricated by in situ polymerization and the physical properties obtained. The nylon matrix composites exhibit the advantage of ductility over epoxy matrix composites. This work was performed because it was expected that in situ polymerization employing latent catalysts would lead to better fiber wetting due to the low viscosity of the monomer system(s). Preliminary results appear to verify these expectations.

The interaction between graphite fibers and epitaxially deposited monomers has been shown to be specific and strong. The edges of the graphite-like planes affect not only the oriented crystallization of monomers, but also affect the subsequent solid state reaction. Instead of polymerization, cyclization occurs for the monomers of nylon 66 and nylon 6, yielding cyclic dimer and cyclic trimer, respectively. It was also found that epitaxial crystallization of the monomer of nylon 66 can be enhanced by application of an electric field.

Polysulfone and polyamide-imide resins were evaluated as matrix materials for graphite fiber reinforced composites. Polysulfone composites were fabricated by winding "Thornel" yarn through a solution containing 20 percent (by weight) polymer in chloroform, followed by compression molding at 270°C; this procedure yielded void-free composites with approximately 50 percent fiber loading. Fabrication of polyamide-imide composites was substantially more cumbersome and involved wet-winding, drying, B-staging, molding, and post-curing. "Thornel" 50 and 50S composites made from both resin systems were evaluated for shear strength. In general, the shear strength values were found to be identical to those obtained on the same yarns in an ERLA 4617 epoxy matrix. However, the stress-strain curves obtained in torsion shear tests on polysulfone composites showed only a gradual yielding, in contrast to the abrupt failure of

both the polyamide-imide and the epoxy composites. "Thornel" 50S, polysulfone composites were also prepared as seven ply (0, 90°) balanced plates for notch-sensitivity testing. The results of these tests are contained in Volume II of this report.

Graphite-fiber, nickel-matrix composites were characterized at room and at elevated temperatures. "Thornel" 50 and "Thornel" 75 graphite fibers were used in the fabrication of virtually all composite specimens. So that fiber damage during fabrication might be decreased, pre-formed tapes (approximately 0.010-inch thick) were prepared and the stacked tapes were consolidated into unidirectional and 5-ply orthogonal plates; however, the mechanical properties of composites fabricated in this manner did not exceed those obtained on specimens fabricated directly from aligned yarns. The average tensile strength of individual "Thornel" 50 filaments was reduced from 267,000 to 207,000 psi as a result of hot-pressing at 1050°C, but no change was evident in the Young's modulus or surface features of the extracted fibers. The properties of "Thornel" 75 filaments were also reduced by the fabrication process. Stress-strain measurements parallel to the fiber axis on unidirectional composites containing "Thornel" 75 graphite fibers showed that a 50 volume percent fiber composite typically fails at 100,000 psi and 0.25 percent strain. Plastic yielding of the matrix is evident at 0.05 percent strain. Failure in compression occurs at 100,000 psi. Compressive and tensile moduli are comparable. Experiments were conducted to rationalize the difference between measured and predicted Young's modulus of unidirectional composites. Factors such as variations in fiber modulus, porosity, carbon solubility, and bonding were considered. The discrepancy is explained most satisfactorily if a fraction of fibers are assumed to be unbonded. Extensive thermal expansion measurements made on composites parallel and perpendicular to the fiber direction are in reasonable agreement with those previously reported. No anomalous irreversible deformation was observed. The effect of thermal cycling on the composite properties was determined for up to 1000 cycles and a maximum  $\Delta T$  of 875°C. Considerable deformation of the composite occurred perpendicular to the fiber direction. Deformation is insignificant parallel to the fiber axis. The change in cross-sectional area is accompanied by an increase in porosity and a decrease in all mechanical properties. This dimensional change is probably related to a "thermal ratchet" mechanism, a consequence of thermal expansion differences between the constituents which results in plastic deformation in compression of the matrix at the higher temperature and a partial recovery of the deformation at lower temperatures. It is believed that better interfacial bonding should reduce the severity of the ratcheting. The Young's modulus of nickel metal and of composites containing "Thornel" 50 and 75 graphite fibers was measured to 1000°C. Short time tensile strength tests were made up to 1050°C on composites containing "Thornel" 75 filaments. A tensile strength of 75,000 psi was measured at 500°C, but this property decreased at the higher temperatures because of extensive fiber pull-out. The trend for flexural strength was characterized by a maximum at 250°C; some specimens failed at 180,000 psi at this temperature. The stress rupture characteristics were measured at 500°C. Failure occurs in less than 100 hours when stress exceeds 40,000 psi.

## Contents of Volume II:

The work presented in Volume II is concerned with the structural mechanics and synthesis of graphite-fiber reinforced composite materials. Optimization studies (minimum weight design) of stiffened cylinders similar to the fuselage component were carried out by two different techniques. The behavior of composite structural elements was investigated in plate buckling and post-buckling studies, buckling of stiffened plates with cut-outs, and application of shell theory to anisotropic cylinders. Micromechanics studies of fibrous composites included development of a photoelastic technique for analyzing frozen stresses, a discrete element microstress analysis of unidirectional fiber composites, an application of the theory of physically nonlinear elastic solids to composite materials, and an investigation of the multiple circular inclusion problem in plane elastostatics. Failure of composite structural elements was investigated through studies of the failure mechanism for off-axis composites, the fracture toughness of composites, the effect of fatigue and sustained loads on cross-ply composites, the notch sensitivity of cross-ply composites, and the effect of a variety of known intentionally interjected defects on the fracture strength. Further studies were concerned with multiaxial stress testing of composite cylinders. The effects of circular and square cut-outs in flat panels and in a stiffened panel, and methods of reinforcement of cut-outs were investigated and correlated with predictions based on discrete element analysis.

## Contents of Volume III:

The work presented in Volume III is concerned with the performance prediction, testing, and post-test evaluation of a representative graphite-fiber, resin-matrix aircraft fuselage component. Additional material properties were determined and structural margins of safety defined by discrete element analysis. After seven response tests under various load combinations, the component was tested to destruction under combined bending and shear loads. Failure occurred at 110 percent of the target design load but below the failure load predicted from tests on flat panels. A weight saving of 27 percent over an aluminum structure of equivalent strength was demonstrated. The component was also three times stiffer than an aluminum structure of the same weight. Performance projections indicate that the same component built with presently available "Thornel" 50S fibers would offer a weight saving of 49 percent. Post-test evaluations included tensile and compression tests on curved skin panels, on stringers, and on stringer-skin combinations. Optical and electron microscopic examination of the fracture surfaces provided further insight into the failure mechanism.

## SECTION III

### CHARACTERIZATION OF GRAPHITE FIBER SURFACES

#### A. Adsorption, Wettability and Adhesion in Fiber Reinforced Composites (Professor Fort, Mr. P. J. Moller, and Mr. S. C. Sharma, Case)

The weakest part of most fiber reinforced composite structures is the interface between the fiber and the polymer matrix which surrounds it. Maximum (theoretical) bond strength is seldom, if ever, achieved. Reasons for failure may be poor contact of one phase with another (poor wetting), weak boundary layers, stresses set up on solidification of the adhesive, or poor attraction of adhesive to adherend. All these failure mechanisms are controlled by the surface character of the materials in contact. Knowledge of this surface character is necessary for systematic optimization of fiber-polymer matrix adhesion, and composite strength.

The objectives of this research are to: (1) characterize the surface area, surface chemistry and surface roughness of selected, high strength, thermally stable fibers; (2) relate these surface properties to fiber wettability, bulk morphology, and adhesion; (3) optimize fiber reinforced composite performance through use of the information obtained. Present work is concerned with fiber surface characterization through measurements of adsorption from the gas phase and from solution.

##### 1. Gas Adsorption Studies

A well-established method for determining surface properties is to study the interaction of the surface with various gases. A solid sample, when weighed in a gaseous atmosphere at various pressures, will increase in weight as the gas pressure is increased. The weight increase is caused by the adsorption of gas molecules onto the surface of the sample. Knowing the weight of one gas molecule, the number of adsorbed molecules can be calculated. The relationship between the number of gas molecules adsorbed and the pressure, at various temperatures, yields information about the nature and energetics of the surface; e.g., whether the surface is porous or nonporous and whether it is energetically uniform or contains areas of high and low energy. The purpose of this study is to make such an investigation of the surface of "Thornel"\* 50 fibers.

The gas adsorption system constructed for use in this work is shown in Figure 1. It consists of a Cahn Model RG recording vacuum microbalance (Cahn Instrument Company, Paramount, California) mounted in an ultrahigh vacuum system pumped by a cryopump and a 50 liters per second ion pump (Varian

---

\* "Thornel" is a registered trademark of Union Carbide Corporation.



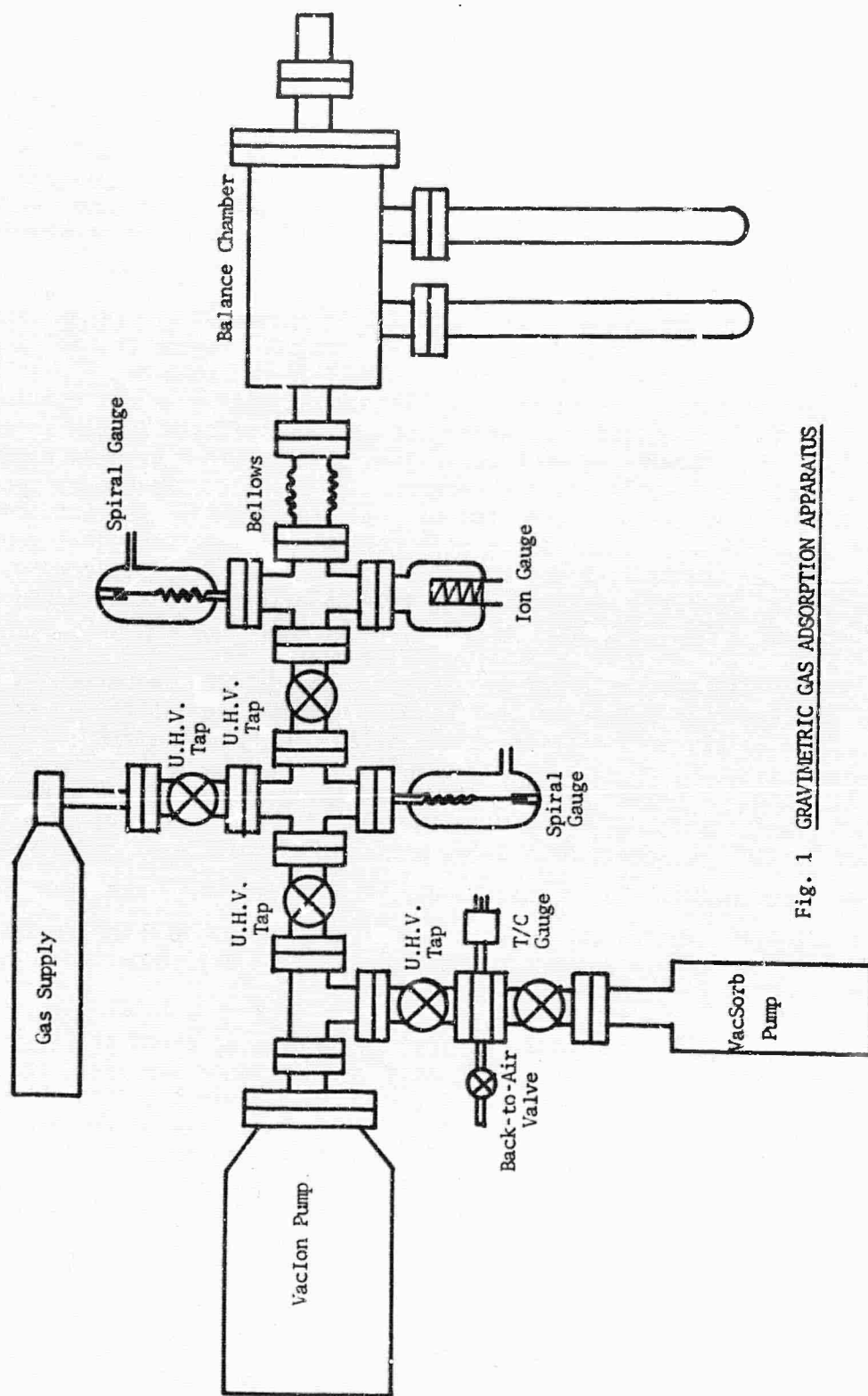


Fig. 1 GRAVIMETRIC GAS ADSORPTION APPARATUS

Associates, Palo Alto, California). Pressures are measured from  $10^{-9}$  torr up to 1 atmosphere with the aid of an ion gage (Varian Associates) and a spiral gage (Electronic Space Products, Los Angeles, California). Temperatures are controlled by a Melabs Model CTC-1A Proportional Temperature Controller (Melabs Inc., Palo Alto, California) by means of the specially designed cryostat shown in Figure 2. The temperature ( $\pm 0.007^\circ\text{C}$ ) is measured by a platinum resistance thermometer attached to the cryostat block. The outer jacket of the cryostat is immersed in a liquid nitrogen bath. For temperatures near  $77^\circ\text{K}$  the outer jacket is filled with helium; at higher temperatures the jacket is evacuated.

Weight changes for a 500 milligram sample are determined with an accuracy of  $\pm 0.2$  micrograms in the low pressure region and  $\pm 3$  micrograms near 1 atmosphere when the sample is at  $77\text{--}90^\circ\text{K}$ . However, a problem of all gravimetric adsorption studies is that of separating weight changes due to adsorption from weight changes due to buoyancy effects as gas pressure is varied. In the present work adsorption experiments have been carried out with the sample at  $77\text{--}90^\circ\text{K}$  and the counterweight at  $23^\circ\text{C}$ . Helium was assumed not to adsorb at these temperatures and was used to determine buoyancy corrections in preliminary work. Experiments with helium, however, sometimes caused damage to parts of the balance due to arcing in vacuum. Buoyancy corrections are, therefore, currently determined by extrapolation of data obtained with nitrogen gas at  $200^\circ$ ,  $23^\circ$ ,  $0^\circ$ , and  $-78^\circ\text{C}$ .

Part of a series of adsorption-desorption measurements with nitrogen gas has been completed on "Thornel" 50 graphite fibers (Union Carbide Lot No. 1001 8T-4E, no finish or size applied during processing). The fibers were pushed, as received as one long piece of yarn, into a pear-shaped quartz pan and then heat treated in high vacuum at temperatures of  $240^\circ$ ,  $400^\circ$ , and  $590^\circ\text{C}$ . Heat treatment was achieved with the aid of a Lindberg Hevi-Duty "Mini Mite" Tube Furnace (Lindberg Hevi-Duty, Division of Sola Basic Industries, Watertown, Wisconsin). Gas pressures over the fibers were less than  $10^{-6}$  torr during bakeout. Before the start of each experiment the pressure was ca.  $10^{-8}$  torr in the balance chamber. Heat treatment at any given temperature was continued until constant weight was attained.

Equilibrium nitrogen adsorption data obtained at  $77.3^\circ\text{K}$  is shown in Figure 3 for the  $240^\circ\text{C}$  and  $540^\circ\text{C}$  heat treated fiber samples. The isotherms for the  $240^\circ\text{C}$  heat treated fibers show a hysteresis loop indicating pores in the fiber surface. The distribution and average size of these pores will be investigated. The experiments on fibers heat treated at  $400^\circ\text{C}$  need to be repeated because of an accident. After bakeout at  $590^\circ\text{C}$  the fibers (the same sample which had been through many  $240^\circ\text{C}$  bakeout experiment cycles) showed a decrease in surface area and no detectable pores.

## 2. Solution Adsorption Studies

The purpose of this study is to characterize the surface properties of "Thornel" 50 graphite fibers by study of their ability to adsorb organic

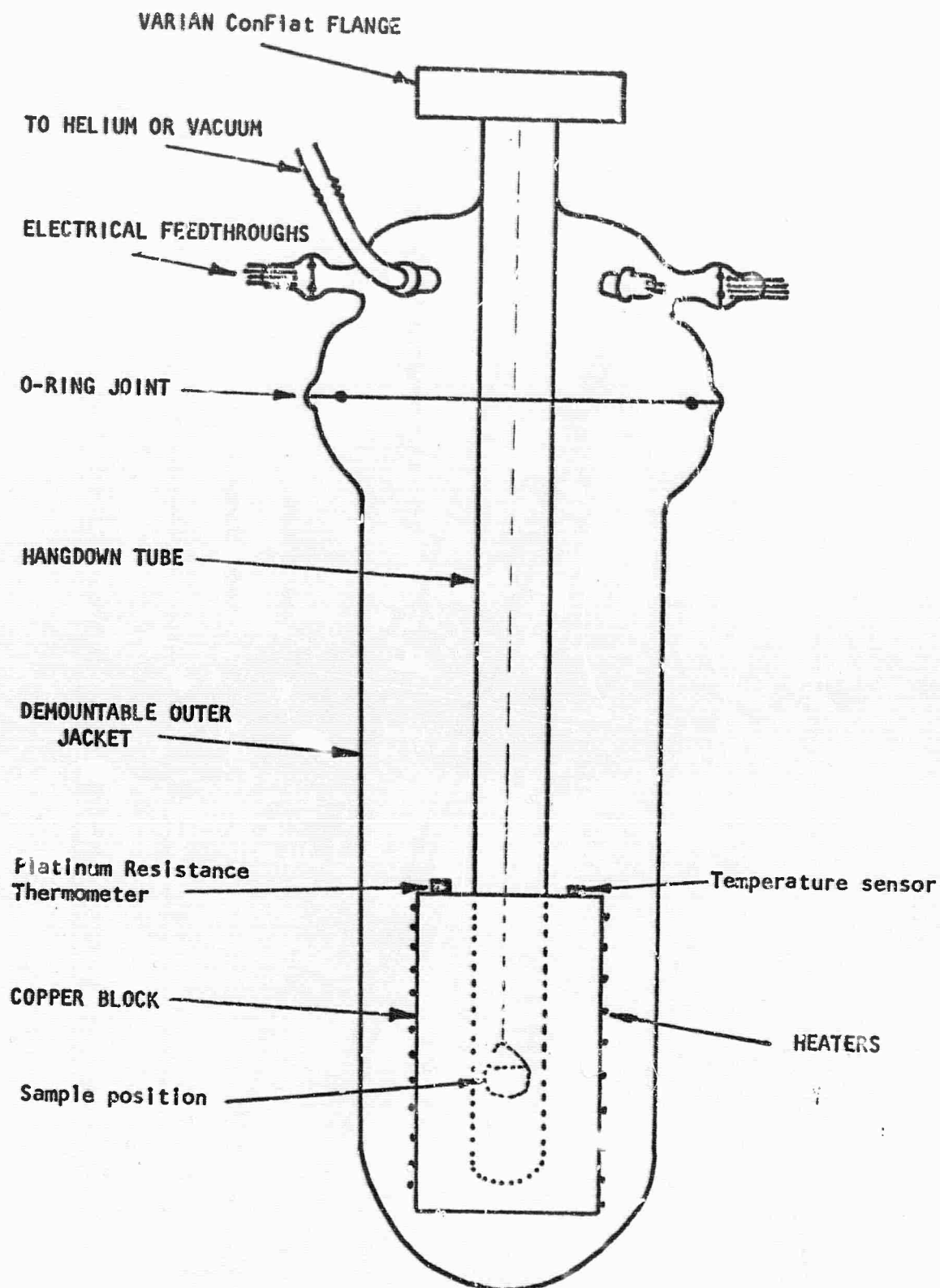


Figure 2. Microbalance Cryostat.

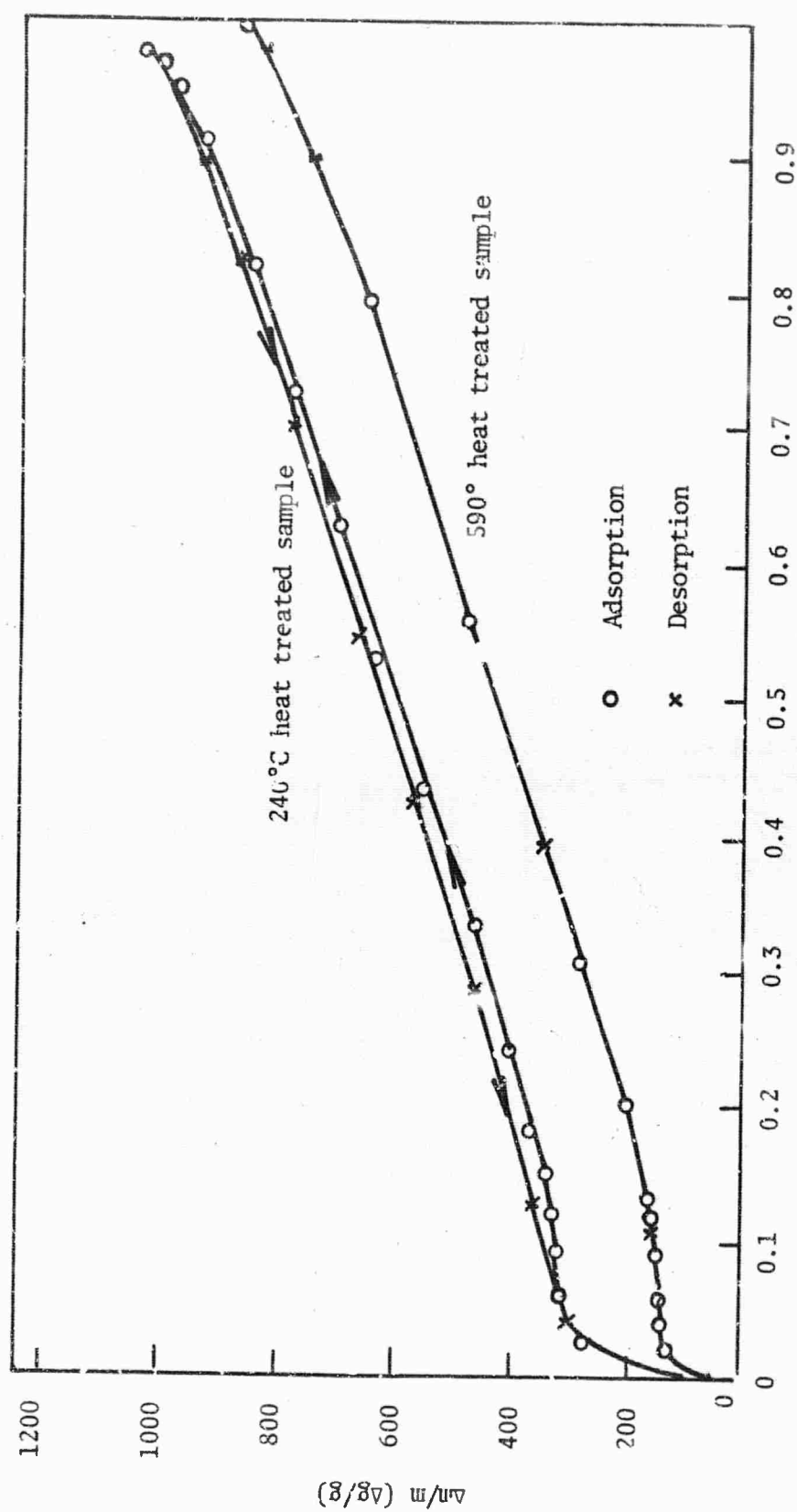


Fig. 3 SORPTION ISOTHERMS FOR NITROGEN GAS AT 77.3°K on "THORNEL" 50

molecules (including polymers) from solutions. Adsorption from solutions comes closer to modelling the actual application of carbon fibers than does adsorption from gases. Because of their very low specific surface area, the amount adsorbed by these fibers is very small and for any quantitative determinations an accurate technique is required. After some preliminary experiments it was decided to use continuous flow liquid chromatography to study adsorption from solutions on "Thornel" 50 fiber surfaces.

A major portion of this year was spent on the design and fabrication of the liquid chromatograph which is shown in Figure 4. The heart of the system is a stainless steel column which holds the fibers. These fibers are wound spirally on a glass-rod, and the assembly is then forced into a stainless steel tube which serves as column jacket. Two pumps, one each for the solvent and the solution, pump the fluids through the fibers in the annular space between the inner rod and outer jacket at any desired flow rate. The column can be heated up to 300°C for baking purposes. The oven temperature can be accurately controlled between 25°C and 100°C for carrying out adsorption experiments. The column can be put under vacuum or purged with nitrogen while heating to clean the fiber surface. The effluent stream from the column is continuously analyzed through use of a LDC-Refractomonitor (Laboratory Data Control, Danbury, Connecticut). By following the change in concentration with time, the amount adsorbed at any solution concentration can be determined. All parts of the system coming in contact with the solutions are made of glass, stainless steel or Teflon so as to avoid contamination of the fiber or solutions.

The dead-volume must be accurately known before the amount adsorbed can be calculated. Dead volume was determined by estimating the volume of the tubing and fittings and adding this to the void volume inside the column. Experimental determination of the dead volume was done by running the solvent through the dry column at a known flow rate and noting the time taken in going from one end to the other. The values of dead volume thus determined are shown in Table I. The experimental values determined at three different flow rates are in good agreement but their average differs from the estimated value by about 4 percent. This difference may be due to an error in the fiber density used (1.63 gm/cc. for "Thornel" 50) or the experimental values can be in error due to a small amount of channeling in the column. Correction for the latter can be made.

The data for the adsorption of stearic acid from cyclohexane on "Thornel" 50 (from the same sample used in the gas adsorption work) at 22°C and 45°C is shown in Figure 5. This system was chosen because the adsorption of stearic acid from cyclohexane on carbon powders had been studied earlier by Kipling et al. (7), and it would thus serve for the evaluation of the performance of the equipment and the applicability of the technique. Also shown in Figure 5 is the data of Kipling et al. (7) for the adsorption of stearic acid from cyclohexane on "Graphon" at 20°C. Only two points could be plotted from their data because other points were at higher concentrations and cannot be accommodated in Figure 5. It is seen that the monolayer is formed at about the same solution concentration on "Graphon" and "Thornel" 50 (22°C data).

# LEGEND

1. Solvent Reservoir
2. Solution. Reservoir
- 3,4. Constant Flow-rate Pumps
- 5,6. Debubblers
- 7,8. Pressure Gauges
9. Oven
- 10,11,12. Equilibration Coils
13. Chromatographic Column
14. LDC Refractometer
15. Recorder

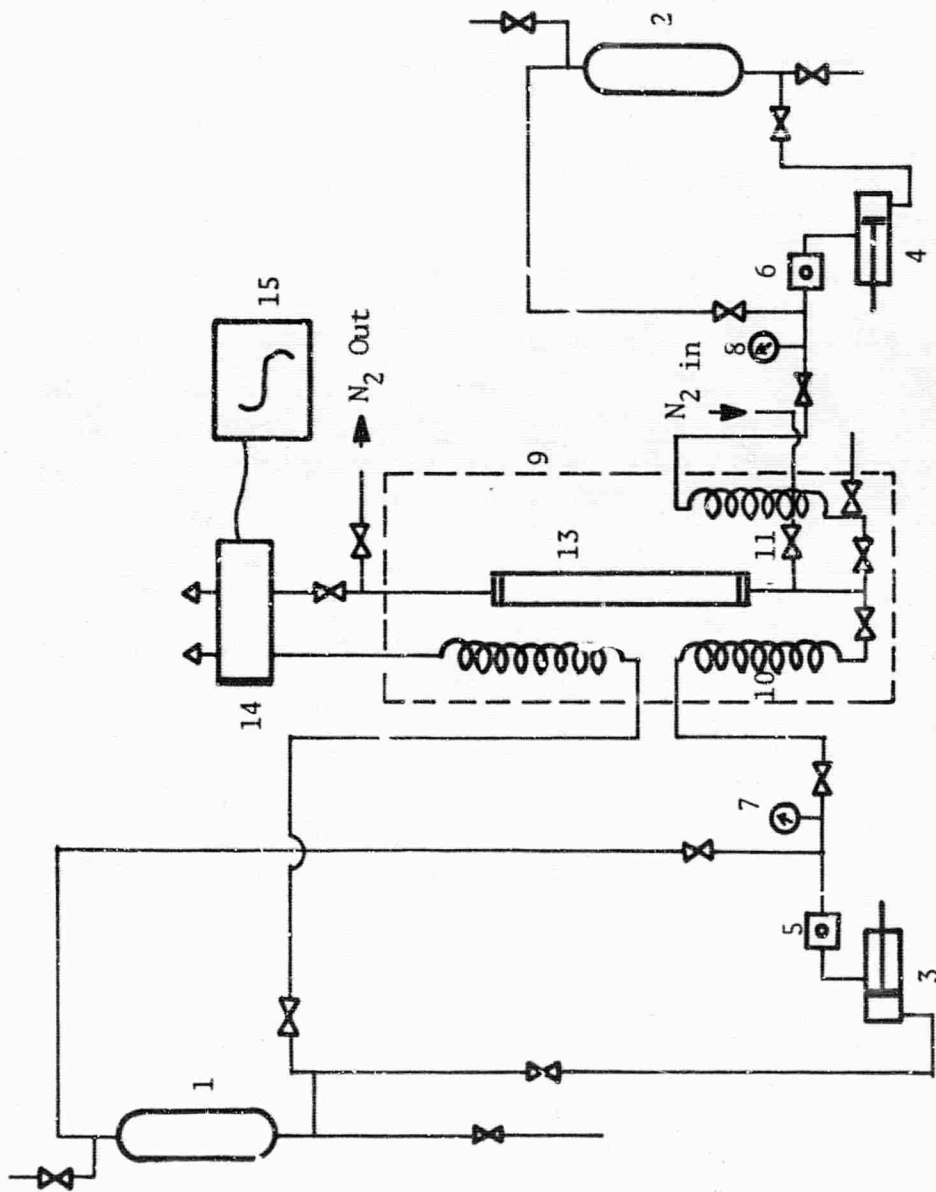


Fig. 4 LIQUID CHROMATOGRAPH

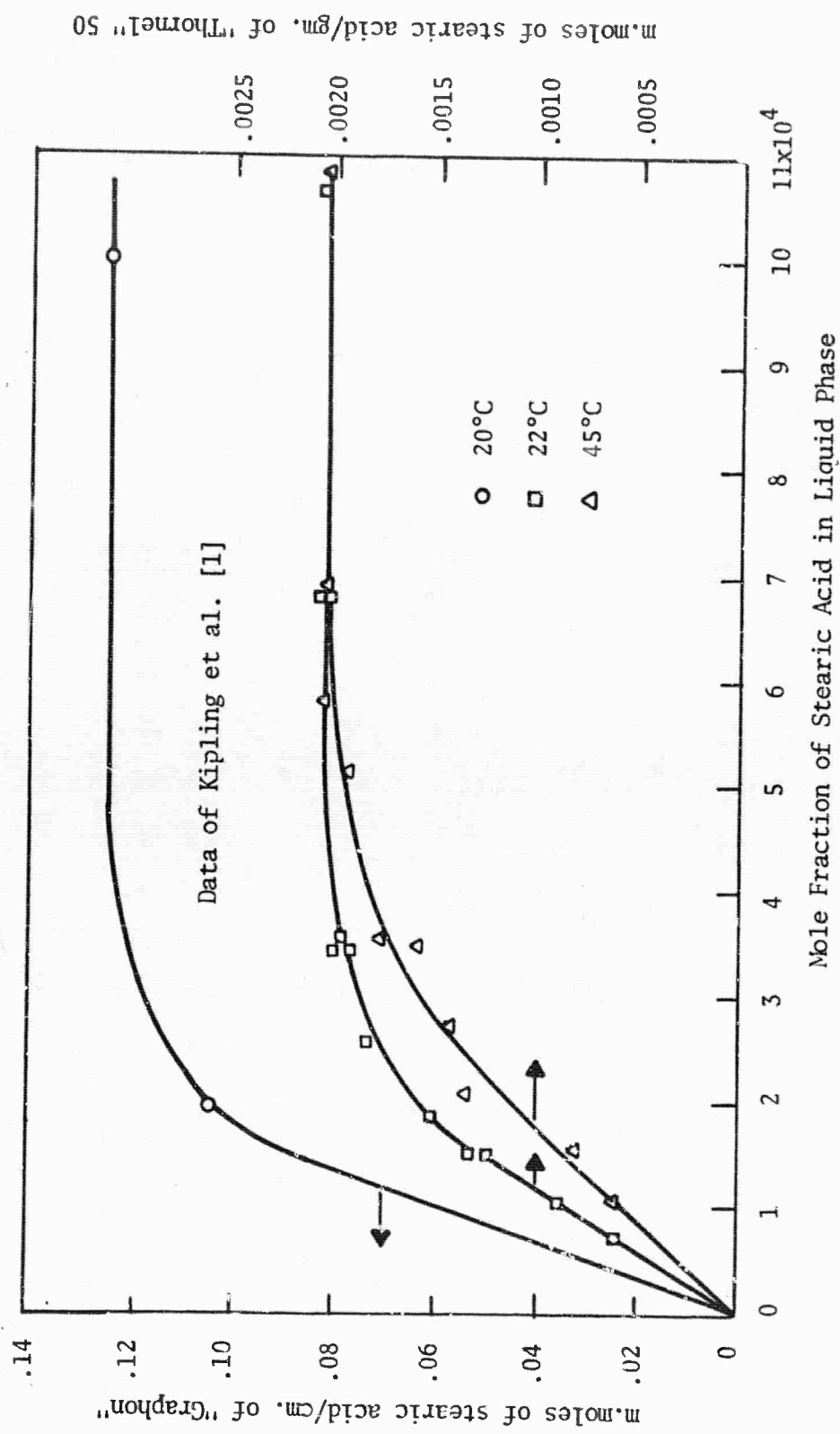


Fig. 5 ADSORPTION ISOTHERMS FOR STEARIC ACID ON CARBON

Similarity between the two surfaces is thus indicated. Kipling et al. found that the stearic acid molecules lie flat on the "Graphon" surface with each molecule occupying an area of  $114 \text{ \AA}^2$ . Assuming the same orientation on "Thorne" 50, the specific surface area of these fibers is found to be  $1.39 \text{ m}^2/\text{gin.}$

TABLE I MEASUREMENT OF DEAD-VOLUME

I. CALCULATED VALUE = 38.86 c.c.

II. EXPERIMENTAL

<u>FLOW RATE</u> (cc/Minute)	<u>TIME</u> (Minutes)	<u>DEAD VOLUME</u> (cc)
0.935	39.7	37.12
0.935	40.2	37.59
0.530	69.9	37.10
0.935	39.6	37.04
1.335	27.9	37.26

Average = 37.22 cc

The isosteric heats of adsorption can be calculated from adsorption isotherms at two different temperatures by using the equation given by Kiselev et al. (8),

$$\frac{\partial \ln a}{\partial (1/T)} \bigg|_{\theta} = \frac{q_{\theta}}{R} \quad \text{(III A-1)}$$

Here  $a$  = activity of solute in solution,  
 $T$  = absolute temperature,  
 $\theta$  = fractional surface coverage,



$q_{\theta}$  = isosteric heat at  $\theta$ ,

and  $R$  = gas constant .

For dilute solutions equation III A-1 reduces to

$$\frac{\partial \ln C}{\partial (1/T)}_{\theta} \approx - \frac{q_{\theta}}{R} \quad (\text{III A-2})$$

where  $C$  is the concentration of solute in solution. The values of isosteric heats thus calculated for the adsorption of stearic acid from cyclohexane on "Thorne1" 50 are shown in Figure 6. The "Thorne1" 50 surface appears to be more or less homogeneous although a very small decrease in isosteric heat with increasing surface coverage is noticeable. No other values for isosteric heats are available in the literature for this system and hence no comparison can be made.

Some scatter is noticed in the adsorption data. This is partly because the amounts adsorbed are small ( $\approx 41$  micro grams at the monolayer). Also the difference in the refractive index of stearic acid and cyclohexane is only .0033. For a solute-solvent system having a larger difference in refractive index greater accuracy is expected. Investigation of other systems is in progress.

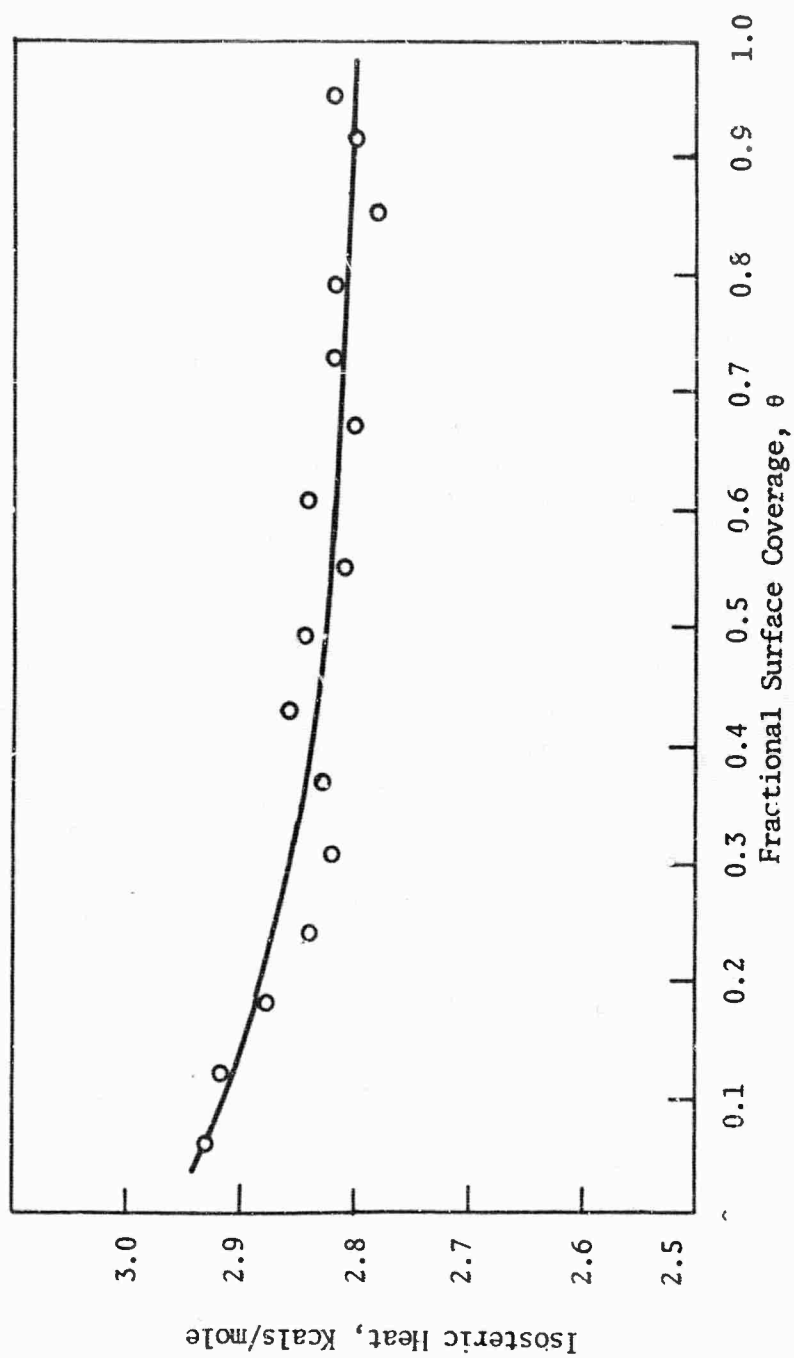


Fig. 6 ISOSTERIC HEATS OF ADSORPTION FOR STEARIC ACID ON "THORNEL" 50

## B. Characterization of Graphite Fiber Surfaces with Raman Spectroscopy (Professor Koenig and Dr. F. Tuinstra, Case)

There is presently a growing interest in carbon and graphite fibers. Reported tensile strengths and Young's moduli of 400,000 psi and  $100 \times 10^6$  psi respectively, for graphite fibers, in addition to a low specific density (2.0 gm/cc), are very promising properties for reinforcing fibers in composite materials. Failure of the interfacial bond between fiber and matrix, however, keeps the composite material from adequately translating internal force fields to the fibers. The present work was undertaken to investigate the origin of the weakness of the interfacial bond.

In a recent paper, observation of Raman spectra of different types of carbons and graphites was reported (19). Raman spectrum is induced in a thin surface layer of the sample due to the high extinction coefficient of the graphite for the laser beam, so the spectrum reflects primarily the properties of the surface. A single Raman line is observed at  $1575 \text{ cm}^{-1}$  in graphite samples consisting of single crystals. This line is assigned to the  $E_{2g}$  species of the infinite crystal. Polycrystalline graphite exhibits an additional line at  $1355 \text{ cm}^{-1}$  and is attributed to a particle size effect. For small crystals of graphite, a  $A_{1g}$  mode of the lattice becomes Raman active. The ratio of the intensities of the two observed Raman lines at  $1355 \text{ cm}^{-1}$  and  $1575 \text{ cm}^{-1}$  is directly related to the "amount of crystal boundary" in the sample. The latter is related to the average crystal diameter in the a-axis direction,  $L_a$  observed with x-ray techniques.

All the techniques used in the structural research of the graphite fibers describe either the internal structure of the bulk of the fiber, like X-ray and E.S.R. do, or they reveal the topology of the surface like optical and electron microscopy do. The Raman spectroscopy of graphite fibers promises to be a unique tool since it characterizes a thin surface layer of the fibers.

In this section, we will discuss the Raman technique and its power for the characterization of graphite fibers with relation to the properties of composite materials.

### 1. Experimental Work

As described in Reference 9, the Raman spectrum of graphite can be obtained using a powerful Ar-ion laser (~500 mW) and a double monochromator (Spex 1400 or Spectra-Physics 700). The laser beam is focused onto the surface of the sample. The illuminated area is carefully imaged on the entrance slit of the spectrometer. For high quality spectra, the laser beam must be focused down to the diffraction limit at the sample. With an appropriate lens, the illuminated area can be as small as  $10 \text{ }\mu\text{m}$  in diameter.

Because of the small focal area and the small dimensions of the graphite filaments ( $\sim 10 \mu\text{m}$ ), a microsampling technique, which is illustrated in Figure 7, was developed. The incident laser beam hits the sample at S. A collecting lens, which normally images S onto the entrance slits of the spectrometer, is temporarily replaced by a microscope which projects its image on a viewing screen V to avoid eye damage to the observer. The microscope is mounted so that it collects the light that normally would pass through the collecting lens. The advantages of this technique are:

1. The focusing of the laser beam onto the sample surface can be controlled,
2. An appropriate area of the sample can be selected, and
3. Effects of the impact of the laser beam on the sample can be examined.

After samples and laser beam are adjusted, the microscope is replaced by the collecting lens, and the Raman spectrum is run. This technique enables one to record the spectrum of one single filament of a graphite yarn.

Samples used in the present work were mostly in the form of a yarn. In the normal runs, the filaments were mounted coplanar with the laser beam and the entrance slit; they made an angle of  $30^\circ$  with the laser beam. Sometimes a goniometer head was used to investigate spectra obtained under different orientations. The samples could be immersed in an inert gas atmosphere to avoid effects from the surrounding air.

## 2. Results for Graphites and Carbons

The Raman spectrum can discriminate between different types of graphite and carbon (9). All types of carbon and graphite fibers investigated showed only two lines at  $1355 \text{ cm}^{-1}$  and  $1575 \text{ cm}^{-1}$ . Differences in the Raman spectra are observed in the linewidth and in the ratio of the intensities of the two lines  $R = I_{1355}/I_{1575}$ .

For a given sample, the linewidths of the two lines are always nearly the same. A small linewidth indicates that the sample is highly graphitic; wide line widths are observed in nongraphitic carbon samples like activated charcoal, lampblack and vitreous carbon.

The ratio, R, appears to be related to the "amount of crystal boundary" in the sample. The band at  $1355 \text{ cm}^{-1}$  is attributed to a vibrational mode of the graphite lattice which achieves Raman activity at the borders at the crystalline areas due to the loss of transitional symmetry. The amount of "boundary" is inversely related to the average crystal diameter,  $L_a$ , in the graphite plane, as determined by X-ray techniques.

The linear relationship between R and  $1/L_a$  is shown in Figure 8.

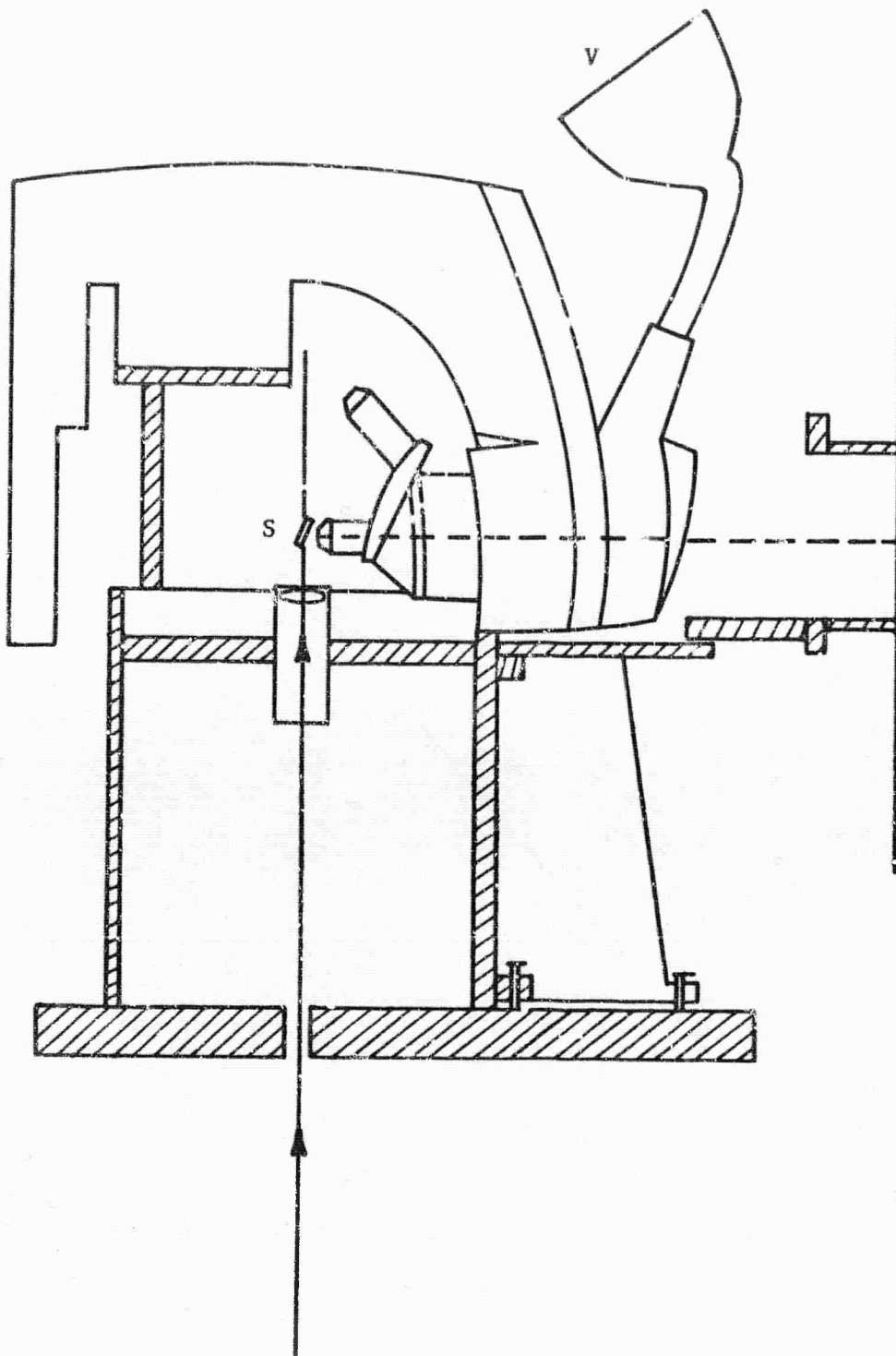


Fig. 7 GEOMETRY OF THE MICROWAVE OVEN

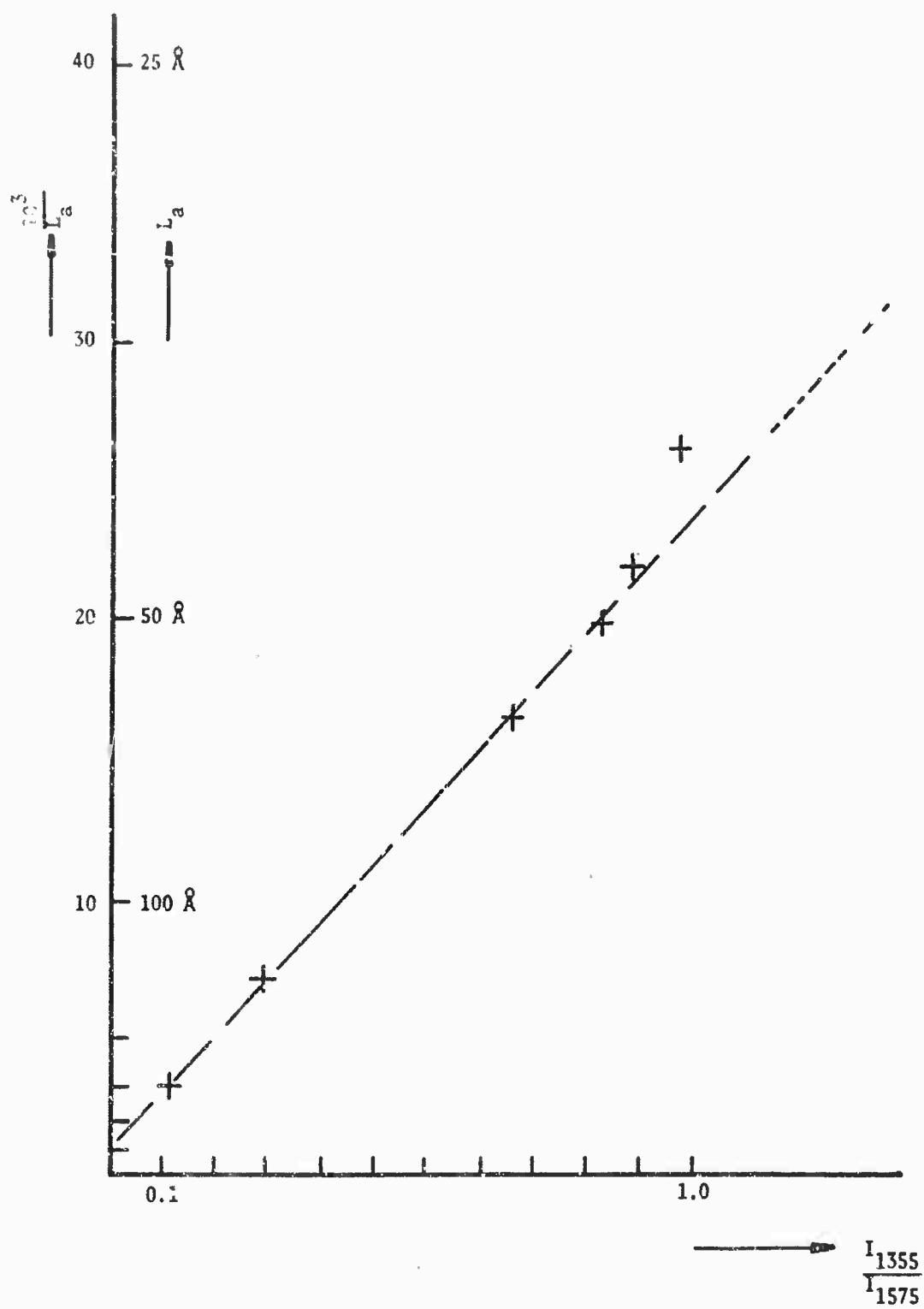


Figure 8. Plot of Relative Intensity versus Crystallite Size for Samples of Different Origin.

The samples used to construct Figure 8 were Thermax (MT), Conitex (FEF), Carbolac 2 (HCC)(10) and a series of samples where the  $L_a$  were measured by Dr. S. L. Strong of the Union Carbide Corporation. All of these samples were powders so that no orientational effects are present.

From the slope of the  $R$  versus  $1/L_a$  curve, an estimate of thickness of the boundary influence for the graphite crystals is  $10 \text{ \AA}$ . The skin thickness of the fiber producing the Raman spectra can be estimated using the extinction coefficient for graphite. It appears that about 70% of the Raman signal results from a surface layer of the order of  $250 \text{ \AA}$  thick; 90% emerges from a  $500 \text{ \AA}$  thick layer. This implies that crystallites with  $L_a$ 's of approximately  $100 \text{ \AA}$  could influence  $R$  by preferred orientation effects.

The amount of crystal boundary seen by the Raman spectrometer in a sample having preferred orientation can depend on the thickness of the sample layer of the fiber producing the spectrum, the diameter of the crystallites, and the amount of impurity or boundary affected molecules inducing the  $1355 \text{ cm}^{-1}$  line. If  $L_a$  is large with respect to the sample layer and thickness of the boundary influence, orientation of the graphite crystal planes perpendicular or parallel to the surface can make a large difference in the ratio of the two lines.

The thickness of the boundary influence of  $10 \text{ \AA}$  makes measurements of  $L_a$  below  $30 \text{ \AA}$  not useful. We have never observed values of  $R$  exceeding 1.4. The orientational effect has been observed in the case of stress annealed pyrolytic graphite, in which the  $c$ -axes of the (large) crystallites are parallel. The value of  $R$  observed on the  $c$ -face of this pyrolytic graphite sample is very low. If, however, the laser beam is aimed at the edge of the sample so that the pyrolytic graphite planes are parallel to the laser beam, a much higher value of  $R$  is found.

### 3. Results for Graphite and Carbon Fibers

The Raman spectra of graphite fibers depend on the fiber source and thermal history. The differences are illustrated for the two Morganite fibers in Figure 9. The differences in linewidth indicate that Morganite II is essentially a carbon fiber (at least its surface) and Morganite I is a graphite fiber. Secondly, the difference in  $R$  indicates that Morganite II contains smaller crystals with more crystal edges in its surface than Morganite I.

The types of fibers investigated in this way are: "Thornel" 10, "Thornel" 25, "Thornel" 50, "Thornel" 75 and "Thornel" 40; further HMG 50, Fortafil 5-Y, Morganite I and Morganite II. Only samples of untreated yarns are reported since the treatments are generally not specified by the manufacturer. Coatings on "Thornel" fibers were taken off by boiling water treatment; in this case no difference was observed in the spectra of coated and un-

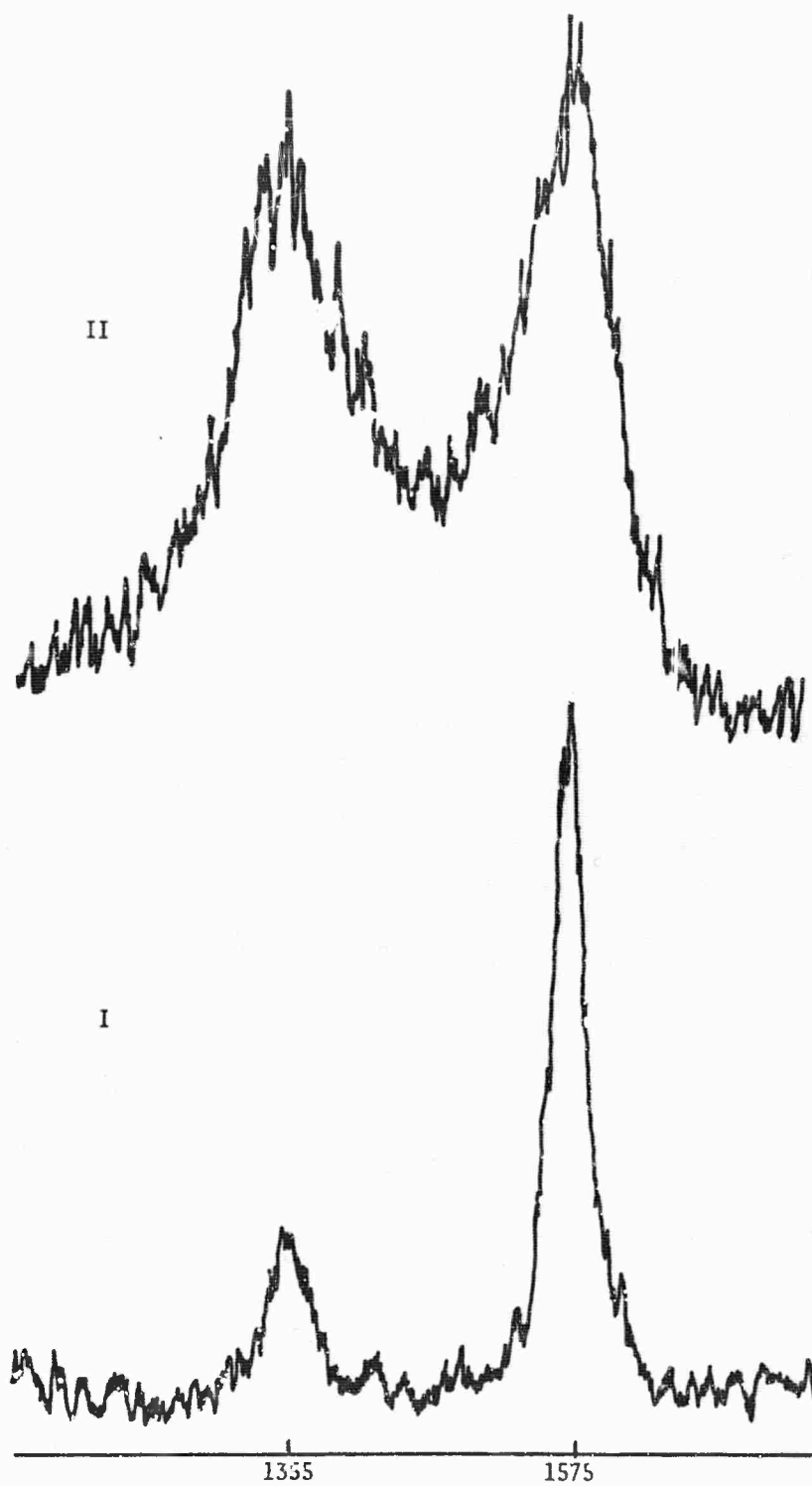


Fig 9 COMPARISON OF THE RAMAN SPECTRA OF MORGANITE I AND MORGANITE II



coated samples because the coating evaporates in the laser beam. For each of these fibers, the  $L_a$ 's were determined through the experimental relationship of Figure 8. For all samples, 5 consecutive runs were made at different spots on a sample 1 inch long. The scattering of the measured values of  $R$  given in Table II was low. Standard deviations were all about 0.03 except for Morganite I where a value of 0.003 was found which is possible due to a high surface homogeneity of this fiber. Spectra taken from the same type of fibers from different lots show considerably more scatter but the general differences are indicated by the values in Table II. The series, "Thornel" 10 - 25 - 50 - 75, can be compared since they are from the same rayon treated at the same temperature on the same lab equipment.

For most fibers, the values of  $L_a$  obtained in this way are larger than the values reported with X-ray techniques (11, 12). The Raman spectra of the powders obtained by grinding the fibers gave  $L_a$ 's measured by the Raman effect much lower than the original fiber. These results confirm that a surface effect is observed. Fibers with high values of  $R$  did not show this effect. Powdering of a yarn sample of "Thornel" 75 ( $L_a = 170$ ) gave  $L_a$  of 85 Å, while powdered "Thornel" 10 ( $L_a = 50$  Å) gave an  $L_a$  of 50 Å. Finally, for a sample of "Thornel" 50, a surface layer was removed by burning in a TGA apparatus. For this sample the  $L_a$  reduced from 215 Å to 110 Å after 5.5% burn off by weight. (This sample was from a different lot than the one from the series reported in Table II). A further burn off to 19.6% did not further reduce the  $L_a$ . Powdering gave a value of 90 Å for  $L_a$ . These results indicate that the crystallites on the surface are larger than in the bulk of the fiber.

Different orientations of the fiber with respect to the sampling geometry did not result in essential differences in the spectra.

#### 4. Relation with the Shear Strength of the Composite

For some of the fibers listed in Table II, mechanical properties of composite materials have been reported (13, 14). From the data given in these references a relation between  $L_a$  (or  $R$ ) of the surface of the fiber and the shear strength of the composite is obvious. To elucidate this point further, some of the treatments specified in Reference 13 were repeated. The "Thornel" 25 yarn was oxidized in nitric acid for a period of 40 hours; another sample of the same yarn was oxidized in air at 400°C for a period of 27 hours. Figure 10 shows the correlation between the  $L_a$  found with the Raman spectrum and the composite shear strength for the same type of sample as reported by Goan and Prosen (13).

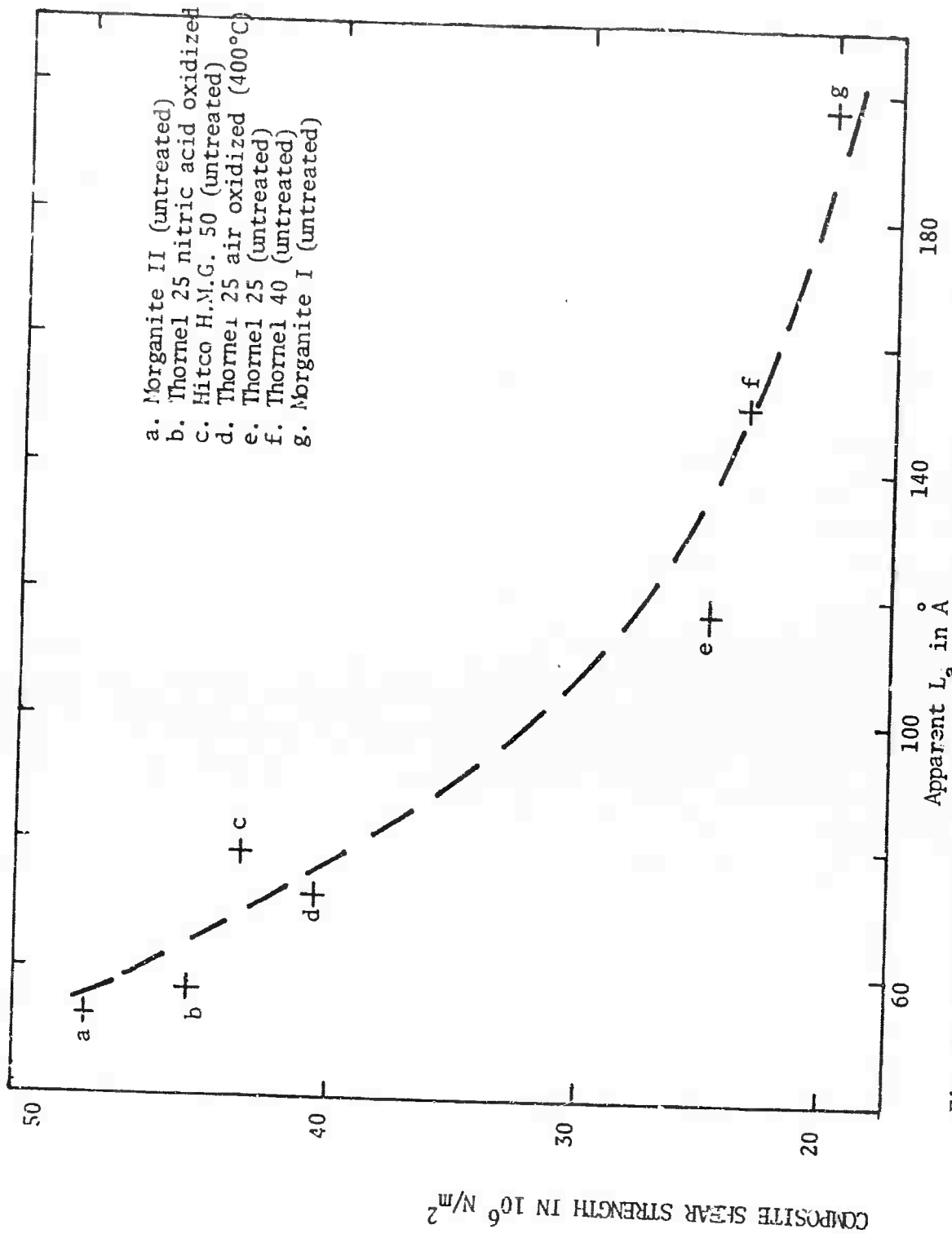


Fig. 10 RELATION BETWEEN COMPOSITE SHEAR STRENGTH AND THE  $L_a$  FOUND THROUGH THE RAMAN SPECTRUM OF THE GRAPHITE FIBER

TABLE II  
RAMAN SPECTROSCOPY RESULTS FOR CARBON AND GRAPHITE FIBERS

Yarn	$R = I_{1355} / I_{1575}$	Apparent $L_a$ (Å)
"Thorne" 10	0.85	50
"Thorne" 25	0.40	120
"Thorne" 50	0.29	155
"Thorne" 75	0.25	170
"Thorne" 40	0.30	150
Morganite I	0.22	200
Morganite II	0.83	50
H.M.G. 50 (Hitco)	0.56	80
Fortafil 5-Y (Great Lakes)	0.25	180

### 5. Discussion

From the present work it is clear that: the "amount of crystal boundary" is closely related to the shear strength of the composite; the higher the apparent  $L_a$  of the surface the lower the shear strength; and the "amount of crystal boundary" in the surface layer of many graphite fibers is unexpectedly low.

The term "amount of boundary" has been used throughout this paper without specifying it precisely. The "amount of boundary" is the amount of crystal boundary seen by the breathing mode of the graphite plane (see Reference 9). This "amount of crystal boundary", which is related to the  $L_a$  from the X-ray technique, can include edge dislocations, vacancies as well as crystal edges. In general, it will be proportional to number of atoms of a graphite plane having one nongraphite-like bond. The number of these atoms is proportional to the potential chemical functionality of the sample. On the other hand, these atoms can considerably increase the shear strength of the graphite composite through possible interlayer linkages. A large amount of boundary is expected to result in a high potential chemical functionality and a high shear strength of the graphite.

The interfacial bond between graphite and polymer matrix can be mechanical, physical or chemical in nature. The mechanical bond can result from purely mechanical interlocking effects at the interface, the physical bond can arise from attractive but nonbonding forces between the two surfaces and the chemical bond can arise from chemical reactions between chemical groupings on the surfaces. It has been shown by Herrick (15) that the mechanical bond, i.e., interlocking of fiber and matrix is a minor influence on the interfacial bond. Recently it was shown (16) that the weak secondary forces acting from the c-face of a graphite crystal are able to induce epitaxial growth of polyethylene. It was observed that the interfacial bond between polymer and the first graphite layer is stronger than the graphite interlayer bond (16). A larger amount of boundary in a graphite sample will enhance the interlayer bond and thus increase the bond between polymer and the bulk of the graphite. The stronger interfacial bonds, which will predominantly determine the interfacial adhesion are, of course, the bonds with chemical (covalent) nature. The result that the potential chemical functionality, which is observed in the Raman spectrum, is directly related to the interfacial adhesion is in agreement with the findings of Herrick (15). The interfacial bond is predominantly determined by the chemical activity and not by the surface area (15).

In the light of the present results, it is not too surprising that different oxidizing agents have different effects on the interfacial shear strength of the composite (13,17). Some agents attack a graphite crystal predominately perpendicular to the c-plane, creating active sites, others affect the graphite layers quickly from the edges as Henning has demonstrated (18). The latter agents will decrease the "amount of boundary" while the former agents will increase it.

The unexpected high values for the apparent  $L_a$  in the surface layer of some fibers can be due to two different effects. Either the  $L_a$ 's are as large as they appear from the Raman spectrum, or an orientational effect gives an apparent  $L_a$  which is larger (19). For the fibers where this surface effect is present, the  $L_a$  for the bulk could be large enough to effectively change the "amount of crystal boundary" in a 250 Å thick layer. The experiments with the stress annealed pyrolytic graphite show that the observed low values of R are due to an orientation effect of the graphite crystallites. In the surface layer of many graphite fibers, the crystallites are oriented with the graphite planes parallel to the surface. This geometry makes it highly probable that "interfacial" failure occurs within the graphite fibers. Some electron microscopic observations of fibers pulled out of a composite confirm these results. "Thornel" 40 fibers left a very thin highly oriented graphite layer on the polymer matrix (nylon 6) as indicated by electron diffraction.

Raman spectroscopy of the graphite fibers indicate that the crystallite size on the surface of the fiber is larger than the crystallite size in the interior of the fiber. The strength of the interfacial bond in the composite depends on the potential chemical functionality of the fiber

surface. This functionality increases with the number of nongraphite-like or crystal boundary carbon atoms, since the number of nongraphite-like or boundary atoms is inversely proportional to crystallite size. Raman spectroscopy can be used to characterize the potential surface activity of graphite fibers. Correlations of the Raman results and composite shear properties can be obtained.

## SECTION IV

### RESEARCH ON GRAPHITE-FIBER, RESIN-MATRIX COMPOSITES

This report section will describe a program on nylon matrix composites in which the nylon is polymerized in situ, a study of polymer formation on graphite fiber surfaces, and a program on polyamide-imide and polysulfone matrix composites.

#### A. In Situ Polymerization of Nylon Matrix Composites (Professor Litt and Dr. J. B. Shortall, Case)

The purpose of this program was to study the viability of using polymer systems such as polyamides and polyurethanes as the matrix element in graphite fiber composites, a special aspect of the work being the incorporation of the fibers in the polymer by in situ polymerization on the fibers. It was anticipated that this method would lead to greater wetting of the fibers by the polymer than would more conventional methods and would also lead to the formation of void-free composites.

The last report (4) described the preparation of a graphite fiber ("Thornel" 25), nylon matrix composite having a fiber content of approximately 20%. This composite was subsequently examined by x-ray and electron diffraction and by electron microscopy.

Slices between 500Å and 1000Å were microtomed from the composite. No obvious voids were present. Figure 11 shows an electron micrograph of sheaths which could be nylon which had crystallized around the fiber during microtoming. Epitaxial crystallization with the polymer chain parallel to the fiber direction is indicated, as the lamellae can be seen perpendicular to the fiber direction. This effect is shown more clearly in Figure 12. While the sheaths clearly indicate epitaxial crystallization of nylon, electron diffraction on selected areas showed only the oriented graphite pattern, Figure 13. Thus, the sheaths must have come from the surface of the fiber and may have a thin film of nylon adhering. Another possibility is that there were two weak regions: one within the fiber and another at the interface; the interface between the fiber and the crystallized lamellae of nylon then sheared, leaving a replica of the lamellae and a sheath of exfoliated graphite.

The fact that the sheaths were easily removed from the fiber indicated that adhesion was poor. This theory was confirmed by strength tests carried out on the composite, which yielded a tensile strength in the longitudinal direction of only  $6 \times 10^3$  psi. This value is the mean of 3 measurements carried out on "dog-bone segments" of the composite using a Tate Emery test machine.

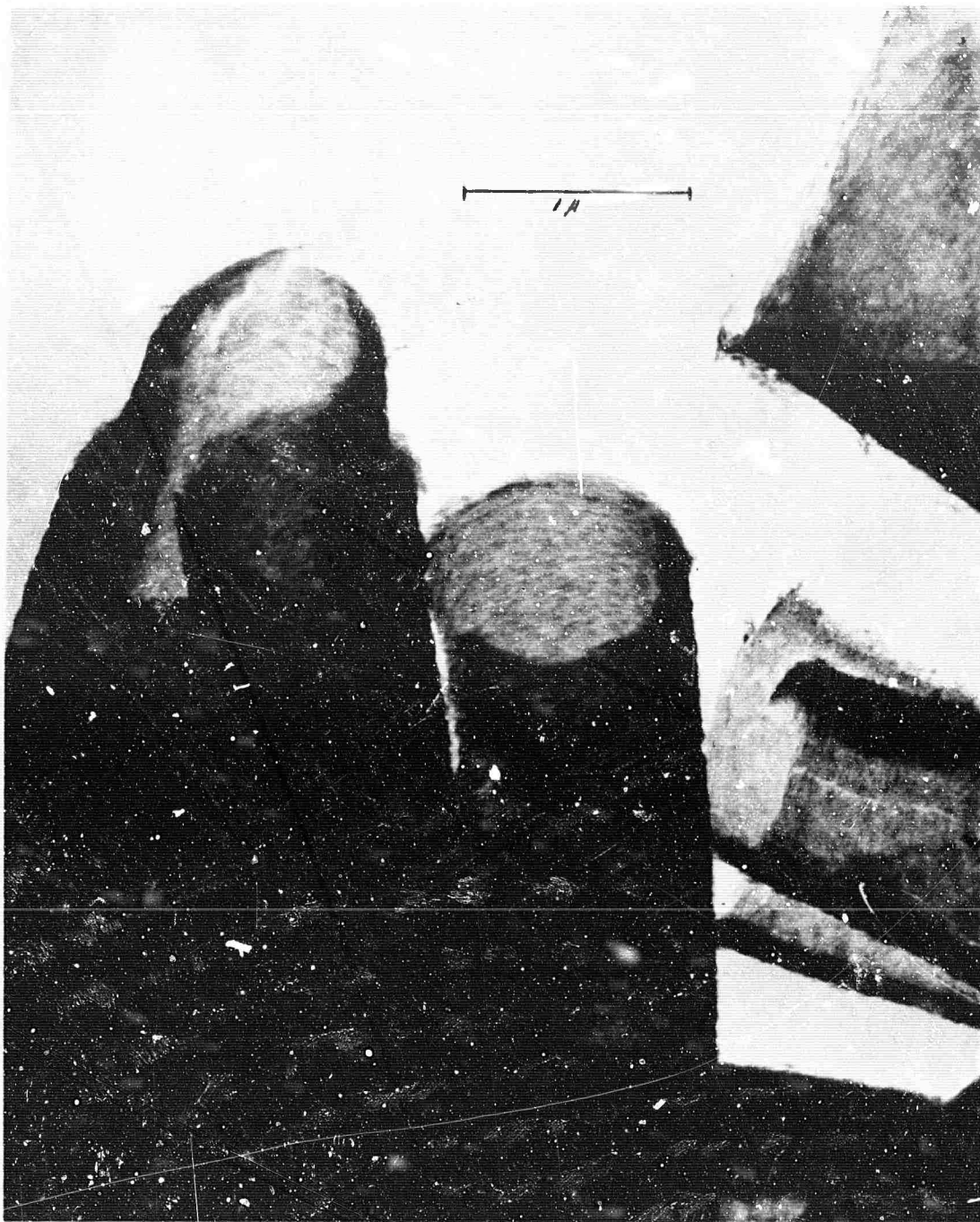


Figure 11. Direct Transmission Electron Micrograph  
of a Section of Composite 1. Magnification = 45,000.

N-22815

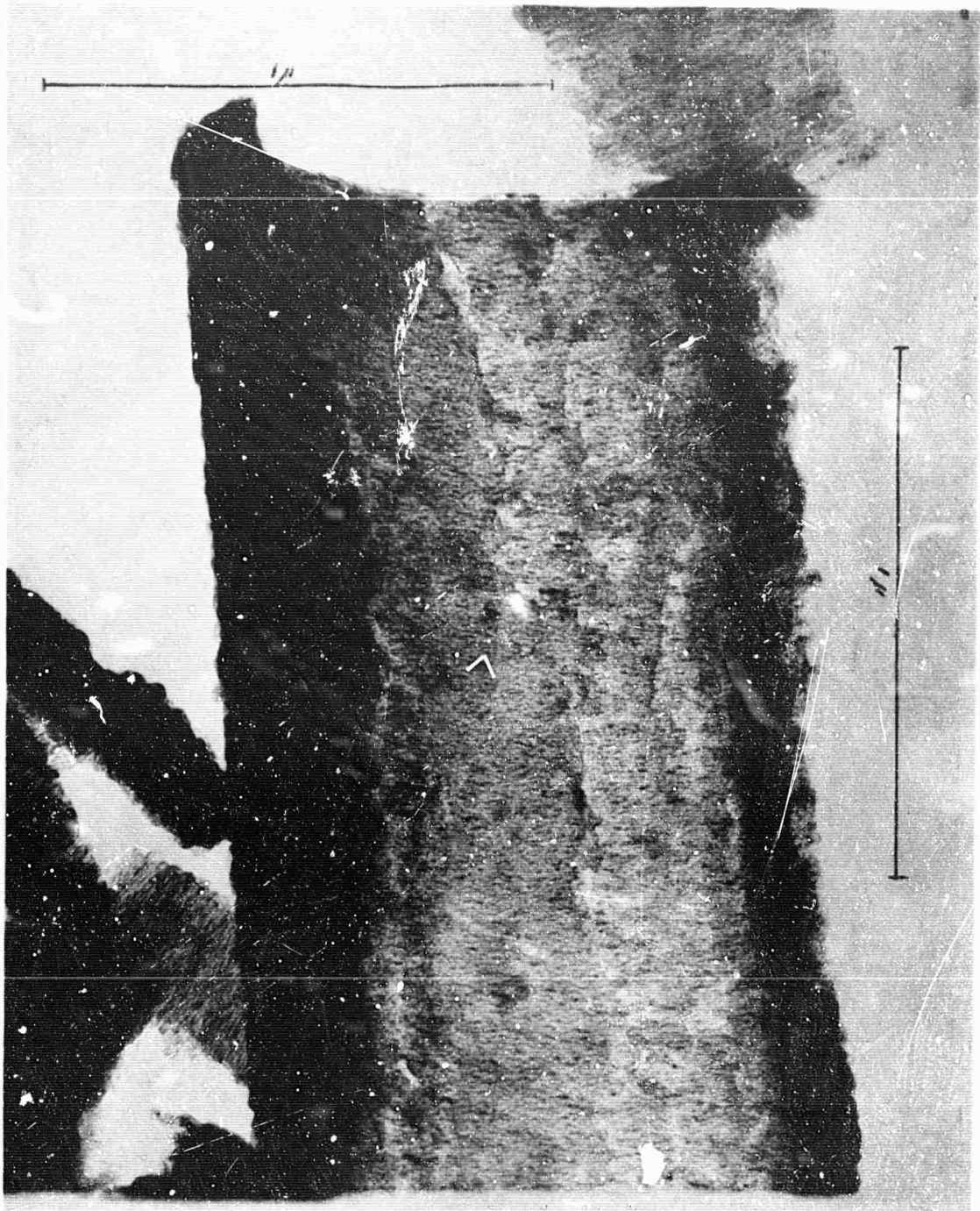


Figure 12. Direct Transmission Electron Micrograph of  
a Sheath from Composite 1. Magnification = 103,000.

N-22818



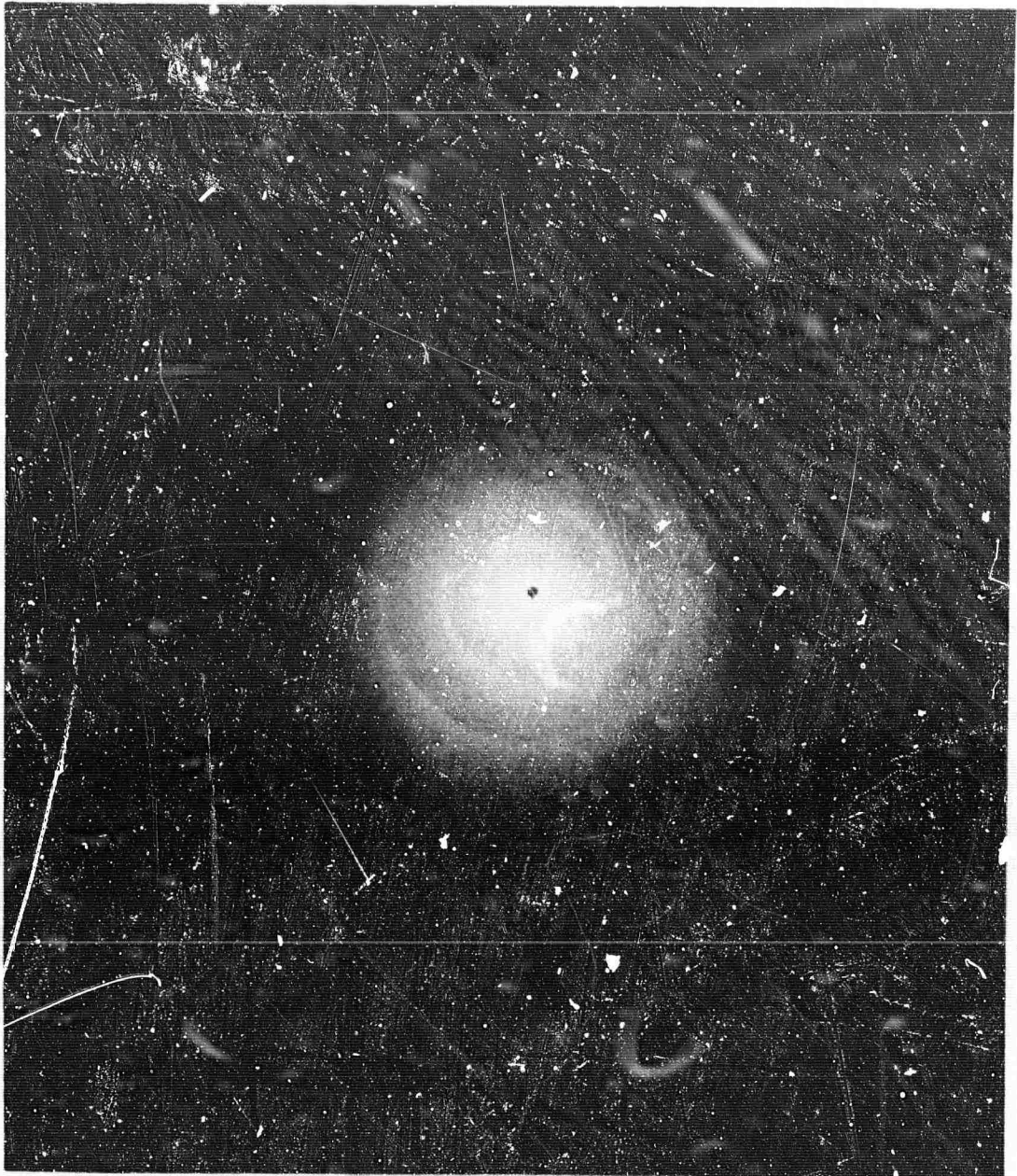


Figure 13. Electron Diffraction Photograph of  
Figure 11 Orientation not Specified.

N-22819

The adhesion was poor because of the polymerization routine used during the initial polymerization. At 170°C, polymer must have crystallized on the surface; the polymer did not melt or recrystallize when the temperature was raised to 200°C, the bulk of the nylon polymerized. Polymer formed at different temperatures would not be linked physically and thus the sheath could be pulled out. Figure 13 is an electron diffraction photograph of a portion of the sheath showing the presence of oriented graphite.

A number of composites were also prepared using "Thornel" 50 and Fortafil 5y<sup>†</sup> graphite fibers in nylon matrices. These composites were prepared by diluting the caprolactam anion to 1/40M and melting the mixture under vacuum at 100°C. This procedure degassed the monomer and prevented air bubble formation during polymerization. When the mixture had melted, the co-catalyst (diethyl carbonate) at a concentration of 1/100 M was added, and after stirring, the mixture was poured onto a mat of graphite fibers in a container in the same oven. The oven was then reevacuated for about 5 minutes; the composite was then transferred to another oven maintained at 235°C through which an atmosphere of nitrogen was passed. This temperature is above the melting point of nylon 6, and the polymerization is homogeneous under these conditions.

Polymerization occurred within 30 minutes, the mixture on the fiber becoming very viscous; on cooling the polymer crystallized out in position on the fibers.

Sections between 500Å and 1000Å thick were microtomed from these samples and studied by x-ray and electron diffraction and by electron microscopy.

The composites were found to be almost void free and had a fiber content of about 40%. The electron micrographs, for example Figure 14, do not appear to show an interface, but apparent sheaths with nylon lamellae can be clearly seen in the lower portion of the photograph. Diffraction patterns from the same composites taken from the area shown in Figure 14, show mainly oriented graphite, Figure 15.

X-ray photographs show that much of the nylon is oriented parallel to the graphite, Figure 16. The 200, 002/202 and 171/271 reflections are clearly highly oriented.

Further composites were made, using the above method, but with the addition of a weight which compressed the mat of fibers after they had been coated with the monomer mixture. Both composites prepared this way were found to contain voids.

Longitudinal and transverse strength tests were carried out on

---

<sup>†</sup>Great Lakes Carbon Corporation



Figure 14. Electron Microphotographs of a Section of Composite 11. Magnification = 13,000. Sheaths and Thin Sections, possibly Carbon Fiber, are Visible.

N-22816



Figure 15. Electron Diffraction of Lower Section of  
Figure 14 , only Oriented Graphite Visible.

N-22817



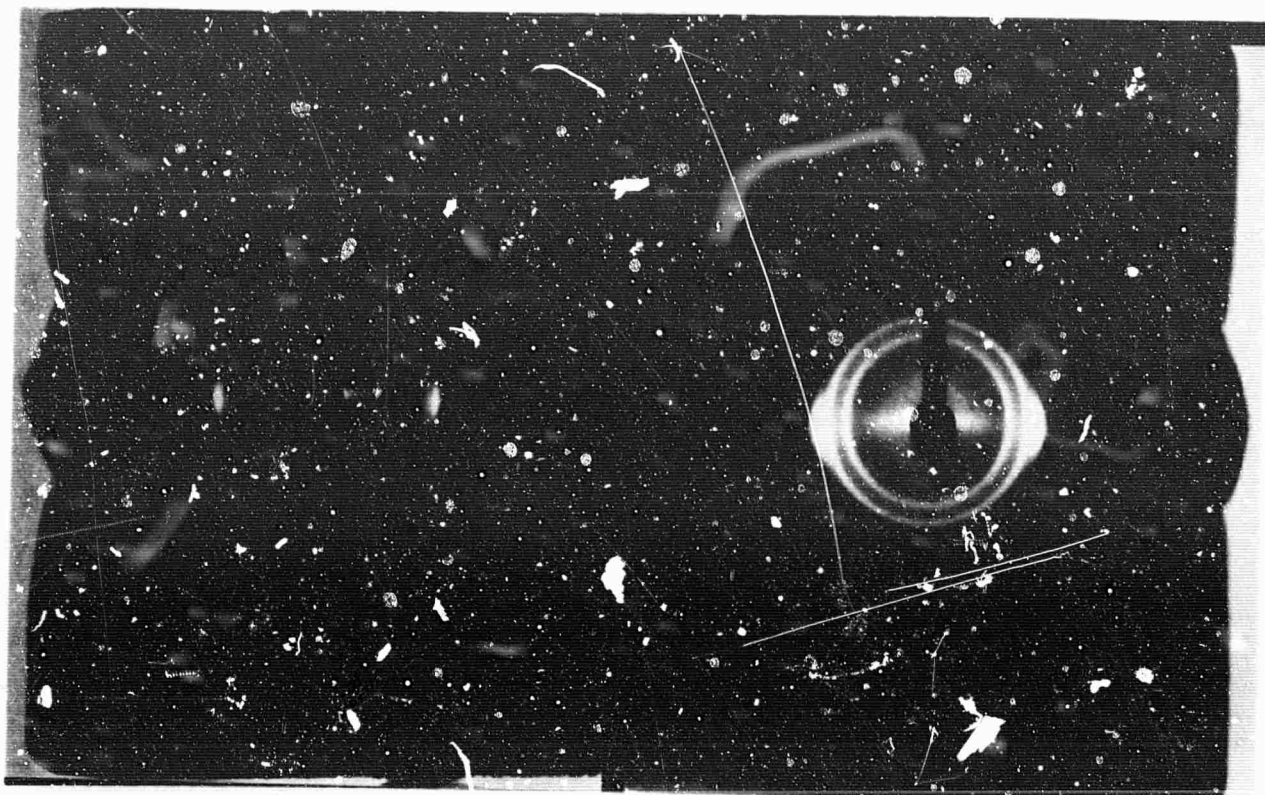


Figure 16. X-ray Photographs of Thin Section of Composite 12.  
(Fiber Density about 60%.) Note High Degree of  
Orientation of Visible Nylon 6 Reflections  
(Two Inner and Outer Vertical Reflections).

N-22814

the composites of "Thornel" 50 and Fortafil 5y graphite fibers, and the data obtained is shown in Table III. The Fortafil 5y uncoated fibers had a modulus of  $50 \times 10^6$  psi and tensile strength of  $274 \times 10^3$  psi.

TABLE III  
NYLON COMPOSITE TEST DATA

Sample No.	Fortafil 5y Composite		"Thornel" 50 Composite
	Tensile Strength (psi)	Young's Modulus (psi)	Tensile Strength (psi)
1	14,320	$3.45 \times 10^6$	17,500
2	11,000		22,500
3	12,000		
4	8,970		
5	8,675		
6	6,240		

Short Beam Test  
(psi)

3,220

2,780

Samples broke in tension, not shear.

The fracture surface of the tensile specimens indicated that the fiber-nylon interface strength was quite good. No extensive debonding propagated from the fracture surface. Also, the sample did not fail in shear in the short beam shear test, indicating a good fiber-nylon bond.

The composites could be machined very well with no chipping and smooth surfaces were easy to obtain.

The results of the electron microscope and x-ray diffraction studies can be summarized as follows:

1. Nylon 6 composites show strong nucleation of crystalline

polymer from the carbon fiber indicating good molecular contact at the interface.

2. Test pieces broke in tension rather than in shear in the short beam bending test. At this fiber loading, there was no shear failure. No quantitative value can be given due to fiber inhomogeneity within the sample.
3. Samples were milled and drilled etc., with no precautions while preparing the test pieces. The composites were found to be very tough.

These factors suggest that the basic objective sought in in situ polymerization has been achieved, viz; polymerization and therefore strong interfacial bonding. Thus the composite had good shear strength, as shown by the bending tests. This result is helped by the ductility of the polymer which probably can relax out any highly strained regions.

The two composites, on close examination, appeared to contain some very small voids. However, these voids were in the matrix rather than at the interface.

The evaluation of possible latent catalysts has continued using very dry conditions (less than 120 p.p.m. water). Also, new methods have been used for the preparation of the sodium salts of caprolactam. In these methods the sodium salts were prepared in situ and the latent catalyst then added, instead of in the previous way which entailed mixing the previously prepared sodium salt with the caprolactam until the correct concentration was obtained, and then adding the latent catalyst.

Potassium tertiary butoxide, sodium borohydride and lithium aluminum hydride were tried but found to be unsatisfactory. Finally, sodium hydride was found to be suitable. The sodium hydride was obtained as a suspension in mineral oil and dried under a stream of dry hydrogen. A 1/100 molar quantity of sodium hydride was added to caprolactam to yield the sodium salt.

The results of the evaluation of some potential catalysts using the system are shown in Table IV.

In studying the reaction in a 60 cycle ac electric field (corona discharge), pure monomer was found to decompose even at room temperature as does epitaxially crystallized monomer on the graphite fibers. In the latter case spark discharge to the conducting fibers was seen to occur. Lowering the voltage or increasing the electrode gap to eliminate discharges resulted in no change in the samples at room temperature. At 120°C with no visible discharges, the crystallized monomer decomposed. Single crystals are observed to melt (lose their shape) and to oxidize under similar conditions. Reactions at voltages under 3000 volts and at higher temperatures (100-160°C) have not been studied.

A similar melting behavior is observed when monomers are put in a dc (20,000 volts) electric discharge. The nylon monomers were found to form oils, waxes and poorly crystallized low molecular weight materials depending on the exposure time. When the epitaxially crystallized monomer of nylon 66 was exposed to a dc discharge at room temperature in air, the sample appeared to catch fire and extinguish quickly when the electric field was removed. This process is not understood. However, highly crystalline oriented nylon 66 formed on the carbon fibers with the polymer chain axis aligned along the carbon fiber axis. Therefore, the graphite fiber surface induces polymerization under conditions where the monomer normally forms only a mixture of low molecular weight materials. The graphite fibers coated with monomer were then reacted with the fiber direction perpendicular to and parallel with the electric field. The parallel case was just described. When reacted perpendicular an oriented polymer reflection occurs on the meridian which definitely shows that the electric field is influencing the orientation of the polymer on the graphite surface. Under these conditions (dc discharge parallel or perpendicular) a bundle of graphite fibers becomes coated with polymer completely throughout, i.e. the polymer wets the surface. The once flexible fiber becomes highly rigid. Studies of depositing nylon melts on the graphite fibers were unsuccessful because of the lack of wettability on the surface and viscous behavior of the polymers. The polymer formed in the electric discharge can be removed by dissolving in formic acid. This is interesting in itself because glow discharge polymers are generally highly branched, cross-linked, and thereby insoluble (21). Once again the strong catalytic influence of "Thorne" 40 graphite fibers on surface reactions has been demonstrated. On the basis of wettability, the deposition of low viscosity monomers followed by in situ polymerization is probably the best method for obtaining graphite-fiber composites with good interfacial adhesion.

Work has been done on corona treated fibers as mentioned previously. The contact angle of water on the fibers was reduced from an average value of 90° before treatment to 65° after treatment for 30 minutes. In the case of corona treated polyethylene surfaces a reduction in the contact angle of water from 100° to 80° resulted in a large increase in ink adhesion from nil to 400g./in., respectively (22). Hines (23) has found corona treatment of polyethylene to increase the polarity of the surface. Thus, an increase in the number of functional groups on the graphite fiber was expected. However, corona treatment did not affect either the crystallization or reaction on the graphite fibers, i.e. the same as untreated "Thorne" 40 fibers.



The monomer of nylon 66 has been found to crystallize epitaxially on other "Thornel" fibers (T25, T50, T75). The monomer apparently does not crystallize well on "Thornel" 10 or Morganite I but does on Morganite II.

TABLE IV  
EVALUATION OF POTENTIAL CATALYSTS

CATALYST	CONCENTRATION (Molarity)	POLYMERIZATION Time (min)	
		Without fiber	With uncoated fiber
Ethyl isobutyrate	1/100	<20	<30
Phenyl isocyanate	1/100	immediate	<5
Phenyl acetate	1/200	<10	<20

Polymerization only occurred when uncoated fibers were used. In every case, fibers coated with polyvinyl alcohol inhibited polymerization. Although ethyl isobutyrate catalyzed the reaction in a suitable interval of time, it was considered unsuitable for further use because of the evolution of bubbles, probably due to ethanol being nucleated at the fiber surface at 200°C, which caused large voids in the resultant composite. The most satisfactory of the tests made with the latent co-catalysts appears to be that using phenyl acetate.

**B. Crystallization and Reaction on Graphite Fiber Surfaces**  
(Professor Lando and Mr. P. Frayer, Case)

The interaction between graphite fibers and epitaxially deposited monomers has been shown to be specific and strong. The edges of the graphite-like planes affect not only the oriented crystallization of monomers, but also affect the subsequent solid state reaction. Instead of polymerization, cyclization occurs for the monomers of nylon 66 and nylon 6, yielding cyclic dimer and cyclic trimer, respectively. A complete description of this previous work is given in the previous report (pg. 37 of Reference 4).

For the past year several approaches have been taken for obtaining polymer on the graphite fibers. The reaction of the monomers at higher temperatures has been studied. Other monomers which might not cyclize have been used. The influence of electric fields and electric discharges on the crystallization and reaction of monomers has been investigated. Finally, the surface of the graphite fibers was found to have increased in polarity when treated in a corona discharge. However, the epitaxial crystallization and subsequent solid state reaction on the corona treated graphite fibers were the same as on untreated fibers.

A single crystal of the monomer of nylon 66 ( $T_m = 197^\circ\text{C}$ ) reacts completely in the solid state at 160°C in 24 hours to form the polymer nylon 66. When epitaxially crystallized on the graphite fibers, the monomer does not react to polymer above 130°C in air but decomposes probably due to the

large surface area exposed to the air. Below 130°C the deposited monomer forms the cyclic dimer of nylon 66. Attempts to use a nitrogen atmosphere and temperatures between 130 and 160°C were unsuccessful. Apparently the decomposition of the monomer is very sensitive to small amounts of oxygen. Normally the monomer can withstand 130°C in air with only slight degradation. In this respect the graphite fibers may be affecting the decomposition reaction.

Three other monomers have been found to crystallize epitaxially on "Thornel" 40 graphite fibers. They are 4-aminobutyric acid (ABA), p-aminobenzoic acid (PABA), and hexamethylenediammonium terephthalate (HMDT). The solvent used affects greatly the quality of epitaxial crystallization. A list of the monomer solvent pairs which gave the best deposition are given below.

HMDA (nylon 66 monomer) - methanol  
ACA (nylon 6 monomer) - water  
ABA (nylon 4 monomer) - water  
PABA (p-aminobenzoic acid) - benzene  
HMDT (hexamethylenediammonium terephthalate) - dioxane

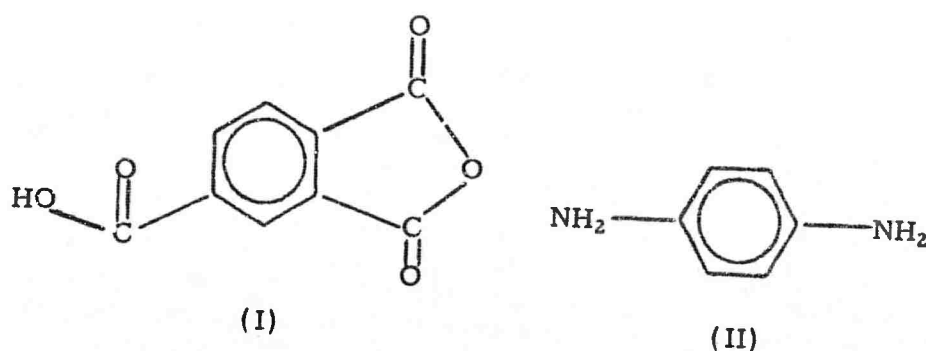
The reaction at 120°C of 4-aminobutyric acid, epitaxially crystallized on "Thornel" 40 graphite fibers, did not cyclize but did polymerize. Four oriented reflections (not due to the monomer) were observed perpendicular to the carbon fiber axis which can be indexed as the  $\alpha$ -form of nylon 4. The solid state reaction of this monomer has not been studied previously. Heating pure monomer at 120°C gave no reaction. There are 3 methylene groups between the amide groups in 4-aminobutyric acid as opposed to 5 for the monomer of nylon 6 and 6 (in the amine component) for the monomer of nylon 66. It was hoped that cyclization would be hindered by fewer rotational degrees of freedom in the 4-aminobutyric acid case. Apparently, this may be an explanation for the fact that polymerization is observed. The reaction of the other two monomers (PABA and HMDT) has not been studied yet.

The epitaxial crystallization of the monomer of nylon 66 is enhanced by ac (10,000 volts, 60 cycle) and dc (20,000 volts) electric fields. The subsequent reaction at 90°C yielded cyclic dimer with improved orientation as evidenced by second layer line reflections when compared with monomer crystallized without the influence of an electric field. This reaction in an electric field will be further investigated. It is hoped that the electric field will inhibit cyclization by restricting the motion of the polar groups. Before understanding this reaction, it seemed necessary to study the reaction of single crystals of the monomer in an electric field. When single crystals were aligned in the dc electric field with the b-axis (chain axis of the molecules) along the field direction and heated at 120°C for 24 hours, no reaction occurred. Normally single crystals do not react in 24 hours until temperatures above 145°C are reached. However, when single crystals were aligned with the a-axis (hydrogen bonding direction) along the dc field and heated at 120°C for 24 hours, crystalline polymer (nylon 66) was obtained. Apparently the breakage of the hydrogen bonds is made easier when under the influence of an external electric field. Previous work of the authors (20) has shown that it is necessary for the hydrogen bonds to break before polymerization occurs.

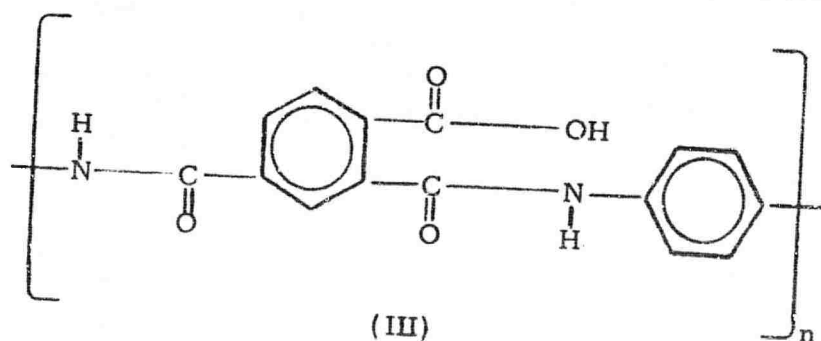
C. Polyamide-imide and Polysulfone Composites  
(Dr. I. C. Lewis and Dr. B. H. Eckstein, Union Carbide)

The objective of this investigation was to evaluate polymers other than epoxies as matrix materials for graphite fiber reinforced composites. For practical reasons and because of the time limitations of this program, only commercially available resins were considered. After a literature search was completed, two polymer systems were selected for initial investigation: the polyamide-imides supplied by the Amoco Chemical Company and the polysulfone P-1700 produced by Union Carbide Corporation. These resins were chosen in order to investigate their specific advantages: (1) polyamide-imide represents a resin with superior thermal stability to the epoxies, and (2) polysulfone resin exhibits extremely high toughness when compared to standard resins.

Polyamide-imides. The polyamide-imide resins are copolymers of trimellitic anhydride (I) and an aromatic diamine such as p-phenylenediamine (II).

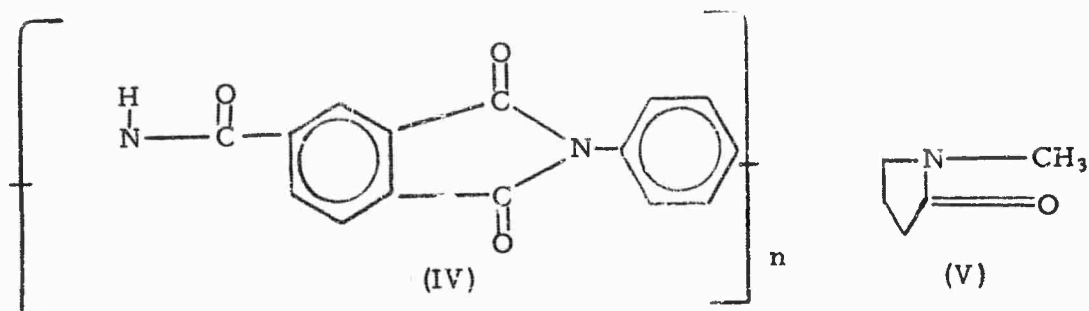


The polymer is generally employed in its soluble ortho-amic acid form (III).

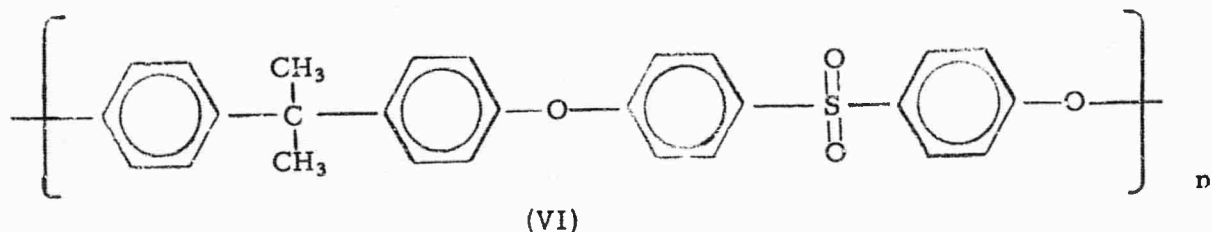


The polyamide-imides show thermal endurance intermediate to that of the polyamides and the polyimides. Although not so thermally stable as the latter, the polyamide-imides are reported to be more readily processible than the polyimides.

The thermoplastic polyamide-imide polymer (III) is converted to an insoluble thermoset polymer (IV) by thermal curing. The curing reaction involves dehydration and cyclization. The cured polymer (IV) is recommended for long-term usage up to temperatures of 600°F. The Amoco Chemical Company supplied two solid polyamide-imide polymers, AI-10 and AI-11. The AI-10 reportedly has long term (1000 hours) stability at 500°F; the AI-11 is thermally stable to 600°F (24). Both polymers are also available as varnishes in N-methylpyrrolidone (V) solution which are designated as AI-1030 and AI-1137, respectively.



Polysulfone - P-1700. The polysulfones have the general structural formula (VI).



Polysulfone P-1700 of Union Carbide Corporation is a thermoplastic material supplied in solid pellet form. The P-1700 has a glass transition temperature of 175°C (350°F) but does not decompose at temperatures as high as 275°C (525°F).

Polymer Properties. Table V lists some properties for the AI-polymers (25) and for the P-1700 (26), as provided by the manufacturers. For comparison, property data are also included for the epoxy resin ERLA-4617 (27), which is a resin system now widely used in graphite fiber reinforced composites. Table VI gives property data for glass reinforced composites prepared with each resin.

The data in Tables V and VI illustrate the superiority in thermal stability of the amide-imide resins and the much greater toughness or elongation of the polysulfone compared with the epoxy material. The thermoplastic polysulfone shows a lower strength and modulus than the thermoset epoxy and amide-imide resins.

TABLE V  
PROPERTIES OF EPOXY, POLYSULFONE, AND POLYAMIDE-IMIDE RESINS

	ERLA-4617 <sup>(27)</sup>	P-1700 <sup>(26)</sup>	AI <sup>(25)</sup>
Specific Gravity, 25°C	1.176	1.24	1.41
Viscosity at 25°C, cps	80 - 150	---	45 - 75 (in NMP)
Heat Distortion, Temp. °C	175	175	280
<u>Cast Resin</u>			
Compressive Modulus, psi	890,000	370,000	---
Compressive Yield Strength, psi	32,700	13,900	35,300
Deformation, %	7.5	0.2	---
Impact Strength (Izod) ft. -lb/in. notch	---	1.3	0.70
Tensile Modulus, psi	783,000	360,000	---
Tensile Strength, psi	19,200	10,200	13,300
Elongation, % at Break	2.8	50 - 100	2.0 - 2.5
Flexural Modulus, psi	815,000	390,000	700,000
Flexural Strength, psi	31,000	15,400	23,400
Recommended Temperature, Usage	Below 150°C	-150°F to 340°F	room temp. to 600°F

TABLE VI  
PROPERTIES OF RESIN-GLASS FILLED LAMINATES FOR EPOXY,  
POLYSULFONE AND POLYAMIDE-IMIDE

	ERLA-4617 <sup>(27)</sup>	P-1700 <sup>(28)</sup>	AI-1030 <sup>(25)</sup> (pressure)	AI-1137 <sup>(25)</sup> (pressure)
Compressive Strength, psi	84,000 - 88,000	25,500	---	---
Compressive Modulus, psi	$4.12 \times 10^6$	---	---	---
Flexural Strength, psi	132,000	27,000	65,000 - 75,000	70,000 - 75,000
Flexural Modulus, psi	$4.3 \times 10^6$	$1.5 \times 10^6$	$3.2-3.5 \times 10^6$	$3.2-3.5 \times 10^6$
Elastic Modulus, psi	---	---	$3.45 \times 10^6$	$3.50 \times 10^6$
Tensile Strength, psi	---	20,000	56,000	56,000
Interlaminar Shear, psi	15,100	---	---	---
Elongation, percent	---	2.0	1.74	1.84
Maximum Recommended Usage Temperature	170°C	175°C	260°C	315°C

## 1. Preliminary Fiber Coating Experiments

So that specific problem areas might be delineated, some preliminary fiber coating experiments were performed with both resin systems. These tests, performed with "Thornel" 25 yarn, involved the dipping of 5-inch long strands of yarn in the resin solution and determining the weight of resin pickup.

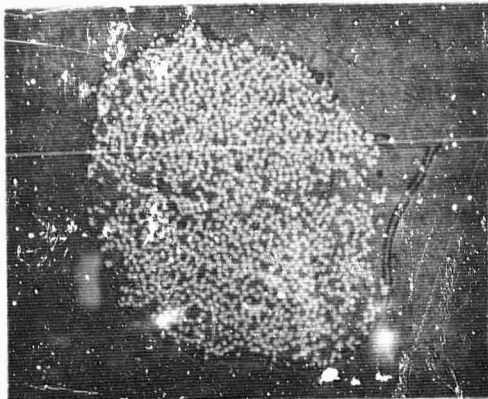
Polysulfone - P-1700. Two solvents, chloroform ( $\text{CHCl}_3$ ) and methylene chloride ( $\text{CH}_2\text{Cl}_2$ ), were used for the coating experiments with the P-1700. Solutions containing approximately 20 percent resin by weight in both  $\text{CHCl}_3$  and  $\text{CH}_2\text{Cl}_2$  could be obtained at room temperature. The resin had to be added slowly while stirring to prevent extensive gelling. The "Thornel" fiber strands were dipped into these solutions, and the volatile solvents were allowed to evaporate at room temperature. Very high resin pickups, in excess of 200 percent, were obtained from both solutions. The  $\text{CHCl}_3$  solutions wet the fibers better than the  $\text{CH}_2\text{Cl}_2$  solutions, resulting in consistently higher resin pickups. The coated fibers were hard and stiff.

Several dilution experiments were performed with the P-1700 solutions in  $\text{CHCl}_3$  and  $\text{CH}_2\text{Cl}_2$ . The resin pickups were approximately linearly related to resin concentration so that predetermined amounts of resin could be coated on the fiber by diluting the starting solution. Consistently high resin contents were obtained with  $\text{CHCl}_3$  solutions. Initial wet-winding experiments performed with the P-1700 -  $\text{CHCl}_3$  solutions (hand-winding of "Thornel" fiber through a resin bath) showed that the relatively rapid winding procedure resulted in lower resin pickup than dipping of individual yarns.

Polyamide-imides. The AI-1030 and AI-1137 varnishes were used in the as received condition. These varnishes contain approximately 30 percent by weight of the solid amide-imide polymer dissolved in N-methylpyrrolidone. The individual "Thornel" fiber strands were immersed in the resin solution for one minute and then dried in an oven at  $150^\circ\text{C}$  for 30 minutes. The resin pickups were determined to be between 33 and 50 percent of the original fiber weight. Several of the coated fibers were cured in an oven by one of the cure schedules recommended by the manufacturer, i. e., two hours each at  $220^\circ\text{C}$ ,  $230^\circ\text{C}$ ,  $260^\circ\text{C}$ ,  $285^\circ\text{C}$ , and  $315^\circ\text{C}$ . The impregnated fibers underwent small additional weight losses during the curing cycle. The cured strands were strong and stiff, although microscopic examination showed the expected presence of voids. Figure 17 presents some cross-sectional photographs of single "Thornel" fiber strands dip-coated in epoxy, P-1700, and the AI-1030 resin. The coating of the individual filaments by the P-1700 resins appears fairly good. However, some void regions are apparent. The AI-1030 varnish appears to have poorer wetting characteristics than the P-1700, as evidenced by filament clumping.

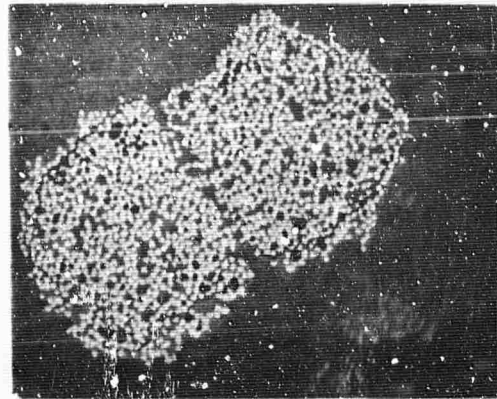
## 2. Preparation of Preliminary Torsion Shear Samples with "Thornel" 25 Yarn

Shear strength is perhaps the best measure of fiber-resin interaction. The torsion shear test was therefore selected for initial property evaluation of the composite systems. This test, described previously (29), requires a molded uniform composite rod five-inches in length, between 0.11 and 0.14 inches in diameter, and containing from 40 to 50 volume percent resin.



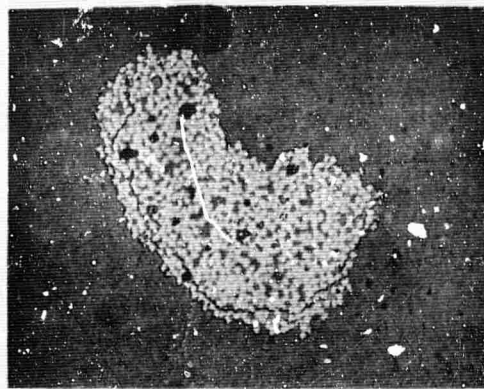
(a) Epoxy 4617

N-22497



(b) Polysulfone

N-22498



(c) AI-1030

N-22499

Figure 17. Cross-Section of Single Strands of "Thornel" Yarn Coated with Epoxy, Polysulfone, and Amide-Imide Resins. (250X)

A hand-winding apparatus was constructed for composite fabrication. The equipment consists of a spool of "Thornel" yarn mounted on a revolving drum, a take-up spool rotated by a hand crank, and a small metal reservoir (approximately 5-inch long, 1-inch wide, and 2-inch deep) for holding the resin solutions. The rectangular take-up spool was made of Teflon, and its dimensions (7-inch long by 1-1/4-inch wide by 1/4-inch thick) were chosen so that enough yarn for two 5-inch test specimens could be obtained in a single operation. "Thornel" 25 yarn was used for the initial experiments designed to solve the problems of preparing adequate torsion-shear rods. The actual resin evaluation was carried out with the "Thornel" 50 fibers.



The measured yarn cross-sectional area of "Thornel" 25 was used to determine that 118 strands of yarn were required to mold a shear rod of proper diameter. After the required number of strands were wound, the coated yarn was cut from the take-up spool, thus providing two strips six-inches long and one-inch wide. These coated strips were inserted into stainless steel molds and cured. Care was taken in all handling procedures to minimize fiber misalignment.

Polysulfone - P-1700. The P-1700, as a thermoplastic resin, requires only relatively simple processing techniques. No cure cycle is needed, and the only variable is the molding temperature. Fiber winding was performed with solutions of P-1700 in  $\text{CHCl}_3$ . Resin concentrations of between 13 and 20 weight percent were used. The more concentrated solutions turned cloudy during storage and were, therefore, employed promptly after preparation. After some experimentation, a molding temperature of  $270^\circ\text{C}$  (approximately  $100^\circ\text{C}$  above the resin glass transition temperature) was employed. The final resin contents were estimated by weighing the molded rods. This determination was only approximate because it also included some excess resin which adhered to the outside of the bar and was difficult to remove.

In the usual procedure, the fibers were wound through the resin solution and onto the Teflon mandrel until 118 turns were on the mandrel. The fiber strips were then cut from the mandrel and inserted in the molds after they had partially dried, but before they had completely stiffened. The molds were placed in a preheated ( $270^\circ\text{C}$ ) furnace and held for 45 minutes. They were then removed and pressed immediately. Machining of the samples to a uniform diameter was difficult due to the hardness of the resin, but wet-grinding procedures allowed the rods to be machined without damage.

After some experiments were carried out so that we might gain experience, a series of seven successful test samples was prepared. The properties and the shear strengths determined for these samples are summarized in Table VII.

TABLE VII  
TORSION SHEAR TEST RESULTS FOR  
"THORNEL" 25 P-1700 COMPOSITES

Sample	Resin Concn. of Coating Soln. wt. %	Resin Content in Molded Rod* wt. %	Shear Strength, psi**	Comments
18C	14.0	39.3	2830	Many voids
20C	16.0	41.9	3310	Voids
14C	16.0	38.5	4350	---
21C	16.0	42.2	4820	No voids
22C	20.0	40.2	3370	Voids
17C	20.0	51.0	4130	Voids
16C	20.0	42.6	4860	No voids, uneven distribu- tion

\*Determined from the final weight of the molded bar.

\*\*Measured from the flat portions of the curve.

Some comments should be made concerning the torsion shear tests. A typical test curve, obtained on Sample 16C is shown in Figure 18.

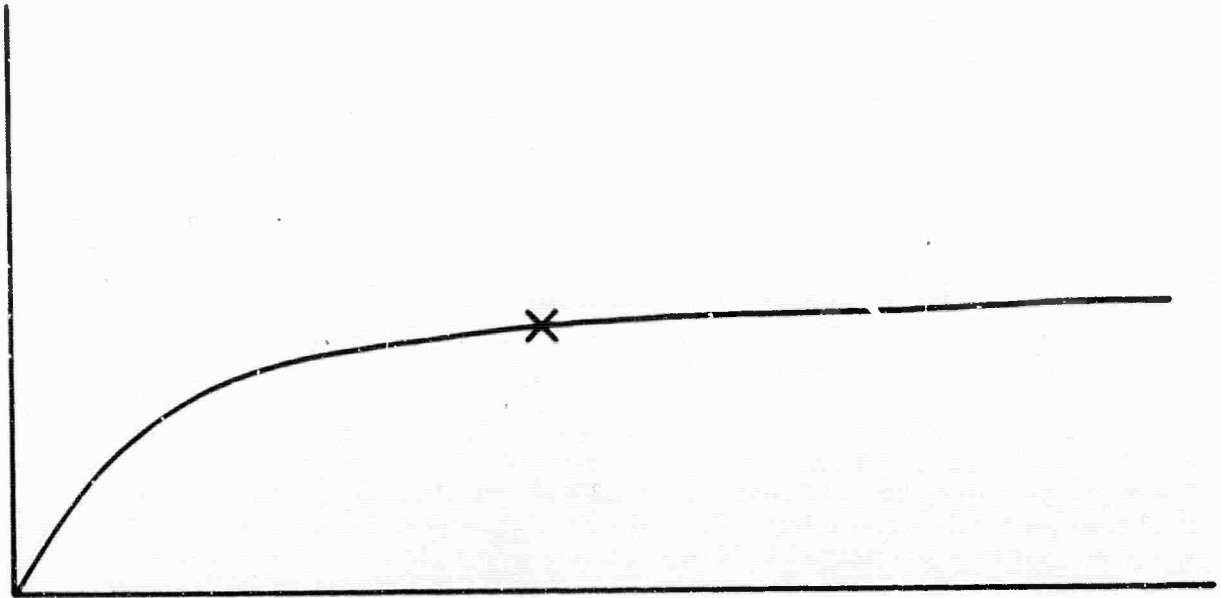
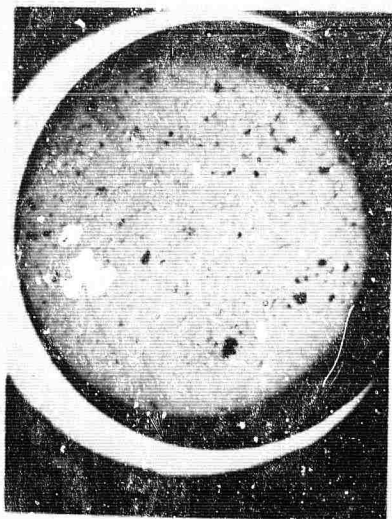


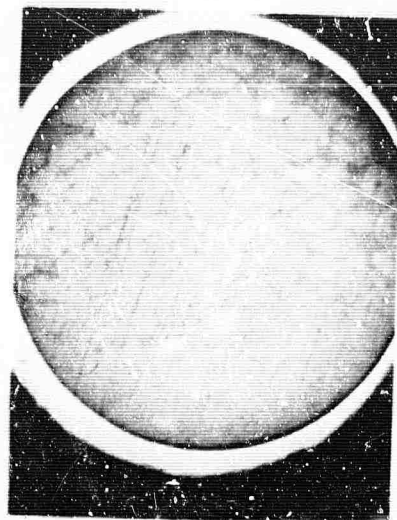
Figure 18. Torque versus Angular Displacement Curve for  
"Thornel" 25 - P-1700 Composite.  
(Shear Strength from Indicated Point = 4860 psi) N-22450

There is no apparent break in the curve to indicate failure; instead, the curve gradually levels off with a slightly increasing slope. The tabulated shear value was taken from a point indicated on the curve. This behavior is different from that of epoxy composites, which show an abrupt break in the curve at the point of failure. (29) The shear strength curves of the polysulfone composites are believed to result from the high elongation of the resin, reflecting a gradual yielding of the resin rather than a drastic failure.

The data in Table VII demonstrate some important effects concerning composite structure and shear strength. The most important factor in reducing shear strength is the presence of voids in the composite. For resin solutions more dilute than 16 weight percent resin, the presence of voids in the composites led to correspondingly low shear strengths. Successful composites were prepared from solutions of 16 to 20 percent resin. The highest shear values were obtained from Samples 16C and 21C, which were essentially free of voids. Figure 19 presents some photomicrographs of the cross-sections of torsion rods 21C and 22C. The poor shear strength of the Sample 22C is a direct result of the voids which are seen as the dark areas in the photograph.



P-21C Shear Strength = 4820 psi  
N-22496



P-22C Shear Strength = 3370 psi  
N-22495

Figure 19. Cross-Section Photomicrographs of  
"Thornel" 25 P-1700 Composites.

Polyamide-imides. The AI-1030 and the AI-1137 varnishes were used in the initial yarn winding experiments for the preparation of a torsion shear rod. The handling of these resins is complicated and requires a B-staging step to remove the high boiling solvent, a high temperature molding step, and an elaborate post-cure. Several variations of the recommended Amoco processing procedures were tried. These included B-staging at temperatures between 150° - 175°C, molding at 210°C and 300°C, and running two post-curing cycles of 10 and 16 hour duration, respectively. So that fiber misalignment would be minimized, all of these operations were performed with the sample in the mold. Final resin contents were estimated by weighing the cured torsion bars and subtracting the fiber weight.

A number of composite samples were prepared, but none was suitable for testing because of low resin contents. The resin contents obtained with these specimens ranged from 20 to 30 weight percent, far too low for a suitable torsion shear rod. Weight loss measurements on a sample cured by one of the standard schedules, but eliminating the molding step showed that the problem was not due to weight loss during curing but resulted from poor wetting of the "Thornel" fibers by the viscous varnish solution. Attempts were made to increase the resin content by prolonged soaking of the wound fibers and addition of solid polymer in the mold. These attempts also proved unsuccessful, and it was concluded that the wetting characteristics of the AI varnishes were too poor for wet winding of graphite yarn.

The wetting problem was solved by using a different solvent system with the solid AI polymers. A mixed dimethylacetamide (DMAC)-acetone solvent will dissolve 30 percent by weight of solid AI polymer to give low viscosity resin solutions. This solvent has the additional advantage of being considerably more volatile than the N-methylpyrrolidone in the commercial varnish.

A resin solution was prepared by dissolving 26 grams of AI polymer in a solvent comprising 35 cc of DMAC and 35 cc of acetone. After it was wound, the coated strip was B-staged at 170°C for one hour, molded at 300°C, and post-cured for ten hours at temperatures ranging from 200°C to 315°C. The resulting composite contained 32 weight percent resin, still too little for meaningful evaluation. The resin content was increased by repeatedly dipping the wound strips in the resin solution before processing. Due to the higher volatility of the solvent, the DMAC-acetone system is much more amenable to this procedure than the NMP varnishes. The resulting rod contained approximately 38 percent by weight of resin. In spite of its very poor structure, this rod had a shear strength of 2000 psi.

After further experimentation, a solution containing 33 percent by weight of resin proved to be the most convenient to handle. More concentrated solutions were too viscous for effective solution winding, and more dilute solutions did not provide sufficient resin pickups.

The redipping process was improved by allowing a ten minute drying period between dippings. In this manner, the resin content was raised to 40 percent in the final rod, and the torsional shear strength increased to 2900 psi. In a further change of the processing procedure, the B-staging operation was performed under vacuum; the resulting sample contained approximately 43 percent resin and had a shear strength of 3880 psi. A cross-section photograph of one of the torsion bars is shown in Figure 20. The use of the DMAC-acetone solvent system substantially improved the fiber wetting problem, but the composites still contained numerous voids.

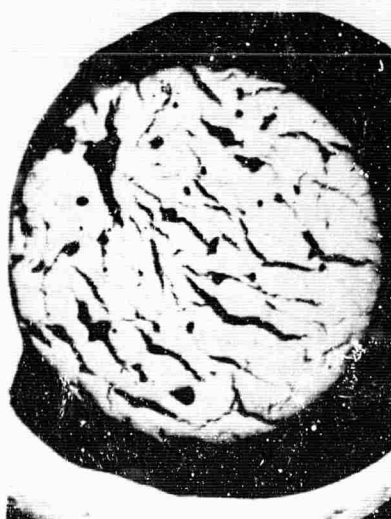


Figure 20. Cross-Section Photomicrograph of Low Shear Strength Polyamide-Imide-"Thornel" 25 Composite Showing Voids. (25X) N-22494

Molding of the B-staged samples proved to be difficult. A Differential Thermal Analysis (DTA) curve for the AI-11 polymer showed no definitive evidence of polymer melting, but a shallow endothermic region between 250° - 320°C gave some evidence of plasticity.

Torsion rod specimens prepared from "Thornel" 25 and the AI-11 polymer were molded after they had been heat-treated at temperatures between 250° - 325°C. The molding temperature was very critical and depended on the resin content. A heat-treatment temperature of 300°C was chosen as the most effective temperature prior to molding the composite rods. Below that temperature, the sample was not plastic enough, while at higher temperatures thermal setting of the resin also prevented molding. After molding, the samples were cured for a 10-hour period at temperatures between 200° and 315°C.

As a result of these trials, ten test specimens were prepared and tested. The shear strength value for these samples ranged from approximately 2300 to 4600 psi, depending on the void content. The higher shear strength composite appeared, under microscopic examination, to be nearly void free. Some molded composite rods which had not been post-cured were also prepared and tested. These rods gave shear strengths ranging from 4200 to 5600 psi. The apparent reduction in shear strength after curing results from void creation during the curing cycle.

3. Evaluation of Torsion Shear Samples with "Thornel" 50 and "Thornel" 50S Yarn

Polysulfone (P-1700) Composites. The evaluation of the P-1700 resin was continued by using composites made with "Thornel" 50 and "Thornel" 50S yarns. The fiber coatings were performed in all cases from a resin solution containing 20 percent by weight of polysulfone in  $\text{CHCl}_3$ . Due to the lower cross-sectional areas of the "Thornel" 50 and 50S fibers (as compared with "Thornel" 25), a larger number of fiber strands were used in the composite sample. The procedure involved the use of 128 lengths of fiber for the "Thornel" 50 sample and 140 lengths for the "Thornel" 50S sample.

P-1700 - "Thornel" 50 Composites. The "Thornel" 50 yarn had an evaluated shear strength of 4900 psi in an epoxy composite. A series of six test samples was prepared from this yarn and the P-1700 resin. The shear strengths and the estimated resin contents are given in Table VIII.

The samples with the lower resin contents contained voids and had low shear strengths. Samples containing approximately 50 percent by weight of resin had no voids and had an average shear strength on the order of 4900 psi (average of last three values in Table VIII).

A molded specimen of the P-1700 resin (without fiber reinforcement) when subjected to the same torsion test gave a shear strength value of 8250 psi, whereas the epoxy resins are known to exhibit shear strengths on the order of 16,000 psi. The shear strength value of 4900 psi, measured for composites prepared from this "Thornel" 50 yarn with either resin, is well below the shear strength value of the epoxy or the polysulfone and is independent of the particular resin employed. This result implies that the "failure" in shear does not occur in the resin but occurs either at the fiber-resin interface or by delamination within the fiber.

TABLE VIII  
SHEAR STRENGTH VALUES FOR P-1700-  
"THORNEL" 50 COMPOSITES

Resin Content (wt. %)	Shear Strength* (psi)
41.0	3680
46.6	3980
45.5	4160
52.1	4800
52.6	4880
49.8	5100

\*Each value is the average result  
of two test specimens.

P-1700 - "Thornel" 50S Composites. The improvement in shear strength obtained for surface treated "Thornel" 50S graphite yarn in epoxy composites is well established, and it was important to determine whether this effect is also present in polysulfone composite. Two different samples of "Thornel" 50S were selected for testing. The torsion shear strength data obtained for these yarns with epoxy resin ERLA-4617, and with the P-1700 resin are shown in Table IX.

TABLE IX  
SHEAR STRENGTH VALUES FOR "THORNEL" 50S  
COMPOSITES WITH ERLA-4617 AND P-1700

"Thornel" Fiber	Shear Strength with P-1700 (psi)	Shear Strength with ERLA-4617 (psi)
50S-1	6500*	6500
50S-2	8300**	8100

\*Average of 8 test results

\*\*Average of 4 test results

The results in Table IX show identical shear strength behavior for composites prepared from the two different resin systems and "Thorne!" 50S in spite of the large difference in shear strength of the individual polymers. Improved shear strengths were obtained for the surface treated fibers with both resins. The shear strengths obtained for the epoxy composites are indicative of a failure at the resin-fiber bond. For the polysulfone composite, the shear strength of 8300 psi equals that obtained for the polymer itself and could indicate a failure in the resin.

The shear stress curves obtained for "Thorne!" 50S composites with the epoxy and the polysulfone are of particular interest. These curves are reproduced in Figure 21 for composites having a measured shear strength value of 8200 psi. A comparison of the torque versus angular displacement curves shows that the epoxy composite increases in torque at a higher rate, reaches a maximum corresponding to a shear strength value of 8200 psi, and then undergoes drastic failure. The curve for the polysulfone composite rises at a lower rate, reaches the same maximum value, and then gradually levels off without indication of failure. This latter effect was anticipated for composites prepared with the high-toughness polysulfone resin.

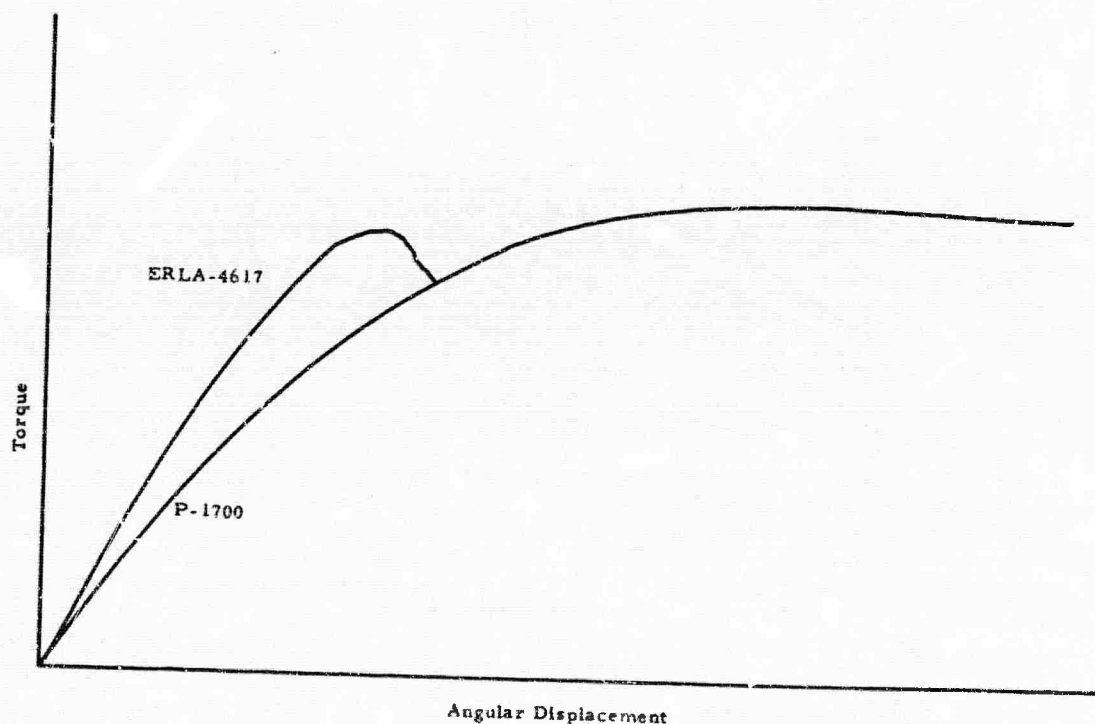


Figure 21. Torque versus Angular Displacement Curves for Composites of "Thorne!" 50S with ERLA-4617 and P-1700 Resins (Measured Shear Strength - 8200 psi)

N-22862



P-1700 - Experimental "Thornel" 50S Composites. So that the ultimate shear strength limit of polysulfone-graphite fiber composites might be determined, a few torsion shear specimens were prepared containing experimental high shear strength "Thornel" 50S fibers. Two samples of yarn, having respective shear strengths of 10,500 psi and 13,900 psi in epoxy composites, were selected. With either yarn, a shear strength value of 9200 psi was achieved in a polysulfone composite. This value of 9200 psi must, therefore, be assumed as the shear strength limit of P-1700 graphite-fiber composites.

One of these torsion rod specimens was repetitively tested to demonstrate the effects of elongation of the resin on the shear-stress behavior. The results of six repetitive tests on a "Thornel" 50S - P-1700 composite sample are shown in Figure 22. The initial test (I) gave a shear-stress curve which leveled off at a maximum torque corresponding to a shear strength value of 9230 psi. The sample was then retested to give the second curve (II) which showed a decreasing slope and gave an ultimate shear strength of 8920 psi. After six tests, the torque versus angular displacement curve is almost linear and still rises to a value of 7080 psi.

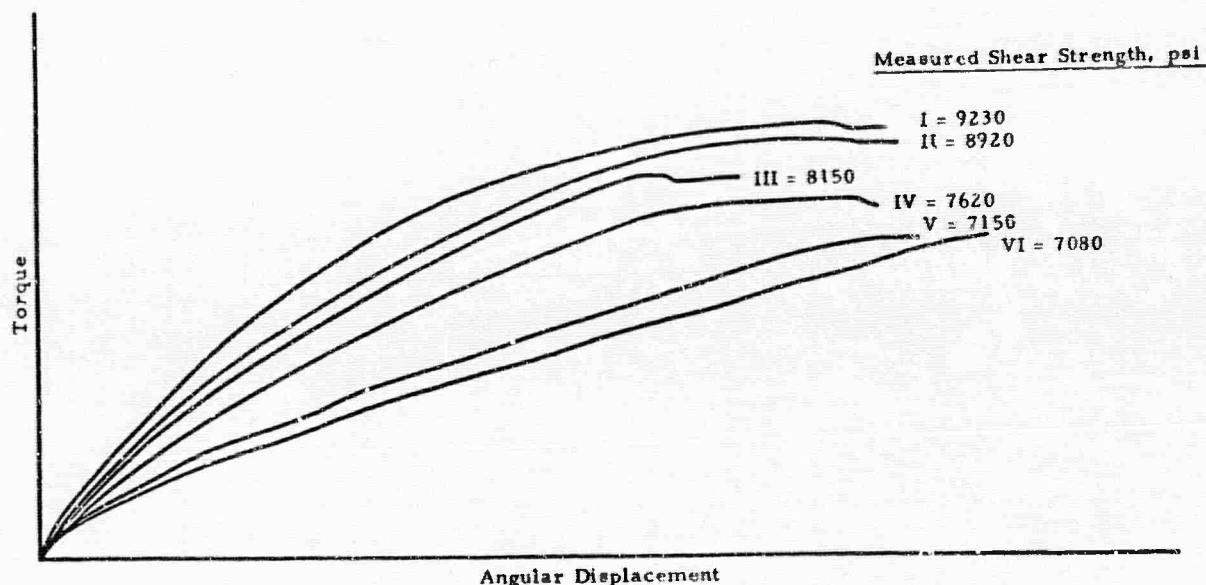
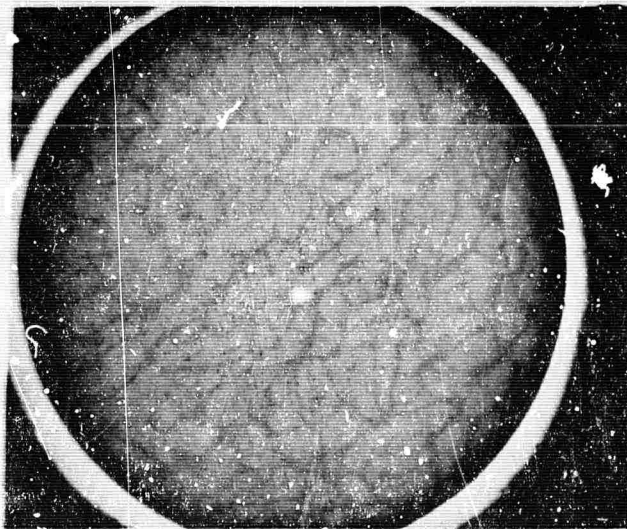


Figure 22. Torque versus Angular Displacement Curves Obtained for a Repetitively Tested "Thornel" 50S- P-1700 Composite.

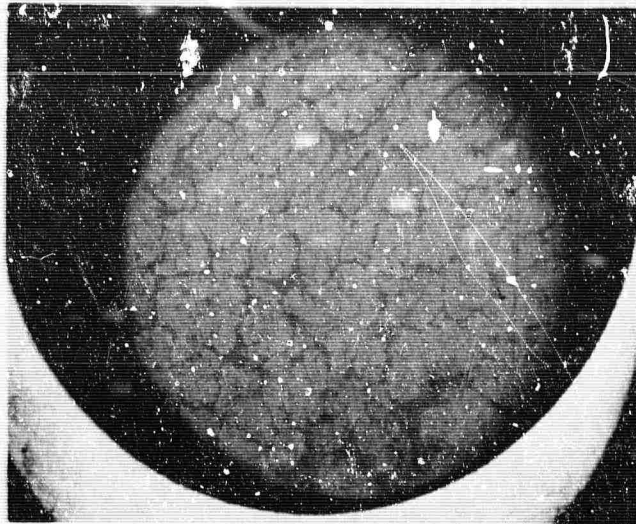
N-22643

Microstructure of Polysulfone - "Thornel" Composites. Some photomicrographs were taken for the P-1700 - "Thornel" 50 and P-1700 - "Thornel" 50S composite rods in order to examine apparent structural differences. Figure 23 presents cross-sectional photographs of the torsion rods prepared for each composite. In the "Thornel" 50S - P-1700 sample, almost every individual strand of yarn is visible and appears to be surrounded by resin.



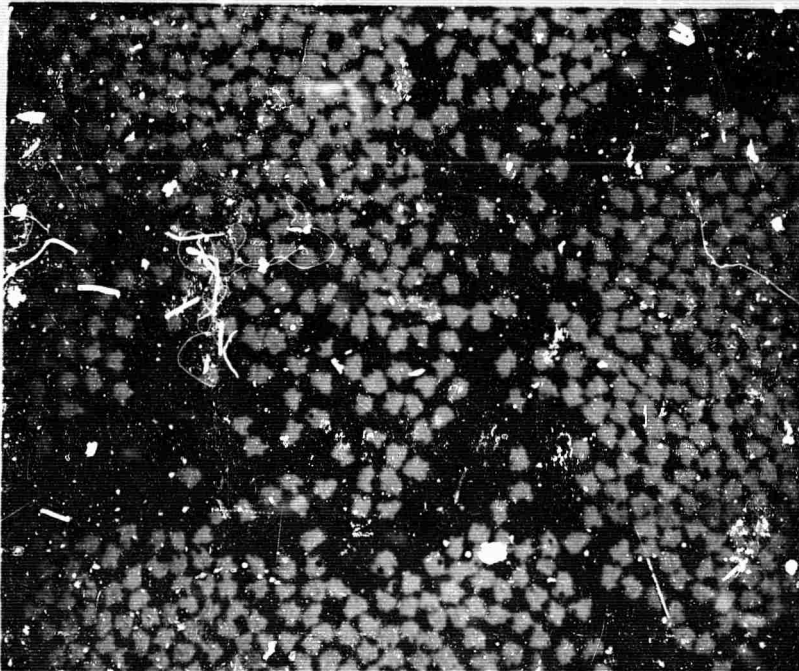


(a) "Thornel" 50S - P-1700  
N-22939  
P-27-C-A



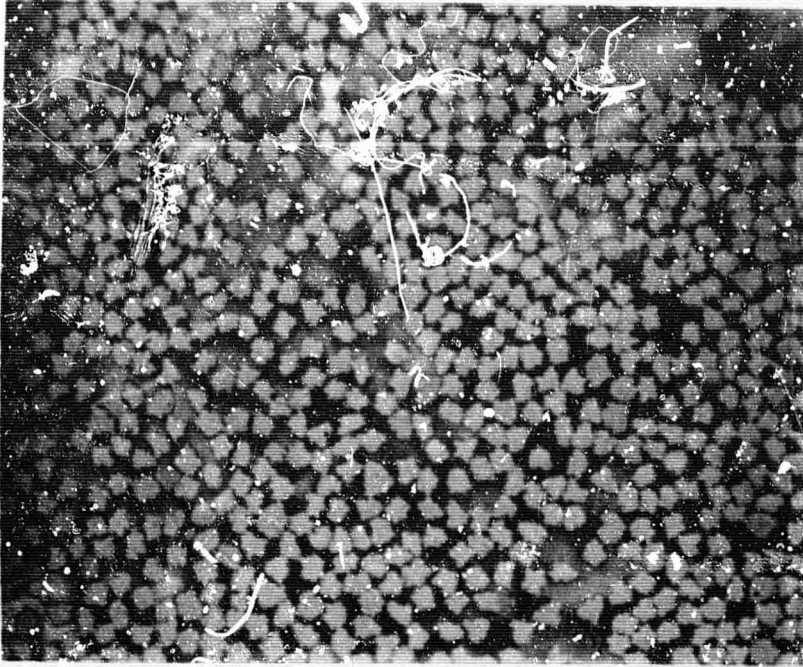
(b) "Thornel" 50 - P-1700  
N-22940  
P-26-A

Figure 23. Cross-Section Photograph of "Thornel"-P-1700 Composite Rods.  
(Magnification 25X)



(a) "Thornel" 50-P-1700

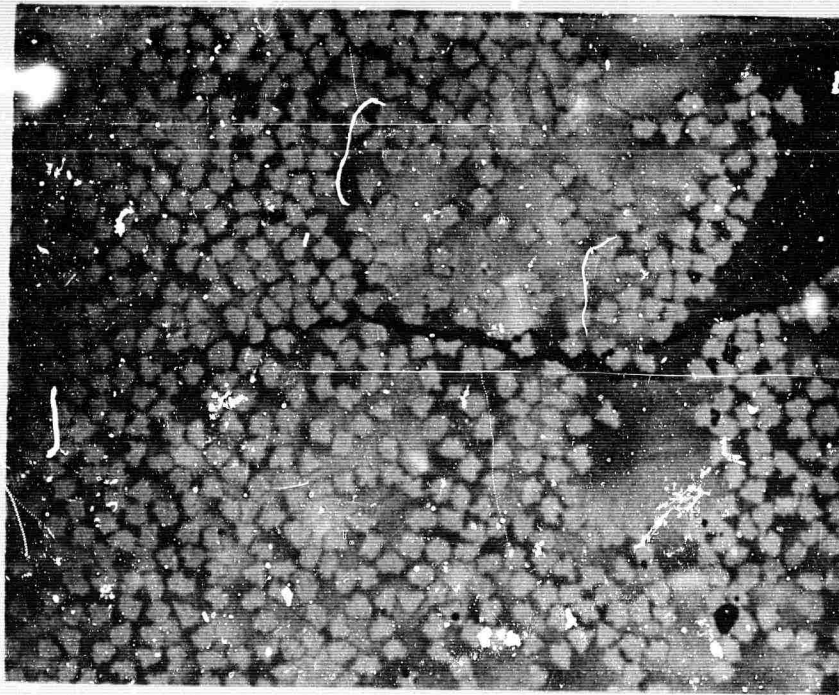
N-22928  
751-2-02



(b) "Thornel" 50S-P-1700

N-22929  
751-1-03

Figure 24. Photomicrographs of "Thornel"-P-1700 Composites.  
(Magnification 500X)



(a) Magnification 500X

N-22926  
751-1-02



(b) Magnification 25X

N-22927  
751-2-01

Figure 25. Photomicrographs of a Shear Tested "Thornel" 50S-P-1700 Composite Showing Cracks.



On the other hand, the "Thornel" 50 - P-1700 rod shows a much poorer distribution of fiber and resin, with many of the yarn strands clumping together. This effect is even more apparent in Figure 24, which shows photographs taken under high magnification of the same specimens. These pictures show the individual graphite fiber filaments embedded in the resin matrix. Again, the more homogeneous distribution of fiber and resin in the "Thornel" 50S composite as compared with the "Thornel" 50 composite is evident.

A careful examination of one of the P-1700 - "Thornel" 50S specimens after shear testing showed the presence of microcracks. These cracks are shown in Figure 25 under two magnifications for a composite sample which had a shear strength value of 8800 psi. The cracks radiate from the outside of the torsion rod, a condition which is typical of failed graphite fiber composites.

Polyamide-Imide Resins. The Amoco AI-11 polyamide-imide resin was also evaluated in composites with "Thornel" 50 and "Thornel" 50S yarn. Low void-content composites, suitable for shear strength measurement, were prepared from both yarns.

The following experimental steps were selected as the preferred procedure for preparing the composites:

- (1) The "Thornel" yarn was hand-drawn through a resin bath prepared by dissolving 35 grams of solid AI-11 polymer in a solvent mixture consisting of 35 ml of acetone and 35 ml of dimethylacetamide (DMAC). One hundred and twenty-eight fiber wraps were used for the "Thornel" 50 samples and 140 fiber wraps were used for the "Thornel" 50S samples.
- (2) The coated rectangular strips were dried in air under infrared heat and then redipped in the resin solution. This procedure was repeated three times to obtain sufficient resin pickup.
- (3) The coated strips were inserted in the molds, and the molds were placed in a vacuum furnace which was held for 45 minutes at 110°C to remove the solvent.
- (4) The molds were placed in a furnace which had been pre-set to 340°C. Thermocouples were inserted into the mold body, and the mold temperature was carefully monitored. When the thermocouple temperature reached 300°C, the mold was removed from the furnace and pressed immediately. Temperature control at pressing was extremely important. At higher sample temperatures, the resin set up and could not be properly pressed. At lower temperatures, the composite showed insufficient plasticity.
- (5) The composites were post-cured at a standard 10-hour schedule of two hours each at 200°C, 230°C, 268°C, 290°C, and 315°C.

"Thornel" 50 Composites. Evaluation was performed with "Thornel" 50 yarn having a shear strength of 4900 psi in an epoxy matrix. A variety of samples was prepared from this "Thornel" 50 and the AI-11 resin. The initial specimens

had high void contents, gave shear strength values between 2000 and 4000 psi, and the shear strength appeared directly related to the number of voids in the composite.

After considerable experimentation, which led to the selection of the processing conditions described above, some low void, completely cured "Thornel" 50-AI-11 composites were prepared. These samples gave average shear strengths identical to those measured for this same yarn in either epoxy or polysulfone resin composites.

A cross-section photomicrograph of one of the torsion rod specimens is shown in Figure 26. The void content of this particular sample is approximately 1 to 2 percent. The voids which are generally found on the outside of the rod are believed to result from the evolution of volatiles during curing. Figure 27 shows an enlarged photomicrograph (500X) of the central region. A good distribution of the individual fiber strands within the polymer matrix is apparent.

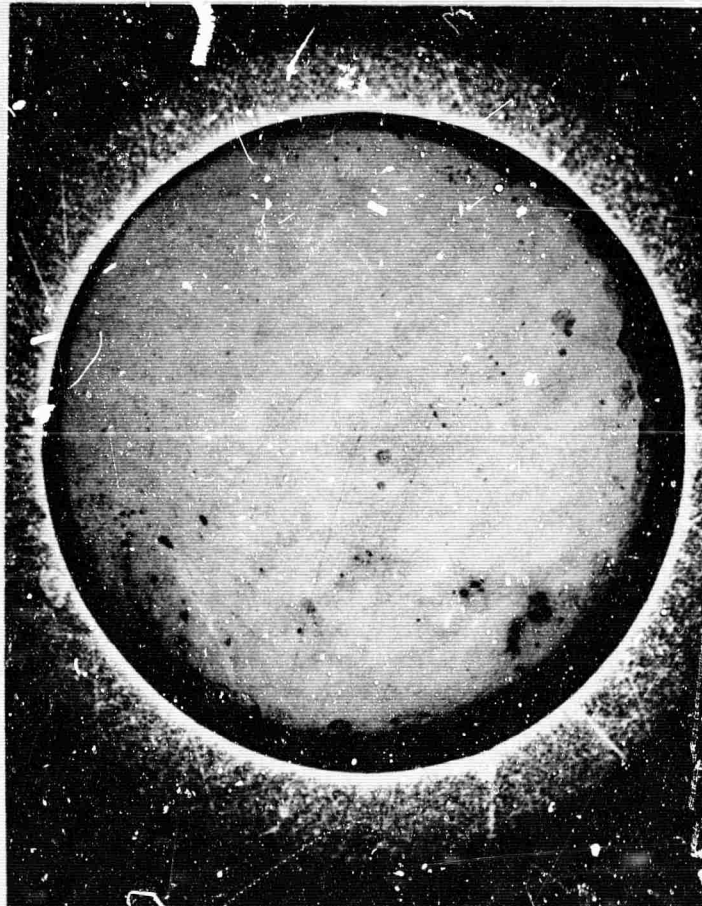


Figure 26. "Thornel" 50-AI-11 Cured Composite. (25X)

N-23418  
916-3-01

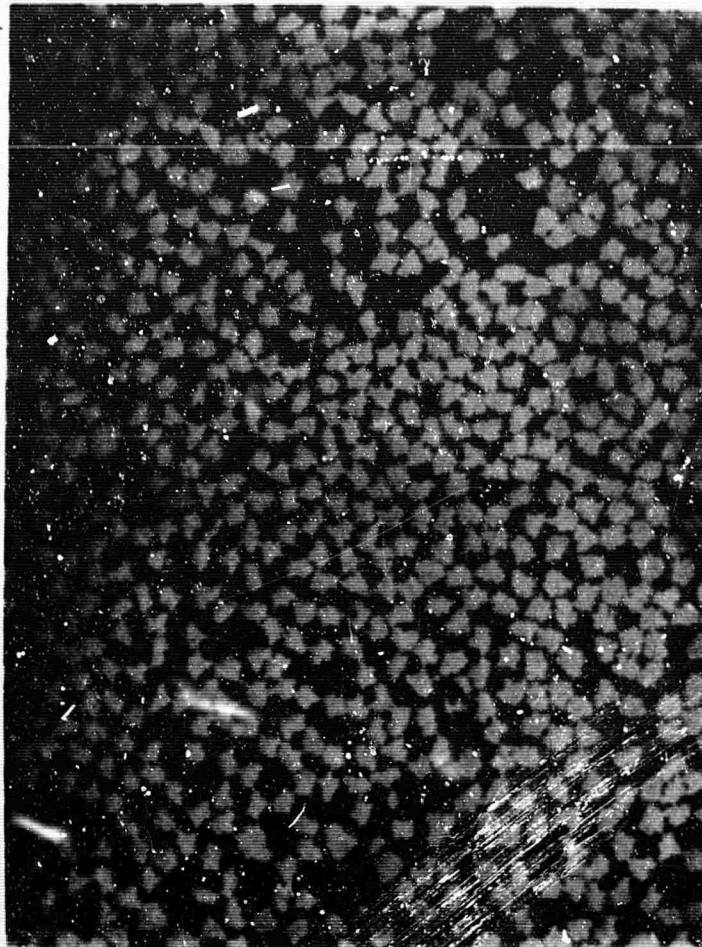


Figure 27. "Thornel" 50-AI-11 Cured Composite. (500X)

N-23419  
944-1-01

Shear strength values of approximately 5000 psi were also obtained on several "Thornel" 50-AI-11 composites which had not been post-cured and were essentially void-free. These results again demonstrate that, for untreated "Thornel," the composite shear strength is limited by the fiber surface and is independent of the resin matrix.

"Thornel" 50S Composites. This phase of the program involved the preparation of AI-II composites in which surface treated "Thornel" 50S was used. A "Thornel" 50S yarn which had a shear strength of 10,400 psi in an epoxy resin composite was selected for this purpose.

First, some torsion rods were prepared from the "Thornel" 50S and the AI-11 without post-curing. A cross-section photomicrograph of such a composite after testing is shown in Figure 28. A few voids are still apparent (less than 1 percent), which probably resulted from some volatilization during molding. The shear strength determined for this torsion rod was 9100 psi.



Figure 28. "Thornel" 50S-AI-11 Composite - Uncured. (25X)

N-23420  
916-4-01

This value is slightly below the epoxy value, perhaps due to the few voids present, but is considerably higher than any shear strength measured for the AI-11-"Thornel" 50 composites. Thus, the shear strength improvement for surface treated graphite fibers is realized in the polyamide-imide as well as in the epoxy composite.

All of the AI-11-"Thornel" 50S composites developed voids after curing, a condition which led to a reduction in shear strength. Figure 29 shows a photomicrograph of one of the best samples obtained. This torsion rod, which contains approximately 5 percent voids (congregated on the outside) had a shear strength of 6500 psi; Figure 29 shows the rod after shear testing, revealing the typical radial crack development.



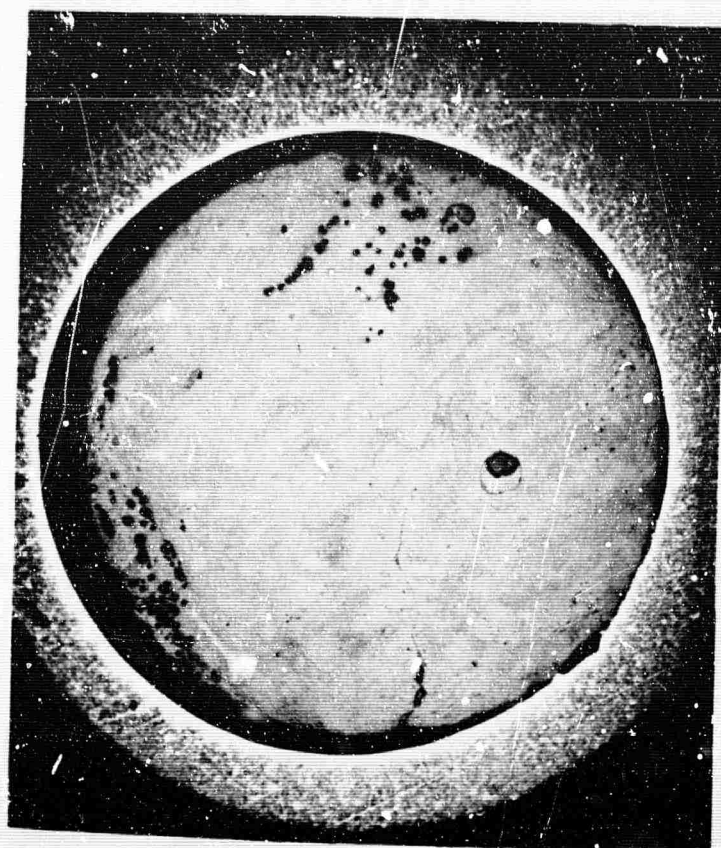


Figure 29. "Thornel" 50S-AI-11 Composite - Cured (25X).

N-23421  
916-1-01

Thermal Behavior. The voids in the cured AI-11 - "Thornel" composites have been attributed to volatile evolution during curing of the resin. Shown in Figure 30 are thermogravimetric analysis (TGA) curves for the AI-11 polymer which illustrate the weight loss behavior in both air and argon.

The TGA curve in air shows that the AI-11 undergoes a 12 percent weight loss at 315°C, which corresponds with the maximum temperature for curing. The polymer shows stability in air at the fast heating rate of 10°C per minute up to 425°C, at which point the weight loss continues. The AI-11 - "Thornel" composite rods which were cured outside of the mold underwent similar weight losses during curing. Curing of the composites in the molds presumably retains a portion of the volatiles and reduces the total amount of voids.



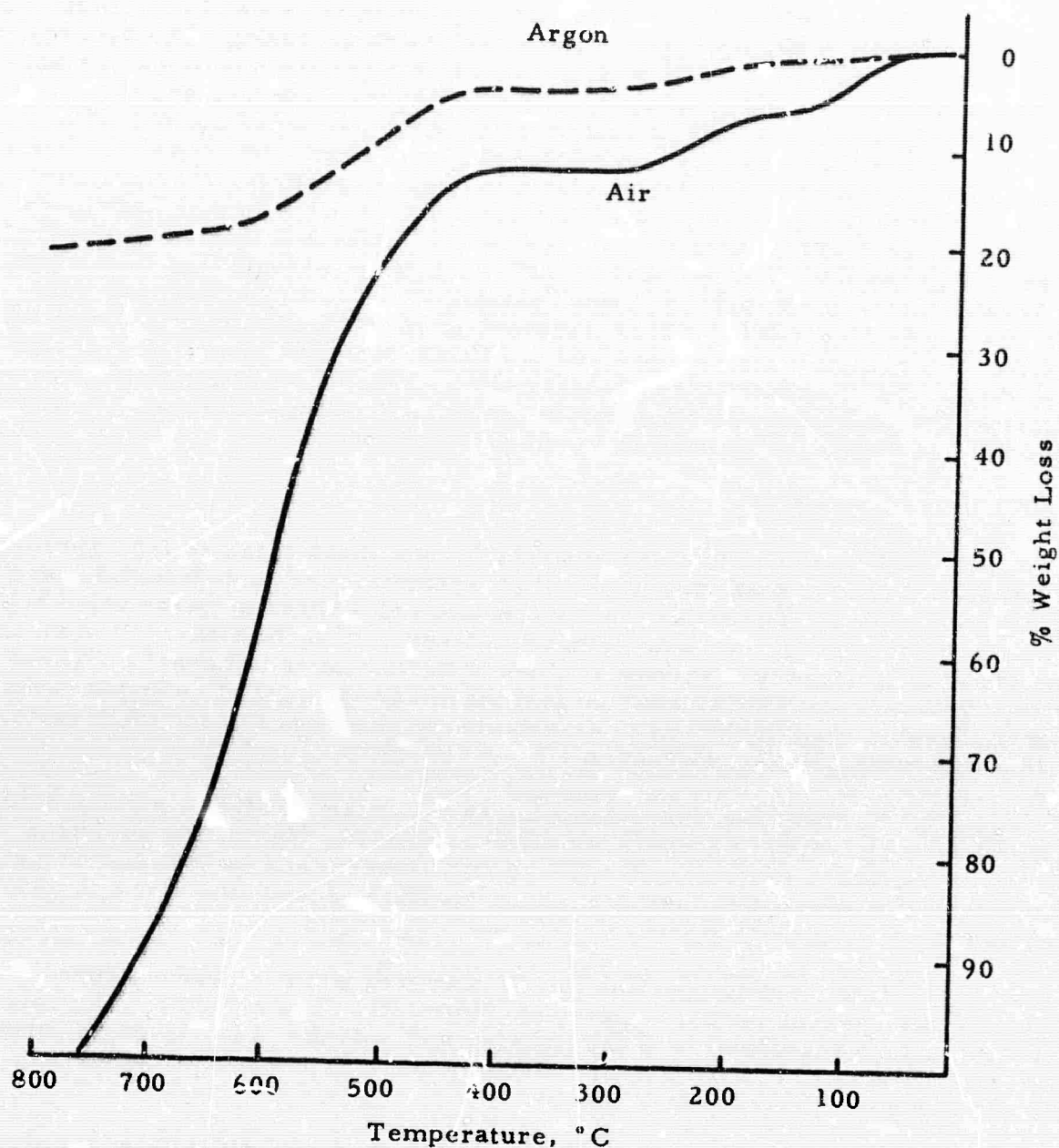


Figure 30. Thermogravimetric Analysis Curves for AI-11 Polymer in Argon and Air.

#### 4. Fabrication of "Thornel" 50S - Polysulfone Plates

The results for the P-1700 composite shear rods were sufficiently encouraging to justify an expansion of the efforts to make flat (0°, 90°) cross-ply laminate plates for further characterization. The preparation of the prepreg required some modification of the wet-winding procedures used for fabrication of shear rods.

The prepreg was made by drum winding six ends of "Thornel" 50S yarn at a time to make broadgoods (tape could also be made). The bath consisted of a solution of 17 to 19 weight percent of P-1700 polysulfone in a solvent containing 80 percent dioxane, 10 percent chlorobenzene, and 10 percent tetrahydrofuran. This solvent system was selected because of the health hazards of working with large quantities of chloroform. The drum was heated with infrared lamps to achieve partial drying of the prepreg. The prepreg was removed from the drum while still flexible and laid out to dry as flat sheets. So that better resin penetration into the yarn could be achieved, the prepreg was pre-pressed to an 8 mil stop at 200° - 215° C and 150 psi for 10 minutes. For fabrication of 12-inch by 12-inch plates, seven layers of prepreg were laid up in the required (0°, 90°) balanced configuration and molded to a 56 mil stop (8 mil per ply) at a temperature of 240° C, with a 10 minute hold at temperature. Teflon-coated glass release cloth was used to facilitate mold release. The physical evaluation (notch sensitivity testings) of these "Thornel" 50S polysulfone plates is reported in Volume II of this report.

## 5. Conclusions

Nearly identical shear strengths have been obtained for "Thornel" 50 fiber with three different polymer matrix systems: epoxies, polysulfone, and polyamide-imide. The failure in shear occurs at a shear strength value below the shear strength of the resin component itself. In each instance, the mechanism of failure appears to involve the propagation of radial cracks. These observations lead to the conclusion that the shear strength of composites made with untreated graphite fibers is determined by the nature of the fiber surface alone and independent of the resin.

All three polymers show improved shear strengths in composites when surface treated "Thornel" 50S fibers are used. Again, for void-free composites, the shear strength appears to be determined by the fiber alone until the point where the fiber resin bond strength exceeds the strength of the resin itself.

Low-void composites can be prepared from completely cured AI-11 resin, but the preparation is experimentally quite difficult. The void content of these composites is the limiting factor in the shear strength, and this characteristic seems to be more important with composites prepared from the higher shear strength fibers.

The polysulfone composites show a gradual yielding at maximum test load rather than the sudden failure encountered in the epoxy resin composites.

## SECTION V

### RESEARCH ON GRAPHITE-FIBER, METAL-MATRIX COMPOSITES

R. V. Sara, Union Carbide

#### A. Fabrication Studies

##### 1. Electrodeposition of Nickel on Graphite Yarn

The apparatus employed for the continuous electrodeposition of nickel on "Thornel" graphite yarn has been described in Section III of the Third Annual Report. (3) No further attempts to increase the output of plated yarn were made beyond the experiments described in Volume I of the Fourth Annual Report. (4) The plated yarn employed to fabricate test specimens which are discussed in succeeding sections was untwisted, four-ply, and ribbon like. The electrodeposited nickel is nodular and has the "corn-cob" appearance of a boron fiber (see Figure 31). Factors responsible for this effect were not analyzed, but the plating rate is probably an important parameter. The yarn used in the present metal-matrix studies was primarily "Thornel" 75; "Thornel" 50 was used to a lesser extent. The two yarns have average physical properties indicated in Table X.

TABLE X  
PROPERTIES OF "THORNEL" 50 AND "THORNEL" 75  
GRAPHITE FIBERS

Graphite Fiber	Fiber Cross- Sectional Area $\mu^2$	Density g/cc	Tensile Strength lb/in. <sup>2</sup>	Young's Modulus lb/in. <sup>2</sup>
"Thornel" 50	33.9	1.65	262,000	51.8
"Thornel" 75	24.8	1.85	333,000	76.5

##### 2. Fabrication of Test Specimens

All specimens prepared for test purposes were plate-like and were prepared from aligned nickel-coated yarns by hot-pressing. Considerable care was taken to assure that the yarns were well collimated in a side-by-side manner before compaction. The majority of specimens were prepared in a furnace having good ( $10^{-5}$  torr) vacuum capability. Virtually all hot-pressing was done in a graphite mold at a temperature of 1050°C for one hour. The pressure employed varied from 2000 to 3500 psi.

A variation to the standard fabrication procedure outlined above was pursued with the intent of densifying at a lower compaction temperature and a lower pressure. It was thought that this potentiality might exist with the use of preformed tapes. A general introduction to this subject and the manner of fabrication was provided in Section V, Volume I of the Fourth Annual Report. (4)

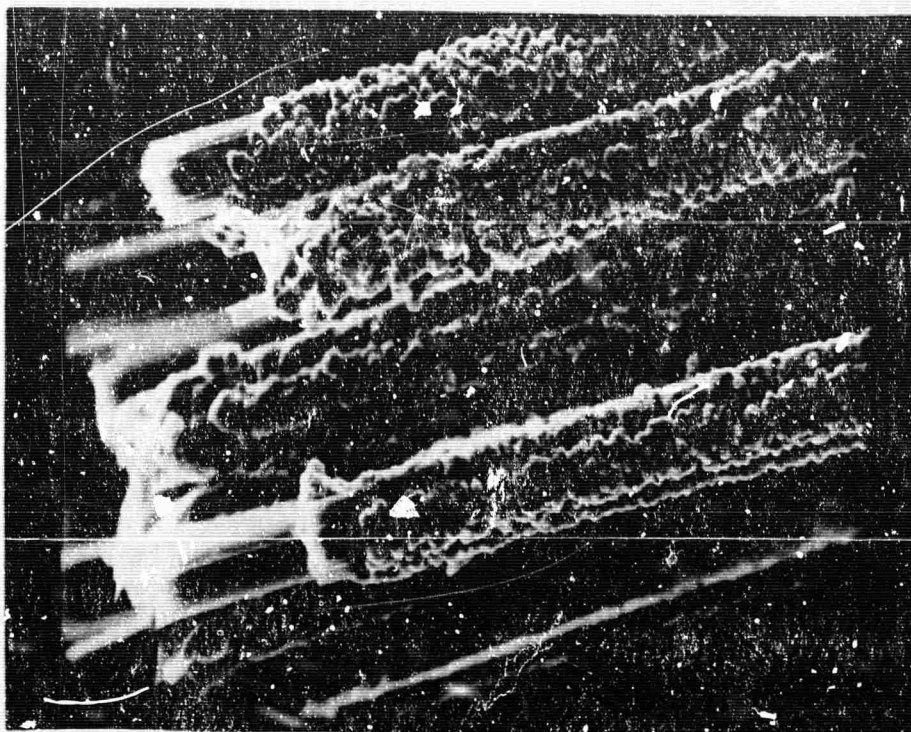


Figure 3i. Electrodeposited Nickel on "Thornel" Fibers. (1000X Mag.)

1223-1-52

A unidirectional plate and a 5-ply orthogonal plate were fabricated by hot-pressing stacked preformed tapes. Nickel sheet (0.00035-inch thick) was positioned between each composite tape to facilitate diffusion bonding. Fabrication of the tapes and final bonding of the stacked tapes in the unidirectional plate were carried out at approximately 700°C at a forming pressure of 3000 psi. The density corresponded to 97.4 percent of theoretical which represents a significant improvement over earlier efforts to fabricate at low temperatures. The orthogonal laminate had the same density characteristics as the unidirectional specimens, but the final bonding was done at 1050°C. The mechanical properties of specimens cut from both plates are discussed in Section V-D.

### 3. Fiber Properties After Fabrication

An accurate assessment of the fiber properties after their incorporation into the matrix is essential for estimating the potential of a composite and for characterizing individual specimens. It is generally assumed that the characteristics of extracted fibers are applicable to those which are encased in a matrix. Results were reported previously (3) on fiber properties as influenced by different fabrication parameters. It has been shown that in the course of fabricating a composite, the fibers are susceptible to physical and/or chemical damage. Physical damage includes factors such as shortened aspect ratio, cleavage, and surface blemishing, which have been discussed previously (3). Because



of the lower fabrication pressure and improved procedures for attaining fiber collimation in the current composites, the extent of physical damage is believed to be less. In spite of these precautions, however, fibers were still not continuous over the entire length of the specimen. It is conceivable that fiber breakage will be curtailed only when the matrix is highly fluid and even lower forming pressures can be utilized. Fiber cleavage is not evident in present composites according to metallographic studies and scanning electron microscope analysis failed to reveal any surface blemishes.

On the basis of annealing studies (3), it was shown that degradation of fiber tensile strength was substantial. The reduced fiber strength accounted for the low composite strength values. Similar results were obtained by Johnson (30) when he heated nickel-coated carbon filaments. He contended that the degradation resulted from graphitization of the filaments. We have conducted additional studies on fiber degradation because it seemed that results obtained on individually heated filaments were not completely consistent with observations made on fabricated composites. For example, the photomicrograph in Figure 32 shows a cross-section of annealed nickel-coated fibers with a deposit on the periphery of the coating. The deposit and altered fiber cross-section is more evident in Figure 33, where the nickel coating has been removed.

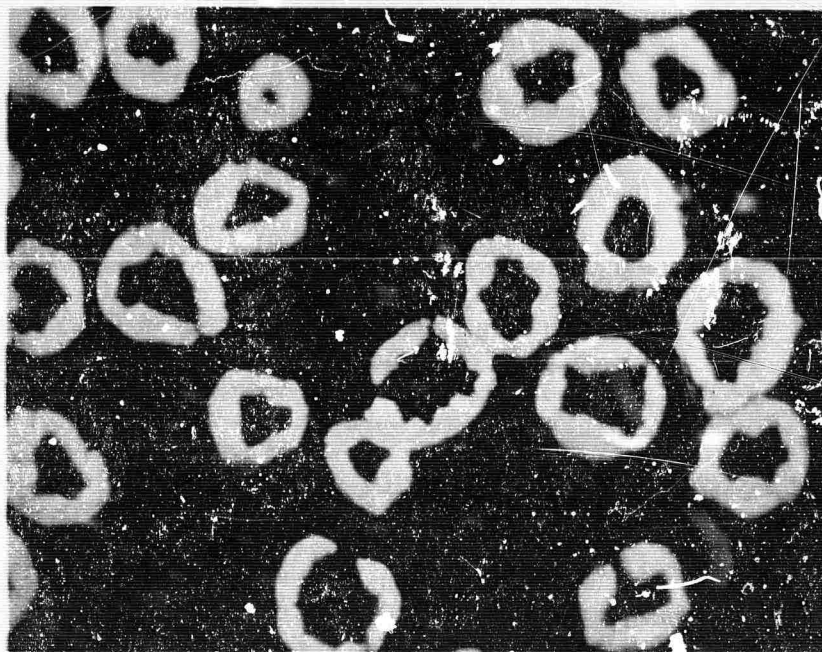


Figure 32. Nickel-Coated Fibers Annealed at 1050°C for One Hour.  
White Areas are Nickel. (2000X Mag.)

A-506

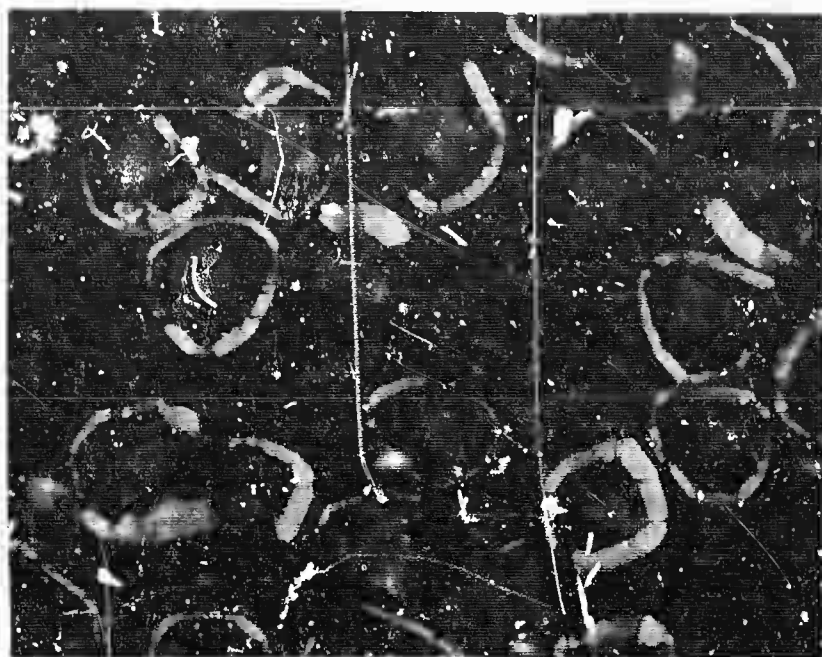
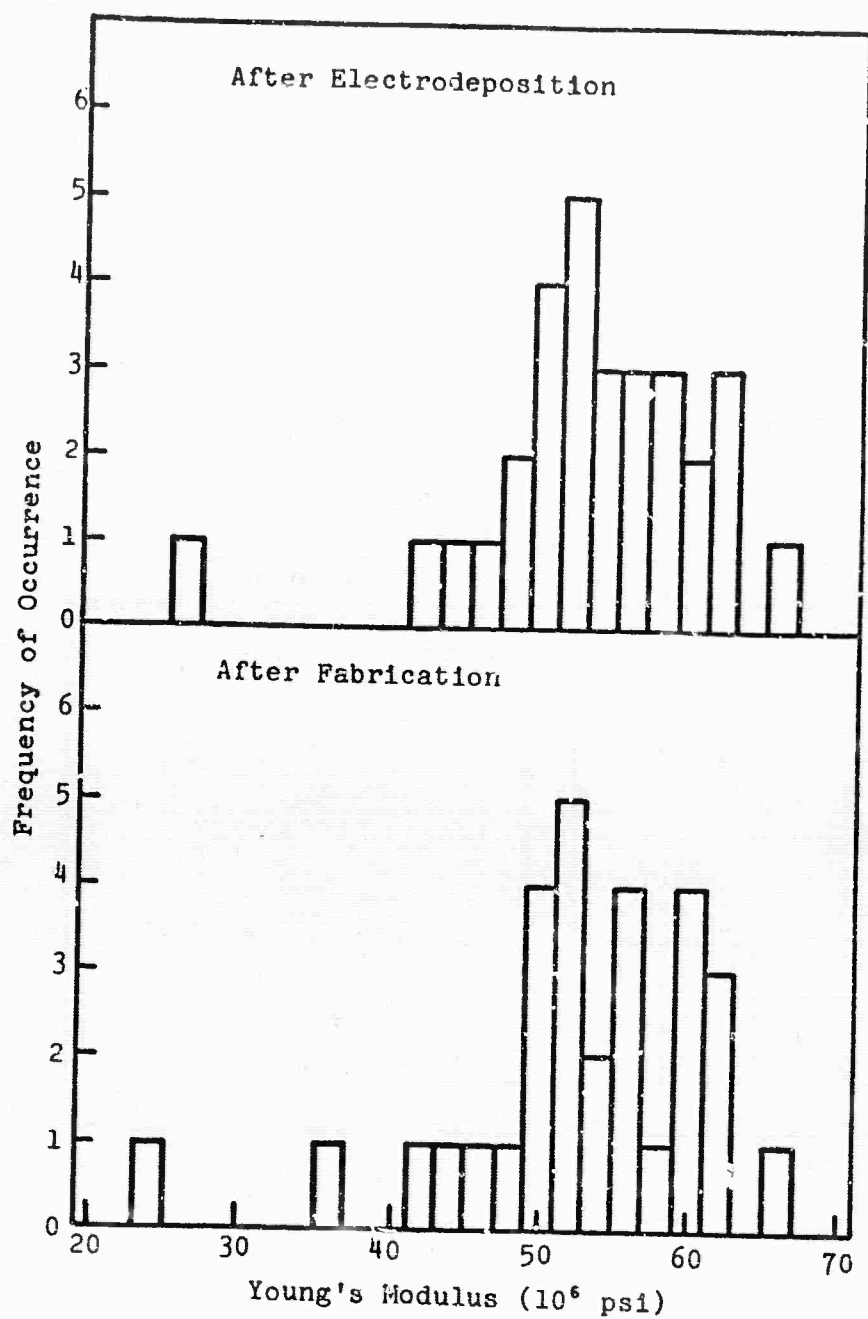


Figure 33. Nickel-Coated Fibers Annealed at 1050°C for One Hour;  
Nickel Removed by Dissolution. (2000X Mag.)

A515

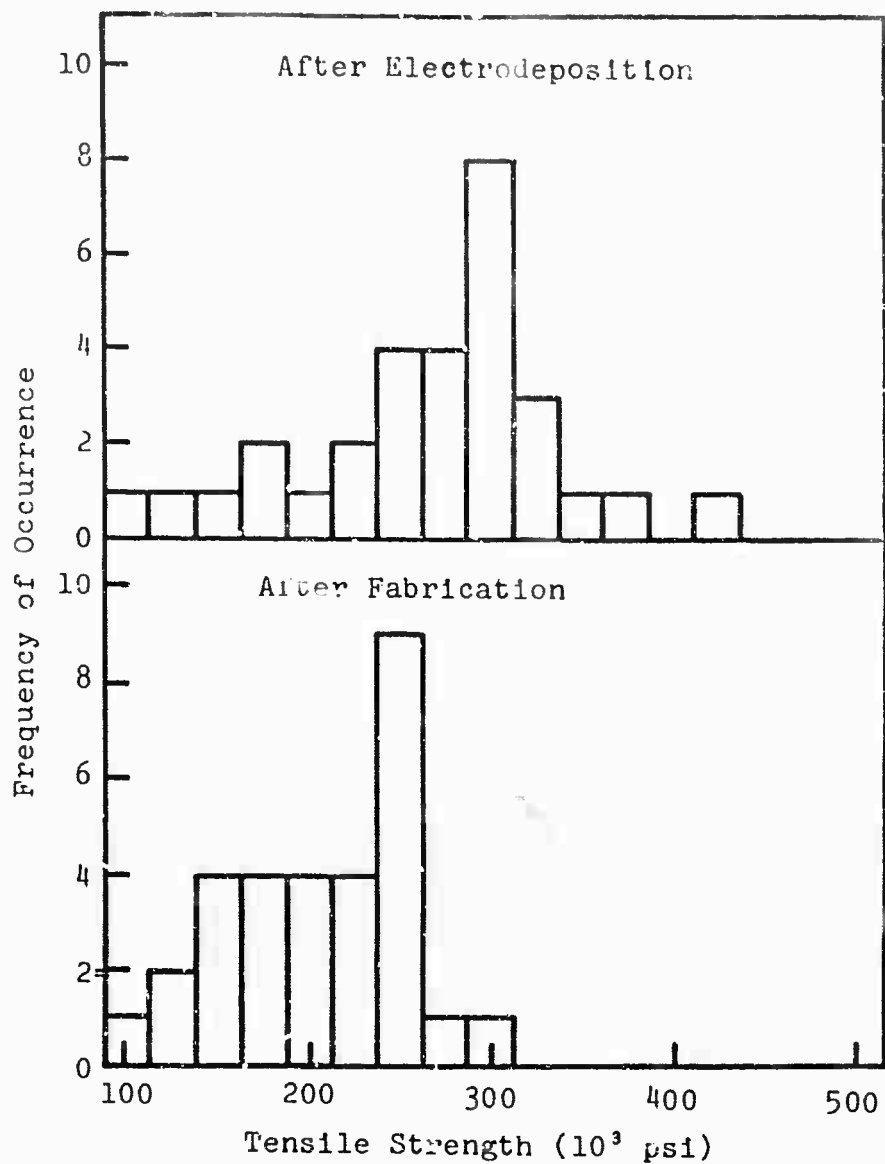
Polarized light and X-ray diffraction indicate the precipitate is highly birefringent and graphitic. Certain fibers had completely diffused through the nickel coating and subsequently precipitated on the periphery of the coating. Structural changes in the fiber of this magnitude have not been seen in fabricated composites even though the thermal conditions are comparable to those employed in annealing the fibers. For this reason, an additional study was made of fiber degradation as a result of fabrication procedures.

The present results are believed to be more reliable than earlier data (3) because of the improved sampling method and the additional statistics available. Sections were removed at regular intervals from nickel-coated yarn in the as-plated condition, and both "Thornel" 50 and "Thornel" 75 graphite fibers were evaluated in this manner. Furthermore, composites were fabricated from the same yarns at 1050°C with pressure applied for one hour. The nickel was removed from the yarns and the composite by dissolution in a 50 percent HCl solution. Thirty filaments from the as-plated and the hot-pressed specimens were tested for modulus of elasticity and tensile strength in the "Thornel" 50 series and a greater number were tested for the "Thornel" 75 series. The data in Figure 34 show that the modulus of the "Thornel" 50 fibers is not altered by the fabrication process, whereas Figure 35 depicts a reduction in tensile strength. The average tensile strength is reduced from 267,000 to 207,000 psi. On the other hand, Figures 36 and 37 show a change in both Young's modulus and tensile strength as a result of fabrication efforts for "Thornel" 75.



N-22375

Figure 34. Young's Modulus of Graphite Fibers After Electrodeposition and After Fabrication of Composite.



N-22485

Figure 35. Tensile Strength of Graphite Fibers After Electrodeposition and After Fabrication of Composite.



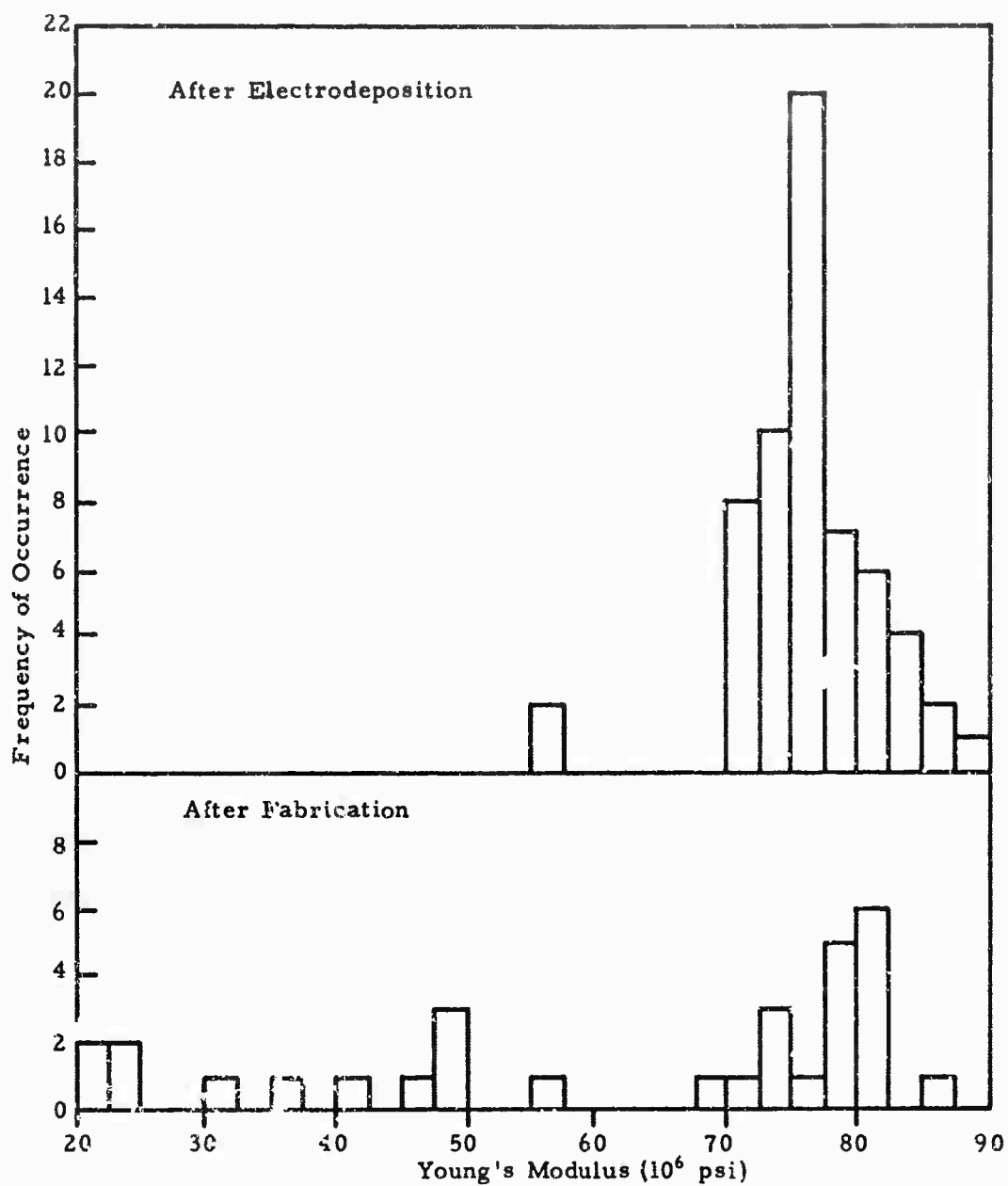


Figure 56. Young's Modulus of "Thornel" 75 Graphite Fibers After Electrodeposition and After Fabrication of Composite.

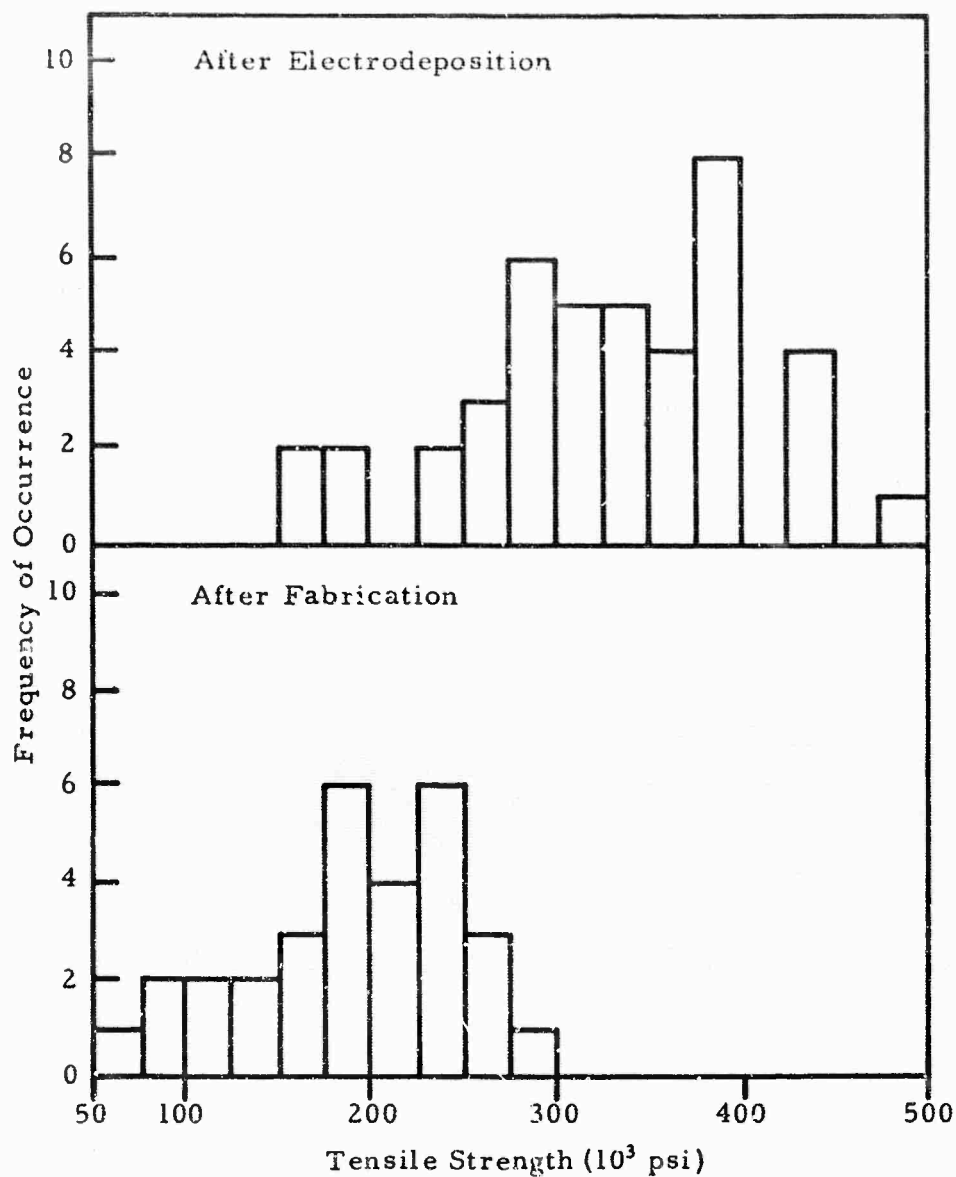


Figure 37. Tensile Strength of "Thornel" 75 Graphite Fibers After Electrodeposition and After Fabrication of Composite.

The narrow scatter-band and average value of  $77 \times 10^6$  psi for E is altered to a broad spectrum of values with an average of  $62 \times 10^6$  psi. The tensile strength, according to Figure 37, is similarly reduced from an average of 333,000 psi to 214,000 psi. The fiber tensile strengths for "Thornel" 50 and "Thornel" 75 are similar after fabricating the composite and concur with values presented (3) previously on individually annealed filaments. The relation between the Young's modulus and tensile strength of individual extracted "Thornel" 75 filaments appeared to be random. That is, fibers with low E values did not necessarily have low strength values, and vice versa. The reason(s) for the apparently more severe degradation of "Thornel" 75 compared to "Thornel" 50 is not known.

Samples of "Thornel" 50 fibers were studied with the scanning electron microscope to determine if fabrication efforts alter the fiber surface features. Nickel was removed from the fibers by dissolution after electrodeposition and after fabrication. The photographs shown in Figure 38a and 38b are representative of the fiber samples. Irregularities were observed on the surfaces of fibers removed from the composite (Figure 38b). The blemishes in question might have been caused by selective solution in the matrix, or the areas might be small graphite flakes which precipitated from the matrix. In either case, solution of the fiber is inferred, a process conceivably connected with the observed reduction of the tensile strength.

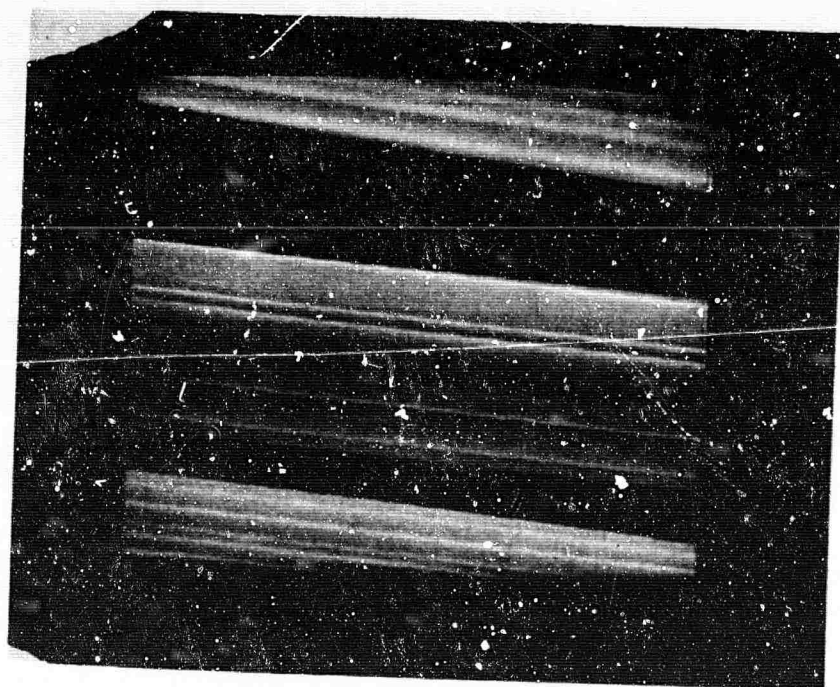


Figure 38a. Graphite Fibers After Electrodeposition;  
Nickel Removed by Dissolution. (3500X Mag)

471-2-S2

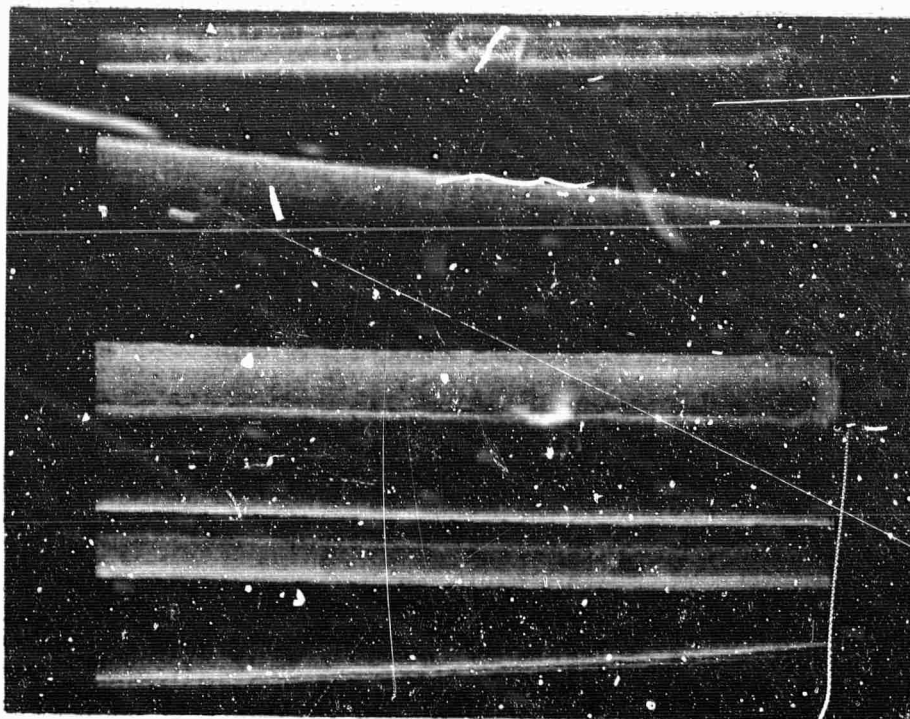


Figure 38b. Graphite Fibers After Fabrication of Composite;  
Nickel Removed by Dissolution. (3500X Mag)

471-2-S2

The interlayer spacing and stack height of graphite comprising the fiber were compared before and after the composite was fabricated at 1050°C. Graphitization of the fiber would result in a smaller interplanar spacing ( $c_0$ ) and increased stack height. It is apparent from Table XI that structural changes are not evident in either "Thornel" 50 or "Thornel" 75 fibers as a result of the processing. These data substantiate the contention made previously that there is a problem in attempting to extrapolate information obtained on individual filaments to composite behavior; the kinetics obviously differ as evidenced by the fiber morphological changes and by the graphite deposits presented in Figures 32, 33, and 38b. The X-ray data presented in Table XI infers that structural changes are not occurring in the fiber as a result of preparing the composite but these results do not rule out the possibility of slight fiber solubility in the matrix. Thus, fiber weakening evidently is not the result of in situ graphitization.

No attempts were made in the past to assess the effect of the compressive force used in hot-pressing on fiber properties. This analysis is complicated by the need for separating the effects of temperature and pressure. Compressing of nickel-coated fibers at room temperature with a force commonly used in hot-pressing is unrealistic because the flow characteristics of nickel vary appreciably between 25° and 1050°C. It was decided that paraffin-coated filaments might approximate at room temperature the consistency of nickel-coated filaments at 1050°C and thus provide a means for separating pressure from thermal effects. Untwisted

"Thornel" 75 yarn, therefore, was drawn through molten paraffin in order to coat each filament. Segments of yarn were then cut to three-inch lengths, carefully aligned in a graphite mold, and subsequently subjected to 3000 psi for one hour. Paraffin-coated filaments were also pressed isostatically. The paraffin-coating was removed with petroleum ether and the filaments were tested for tensile strength and Young's modulus. The results in Table XII represent the averages of ten determinations. The Young's modulus does not change, but the tensile strength is reduced approximately twenty percent by the 3000 psi pressure. Very little fiber breakage was evident in either of the two pressure specimens; a feature which differs from that observed in fibers extracted from nickel-matrix composites.

TABLE XI  
STRUCTURAL PARAMETERS OF GRAPHITE FIBERS BEFORE  
AND AFTER COMPOSITE FABRICATION

Fiber	Before Fabrication		After Fabrication	
	$c_o$ Å	$L_c$ Å	$c_o$ Å	$L_c$ Å
"Thornel" 50	3.434	57.6	3.430	61.5
"Thornel" 75	3.419	79.3	3.425	78.5

TABLE XII  
"THORNEL" 75 FIBER PROPERTIES BEFORE AND AFTER  
PRESSING IN A PARAFFIN MATRIX AT 3000 PSI

Fiber	Tensile Strength (psi)	Young's Modulus (psi)
As-Received	362,000	$75 \times 10^6$
Double Acting Pressure	309,000	$78 \times 10^6$
Isostatically Pressed	296,000	$75 \times 10^6$

This difference illustrates the complexity of the problem and the need for additional testing and statistics. These results, however, suggest that the fiber properties are degraded more by thermochemical processes than by the compaction operation. Degradation of the fiber strength appears to be caused most by limited solution in the nickel matrix. It is conceivable that a loss in strength might result under these conditions if areas are selectively dissolved, thereby creating notches or stress risers. The Young's modulus is a bulk property and should not change if the preceding reasoning is correct. In this regard, the data in Figures 34 and 36 are inconsistent for reasons that are not known at this time.

#### B. Filament and Strand Tests

Experimental evidence presented in the Third Annual Report (3) depicted good agreement in the Young's modulus and tensile strength values of "Thornel" 50 fibers as determined by single filament and strand test techniques. The procedure which was employed in those tests was extended in the present study to include "Thornel" 75 and nickel-coated "Thornel" 50 and 75. The primary advantages of the strand test are lower cost, less time, and results which are probably more indicative of fabricated composite characteristics. Results of the present tests are shown in Table XIII.

TABLE XIII  
PROPERTIES OF NICKEL-COATED AND AS-RECEIVED FIBERS  
BASED ON FILAMENT AND STRAND TESTS

Fiber Volume (%)	No. of Tests	Average Tensile Strength ( $10^3$ psi)	Coeff. of Variation (%)	Average Mod. of Elasticity ( $10^6$ psi)	Coeff. of Variation (%)
<u>Strand Tests - "Thornel" 50</u>					
100	6	274	4.7	43.5	1.3
45	4	132	5.4	30.8	0.4
44	5	109	14.7	29.1	3.6
<u>Strand Tests - "Thornel" 75</u>					
100	16	315	14.3	75.4	3.6
64	4	174	10.9	76.0	6.6
47	3	165	5.4	47.2	3.2
45	6	143	11.2	58.8	3.
42	4	122	15.6	56.7	7.2
33	5	106	13.2	54.8	18.2
<u>Filament Tests - Unplated "Thornel"</u>					
"T" 50	40	262	24.4	51.8	13.2
"T" 75	40	335	20.6	76.4	8.4

Filament test data for both Young's modulus and tensile strength show a greater variation than the data obtained by strand tests, but, the correlation between average filament and strand values is good. Results of the strand tests on nickel-coated "Thornel" 75 yarn is shown in Figure 39.

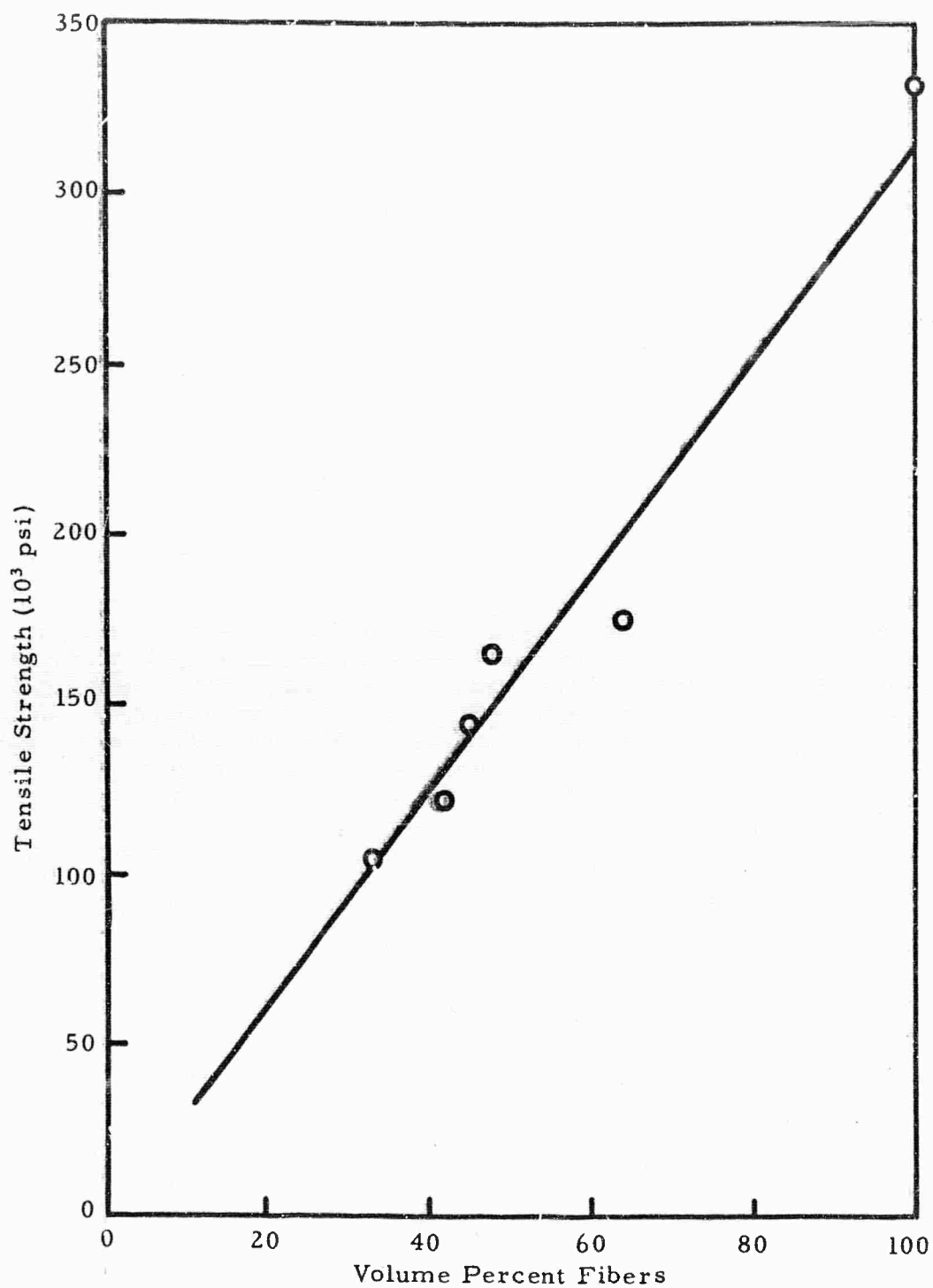


Figure 39. Strand Tensile Strength Values of Nickel-Coated "Thornel" 75 Graphite Fibers.

The linear curve drawn through the points is a least squares fit which passes through the origin and 315,000 psi at 100 v/o fiber. The nickel coating apparently does not contribute to the strand strength. Young's modulus of the nickel-coated "Thornel" 75 strands are more erratic and, with the exception of E for 47 v/o fiber yarn, strand values are greater than rule-of-mixtures estimates.

### C. Composite Behavior-Room Temperature

#### i. Tensile Stress-Strain Behavior of Unidirectional Composites

The stress-strain behavior in tension was measured on three composites with the aid of strain gages. The specimens contained 37, 45, and 51 v/o "Thornel" 75 fibers. Figure 40 shows stress-strain behavior of the three aforementioned specimens, and, for comparison purposes, the characteristics of a composite fabricated with 45 v/o "Thornel" 50 graphite fibers is included. Initial modulus of the "Thornel" 75 composites increases from  $40 \times 10^6$  psi to  $50 \times 10^6$  psi as the fiber content increases from 37 to 51 v/o. The secondary modulus and failure strengths also increase with fiber loading but strain at failure decreases. The "Thornel" 50 composites characteristically deform more at failure than the "Thornel" 75 composites.

#### 2. Compression Stress-Strain Behavior of Unidirectional Composites

A specimen which had been previously loaded in compression to failure (4) was examined metallographically and hardness measurements were made. The microhardness measurements were prompted by cracks observed in the nickel near the fracture edge as shown in Figure 41. The separations are believed to be in the grain boundaries and imply poor intergranular cohesiveness. The grain boundaries etch very rapidly (see Figure 42) suggesting that impurities might be concentrated in those regions of the matrix. Microhardness measurements indicated that the bulk nickel is soft and ductile and, as shown in Figure 43, indentations within the grain and in the grain boundary are approximately equal. A slight distortion was evident in the diamond impressions made in the grain boundaries, but this evidence is probably insufficient to signify irregularities in the grain boundaries.

The photomicrographs in Figures 41 and 42 indicate numerous regions in which nickel grains were removed from the composite during polishing. A similar effect is evident in areas of the specimens further removed from the fracture edge (see Figure 44). The extensive pull out noted in these photographs appears to be additional evidence of poor intergranular bonding. Microstructural irregularities of this sort were not observed in tensile specimens stressed to failure. On the contrary, the photograph in Figure 45 shows that it is difficult to retain the fibers during polishing. Deformation in the compression specimen just prior to failure was approximately 0.65 percent; tensile failures generally occurred at strains of 0.4 percent. The additional deformation encountered in compression may be responsible for the microstructural differences between tensile and compression specimens.



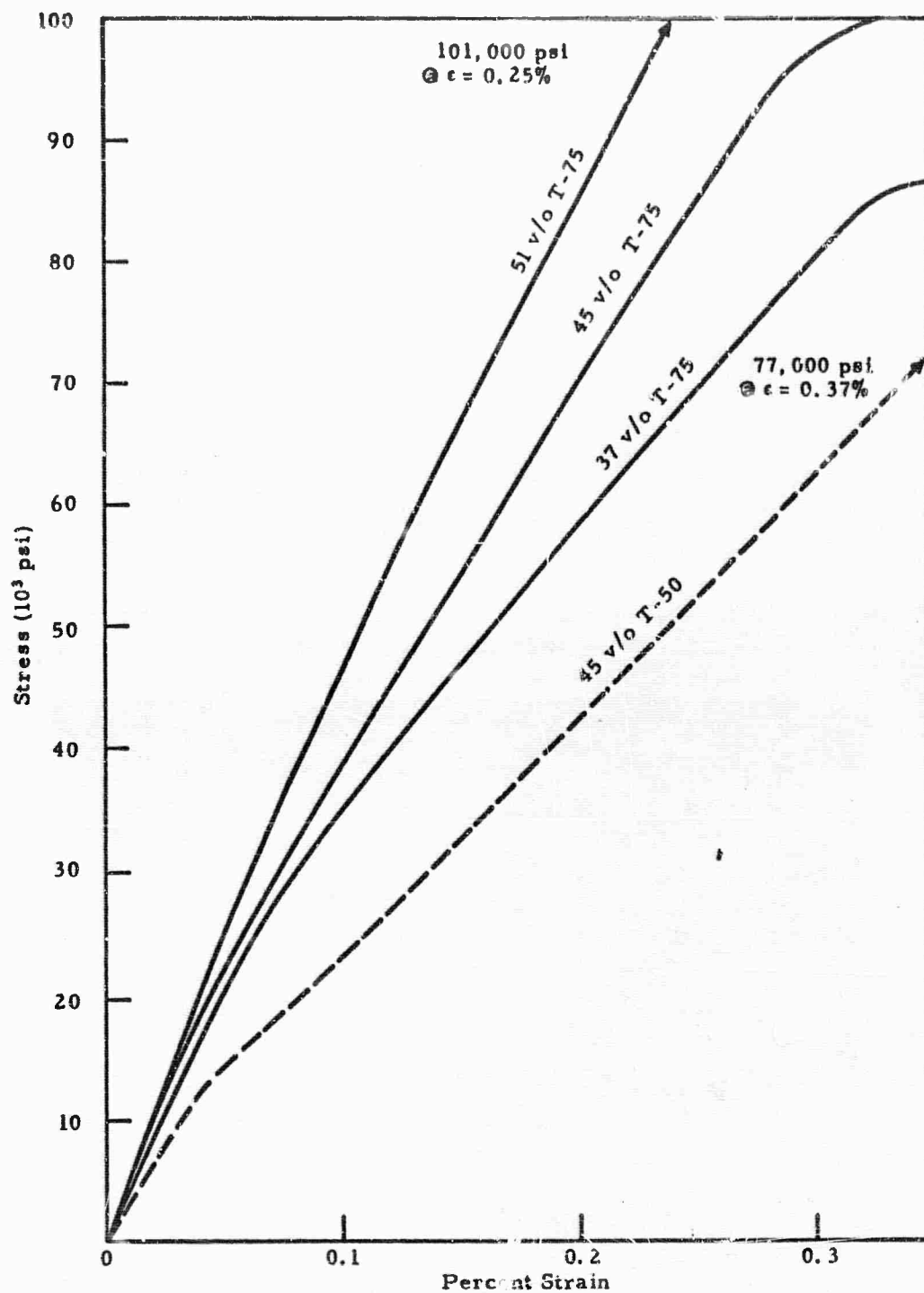


Figure 10. Stress-Strain Behavior of "Thornel" 50 and "Thornel" 75 Fibers in Nickel Matrix.

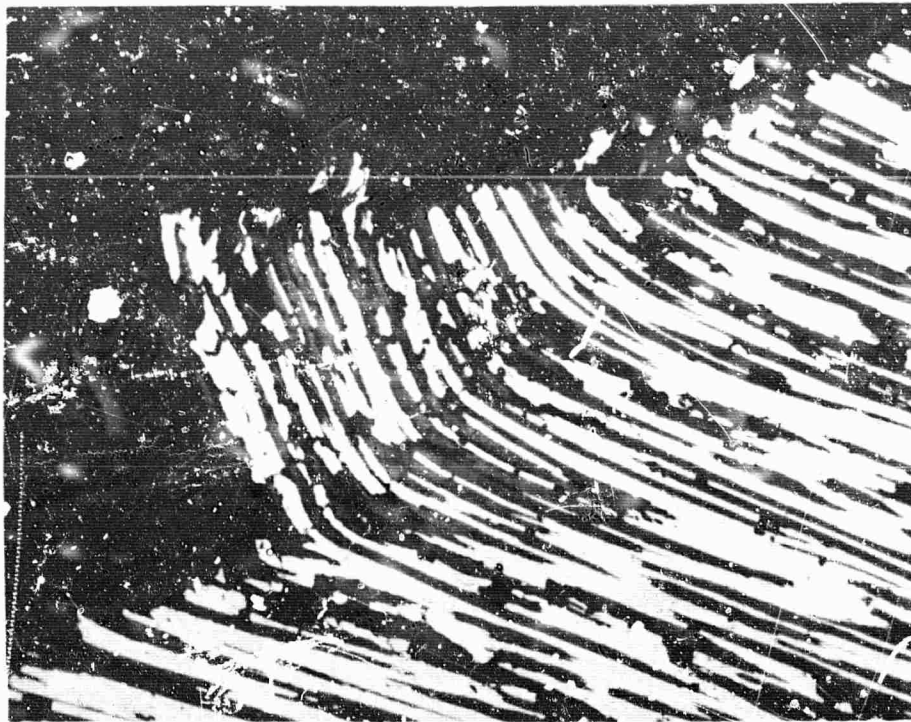


Figure 41. Fracture Edge of a Graphite-Fiber, Nickel-Matrix  
Compression Specimen. (250X Mag.)

470-1-0-2

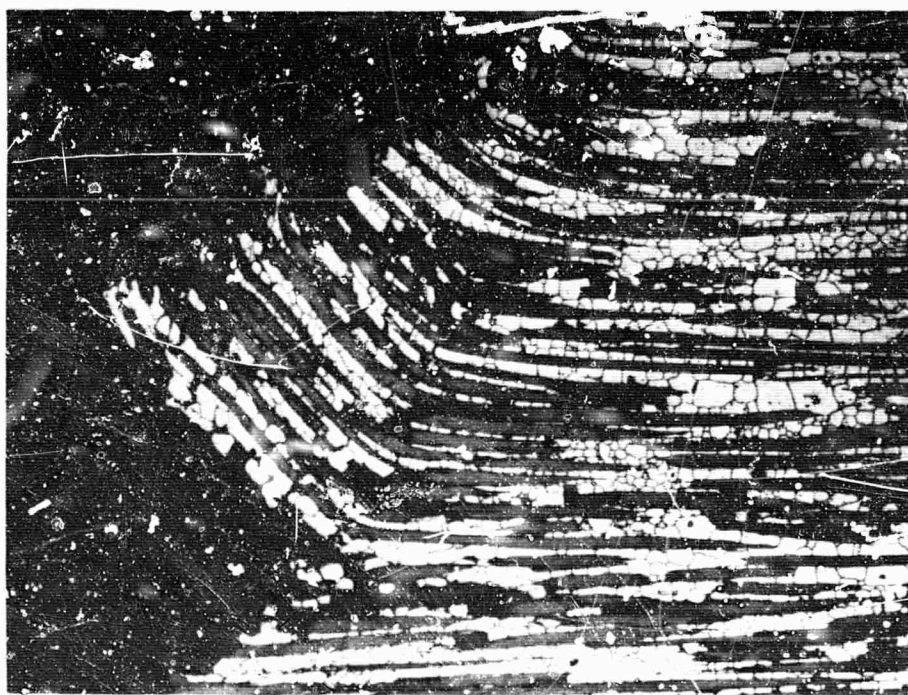


Figure 42. Etched Fracture Edge of a Graphite-Fiber, Nickel-Matrix  
Compression Specimen. (250X Mag.)

470-1-0-3



Figure 43. Microhardness Indentations in the Nickel Matrix and in the Grain Boundary.

N-22338



Figure 44. Microstructure of Graphite-Fiber, Nickel-Matrix Compression Specimen. (250X Mag)

470-1-0i



Figure 45. Fracture Edge of a Graphite-Fiber, Nickel-Matrix  
Tensile Specimen. (750X Mag)

N-22534

One might suspect that graphite may concentrate in or near the grain boundaries as a result of solution and diffusion processes. Limited quantities of impurity graphite have been observed in microstructures, but under conventional fabrication conditions, the graphite is dispersed in isolated areas. The nickel plated on graphite yarn generally has a tarnished appearance which possibly might be indicative of oxygen contamination and could be a possible cause of grain boundary embrittlement. Even though microhardness measurements did not substantiate irregularities in the grain boundaries, a compression specimen was prepared from nickel-plated yarn which previously had been annealed in an 85 percent argon-15 percent hydrogen environment at 750°C for two hours. This procedure removed the tarnished appearance of the nickel (which presumably was caused by nickel oxide) and resulted in a weight loss of approximately 0.25 percent. Four tensile and one compression specimens were fabricated from the hydrogen-treated yarn. The extent of densification (96.2 percent of theoretical) was no improvement over that obtained with untreated yarns, and the tensile strength values (84,000 psi) were average. A single measurement of Young's modulus gave  $34.1 \times 10^6$  psi, a value that is slightly higher than expected for this densification. The compression stress-strain curve for the present composite and for a conventionally prepared specimen are shown in Figure 46. The differences are not great. The composite containing hydrogen purified yarns had a modulus of  $32.8 \times 10^6$  psi and failed at 101,000 psi, whereas the corresponding properties for the conventional specimens were  $28.7 \times 10^6$  psi and 96,000 psi. The elastic limit of both specimens is exceeded at stresses greater than approximately 25,000 psi.

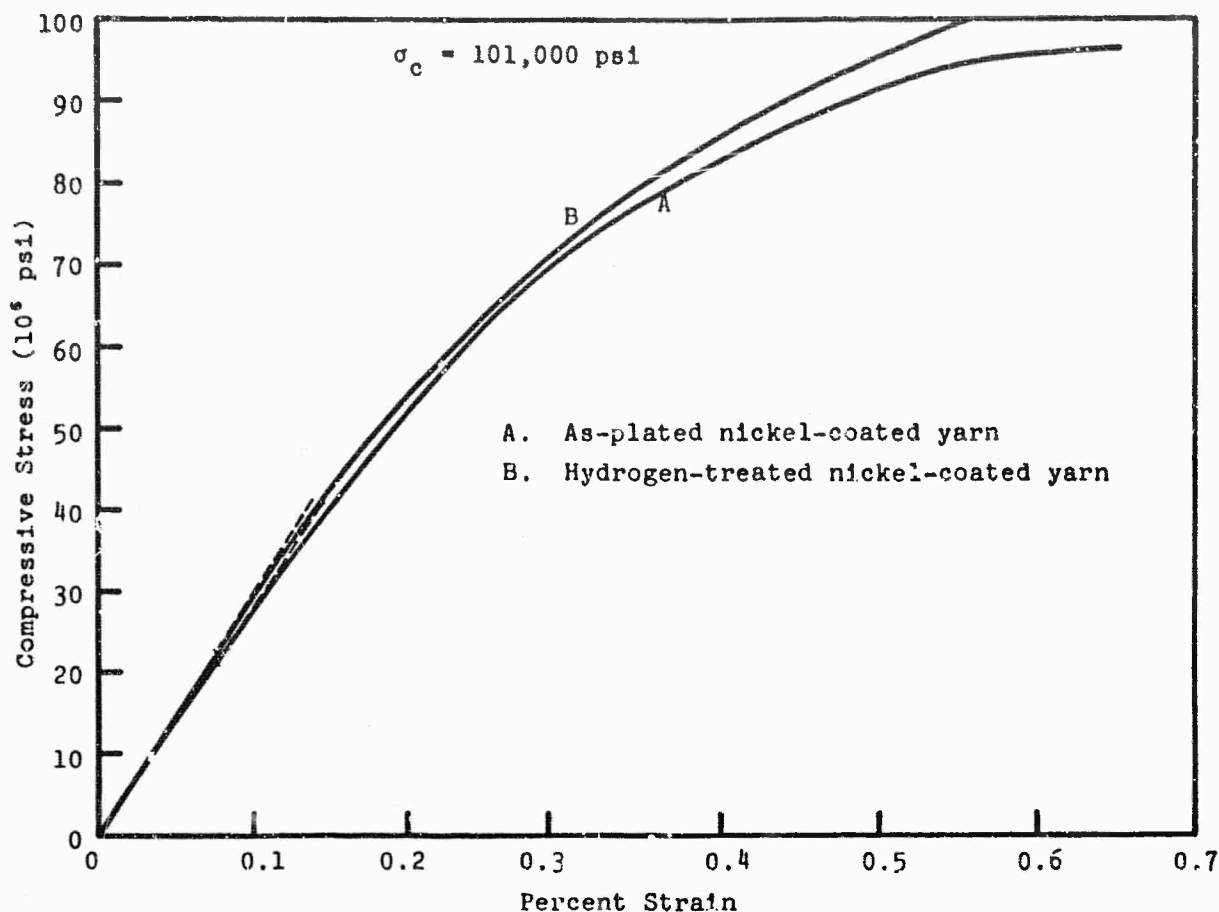


Figure 46. Compression Stress-Strain Behavior of Graphite-Fiber, Nickel-Matrix Composites Fabricated from As-Plated and Hydrogen-Treated Nickel-Coated Fibers.

N-22942

The compression stress-strain curve is very curvilinear and resembles the behavior of nickel stressed in the same manner. Metallographic observations suggest poor intergranular cohesiveness might be instrumental in this behavior but additional evidence is lacking at this time.

### 3. Tensile Strengths of Unidirectional Composites

The relationship between tensile strength values of "Thornel" 75 composites and strand test results is shown in Figure 47; experimental details relative to the strand values were discussed in a previous section. Approximately two-thirds of the strand tensile strength is realized in the fabricated specimens. Results on fibers extracted from the composite were shown in Figure 37; the 214,000 psi value also is approximately two-thirds of the strand tensile strength. It is evident that composite strengths are generally consistent with values estimated from the reduced fiber tensile strength. Failures in the fabricated composite specimens containing 50 v/o<sub>f</sub> were shear-like, a behavior aggravated by the "dog-boned" features of the test specimens.

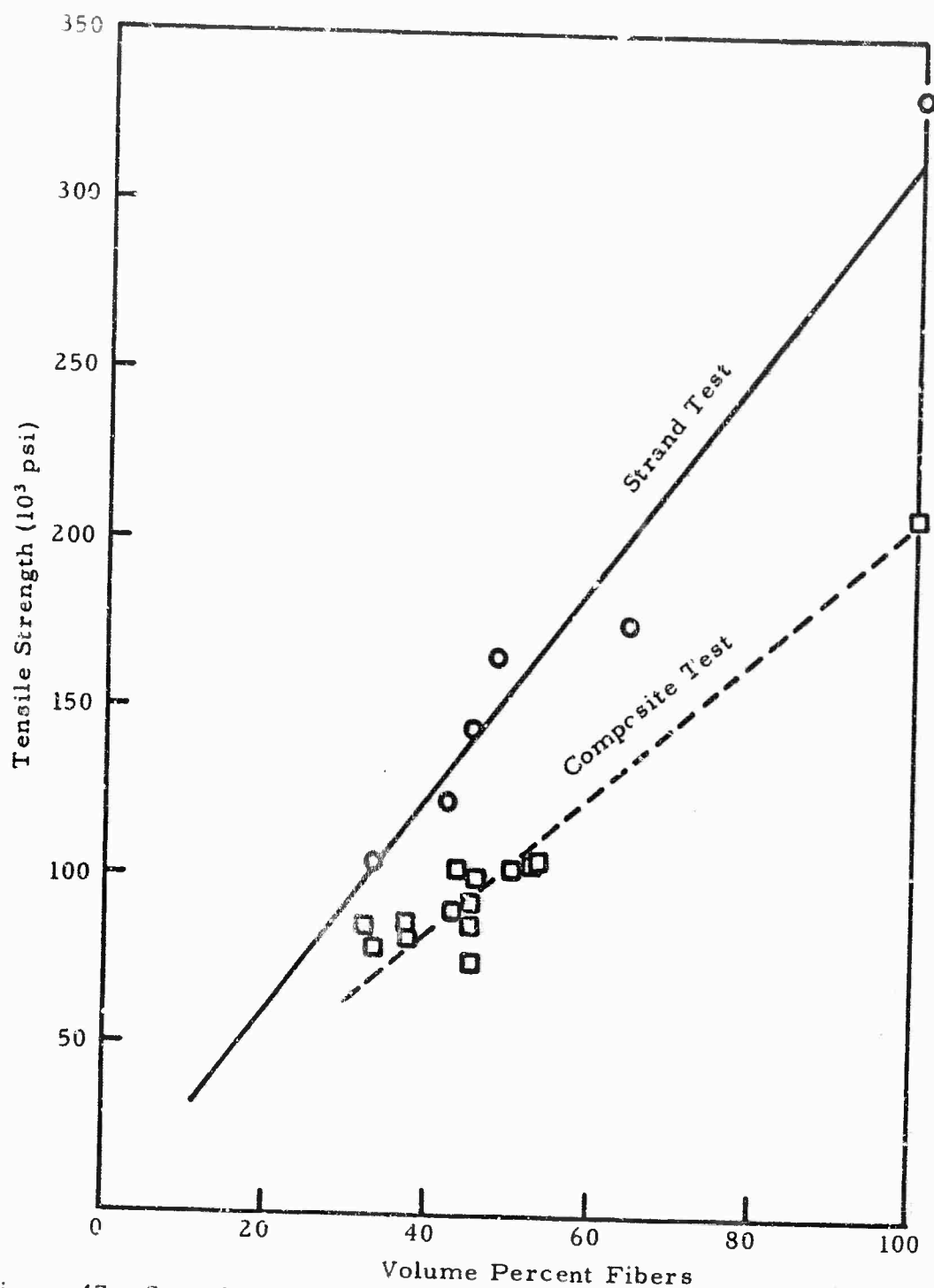


Figure 47. Strand Tensile Strength Values of Nickel-Coated "Thornel" 75 Graphite Fibers Compared with Composite Tensile Strengths.

The tensile strength of unidirectional composites containing different volume fractions of "Thornel" 50 fibers was reported in the Third Annual Report. These data are compared in Figure 48 with strand data described previously in Table XIII. The rule-of-mixtures curve constructed through the data has a terminal value for the fibers of 207,000 psi. The latter is based on measurements conducted on extracted fibers (see Figure 35). Again, it is evident that the full potential in composite tensile strength is not attained because of degradation processes accompanying the fabrication, but results are proportionately better in this instance than was noted previously for "Thornel" 75 composites. The tensile strengths of composites containing 45 v/o "Thornel" 75 have, on the average, exceeded comparable "Thornel" 50 tensile strengths by approximately 20,000 psi.

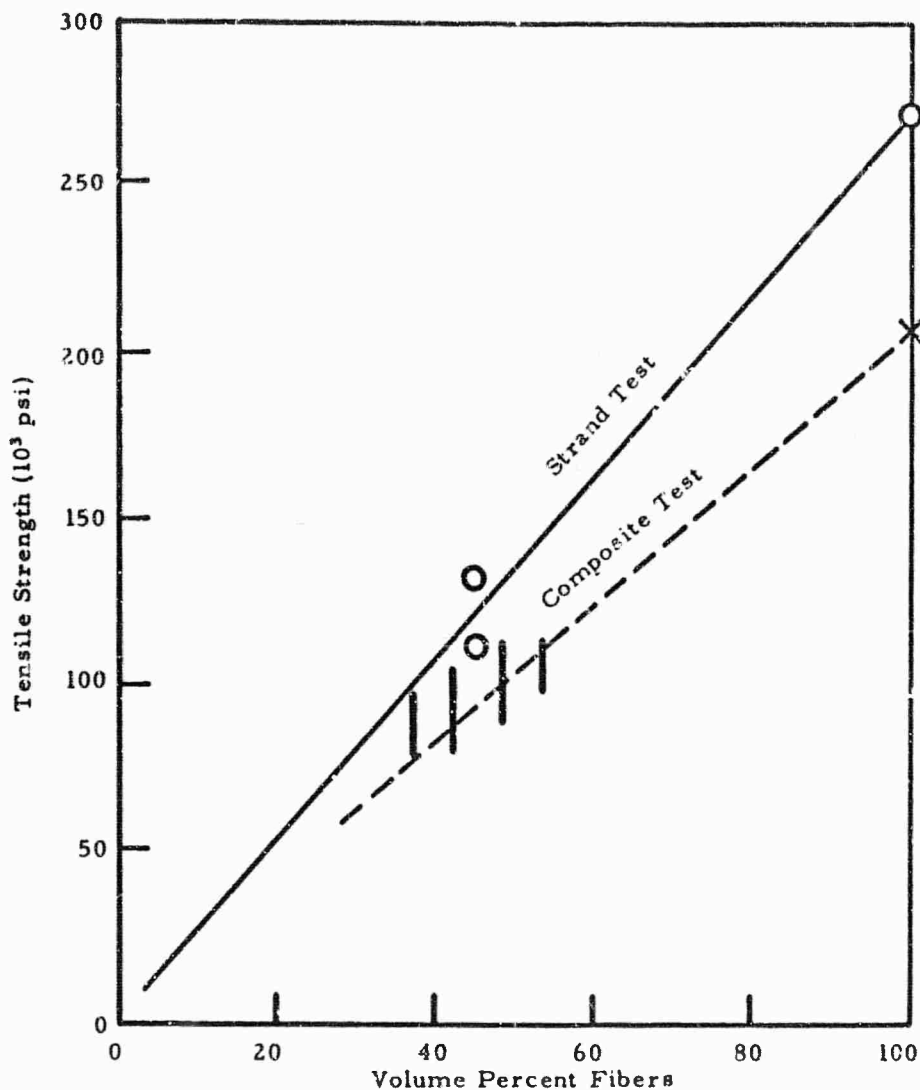


Figure 48. Strand Tensile Strength Values of Nickel-Coated "Thornel" 50 Graphite Fibers Compared with Composite Tensile Strengths.



#### 4. Young's, Shear Modulus, and Shear Strength Studies

Several studies related to the Young's modulus were conducted because of the apparent discrepancy which exists between experimental and calculated Young's modulus. According to an earlier study (Section V-C, Volume I of the Fourth Annual Report (4)), a "best fit" was obtained if the nickel matrix modulus was assumed to be  $17 \times 10^6$  psi instead of  $30 \times 10^6$  psi. Unfortunately, the composite matrix cannot be assessed in situ. The modulus of elasticity of metals is one of the most structure-insensitive mechanical properties. Characteristically, it is only slightly affected by alloying additions, heat-treatment, or cold work. Nevertheless, it appeared advisable to ascertain the effects of carbon solution on the Young's modulus. Particulate composites were fabricated from blended mixtures of a chemically pure nickel powder and Union Carbide Grade SP-1 spectroscopic graphite powder. Cold-pressed bars were heated in hydrogen to  $750^\circ\text{C}$  prior to hot-pressing by the process typically used to fabricate the fiber-based composites. The test specimens contained one to two percent porosity. The Young's and shear modulus values are shown in Figure 49. According to the phase diagram data, the solubility of carbon in nickel corresponds to approximately one atomic percent at the fabrication temperature of  $1050^\circ\text{C}$ . Equilibrium conditions evidently were not obtained because SP-1 graphite powder was still evident in the specimen containing 5 v/o (corresponding to one atomic percent) graphite. It is unlikely that solubility conditions would be much different in the fiber-based composites from that encountered with the particulate system. Hence, the slight decrease in modulus noted for the 5 v/o specimen in Figure 49 is inconsequential in terms of the required reduction to  $17 \times 10^6$  psi specified previously for the nickel matrix.

The effect of voids on composite elastic properties has not received much attention, partly because analytical predictions have not been developed for composite systems containing fibers and voids. Greszczuk (31) proposed simple corrections for voids which could be applied to the measured values, recognizing that a rigorous solution would require information on the size, shape, and distribution of voids. The following effort was made principally to determine, by using Greszczuk's correction principles, the degree to which the Young's and shear modulus values in graphite-fiber, nickel-matrix composites are influenced by voids. This information seemed necessary for assessing the reliability of measured elastic constants which have been used for correlation with predicted values. In this context, it is important that small errors in calculated porosity are not overshadowing the discrepancy observed between calculated and measured Young's modulus.

Figure 50 shows the Young's and shear modulus values which were used in this analysis, except for three data points obtained on composites with volume fractions of porosity greater than 0.16 percent. The elastic property measurements were made over the course of this program on specimens containing  $45 \pm 3$  v/o "Thornel" 50 fibers. All measured data were included in this analysis, regardless of the fabrication parameters.

The longitudinal Young's modulus  $E_L$  can be calculated from the familiar rule-of-mixtures expression

$$E_L = E_f k + E_m (1-k).$$



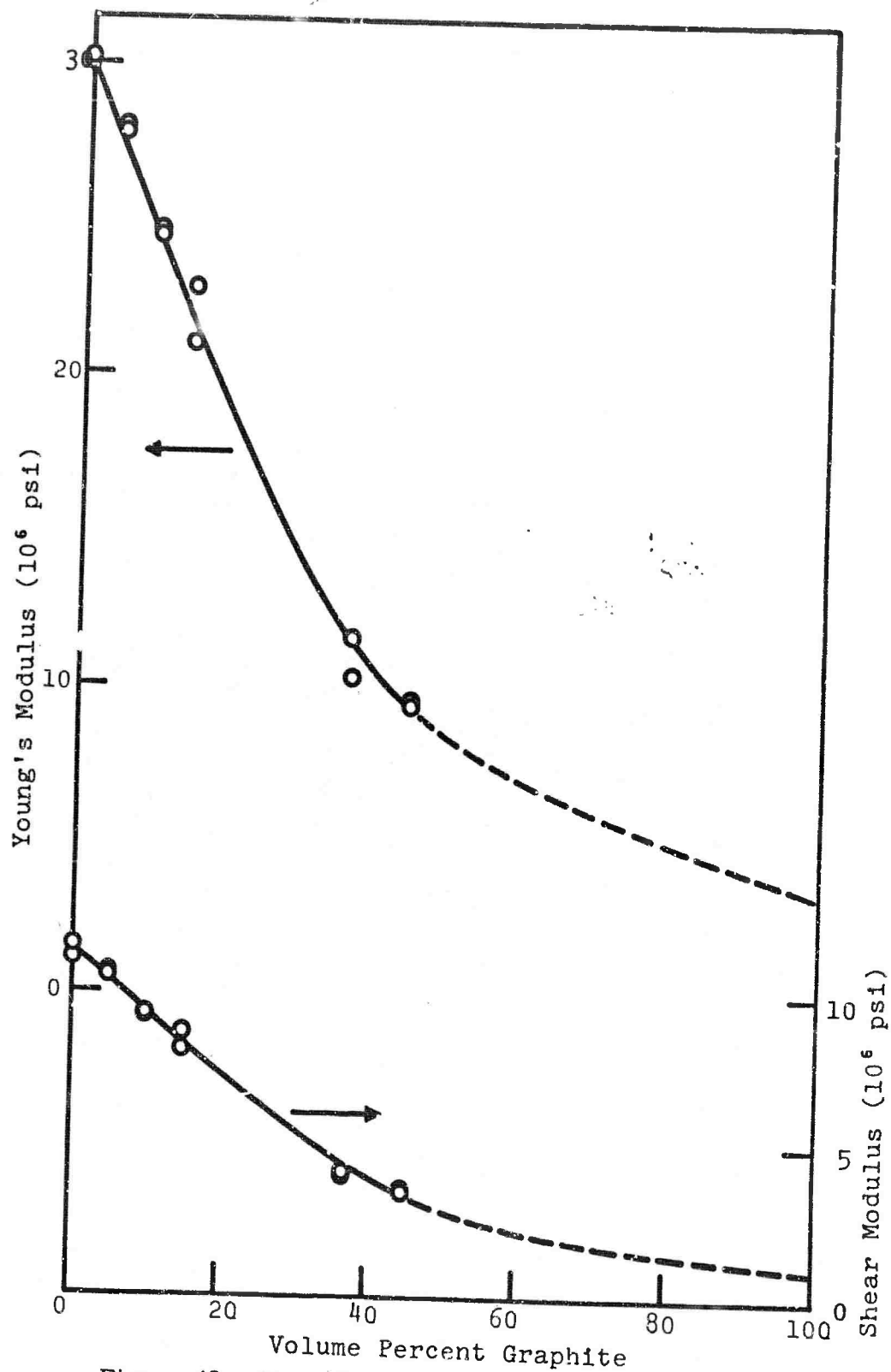


Figure 49. Young's and Shear Modulus of Graphite-Particulate, Nickel-Matrix Composites.

N-22943

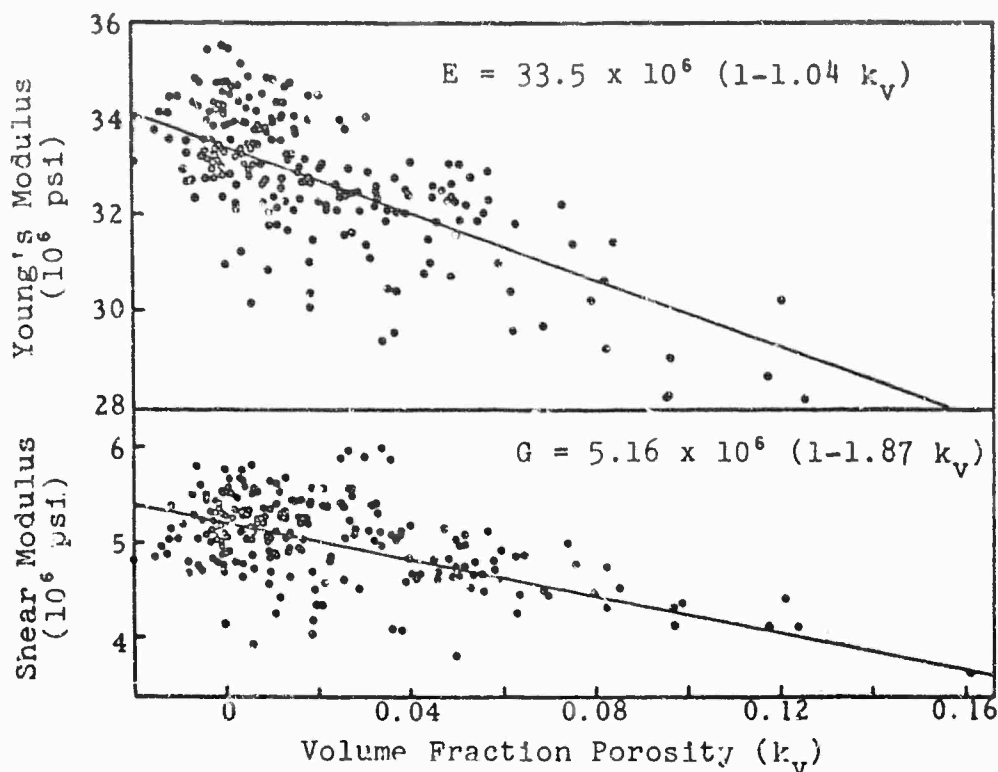


Figure 50. Variation of Young's and Shear Modulus with Porosity. N-22425

The correction proposed by Greszczuk for the effects of voids is made by replacing  $k$  and  $E_m$  by the quantities  $\bar{k}$  and  $\bar{E}_m$ , where

$$\bar{k} = (1 - k_v) k$$

$$\text{and } \bar{E}_m = E_m \frac{(1 - k_v)}{1 - k}.$$

In the preceding equations,

$$k_v = \frac{V_v}{V_f + V_m + V_v},$$

$$k = \frac{V_f}{V_f + V_m},$$

$$\text{and } \bar{k} = \frac{V_f}{V_f + V_m + V_v}.$$

where  $V_v$ ,  $V_f$ , and  $V_m$  represent the volume of voids, fibers, and matrix, respectively. After these substitutions are made, the relationship between longitudinal modulus and porosity becomes

$$E_L = [E_f k + E_m (1 - k)] - k_v [E_f k + E_m (1 - k)].$$

Young's and shear modulus data were fitted to this type expression by least squares procedures. Treatment of the shear modulus data in this manner is tentative until the equations pertinent to this elastic constant are analyzed more thoroughly. The solid lines drawn in Figure 50 summarize this effort.

Expressions which describe both curves are

$$E = 33.5 \times 10^6 (1 - 1.04 k_v)$$

$$\text{and } G = 5.16 \times 10^6 (1 - 1.87 k_v).$$

The empirical equation proposed for the effect of porosity on Young's modulus concurs quite well with the experimental expression. The dependence of shear modulus on porosity is evidenced by the higher coefficient of 1.87. The Young's modulus,  $E_L$ , predicted for a composite containing 45 percent fibers is  $39 \times 10^6$  psi. According to Figure 50, the experimental Young's modulus indicated for a pore-free composite is  $33.5 \times 10^6$  psi. The volume fraction of porosity bridging these two modulus values on the basis of Figure 50 is approximately 0.20. This change is indicative of the large and rather unrealistic correction which must be added to the measured values of  $k_v$  if the difference in modulus data is the result of voids. These results suggest that  $33.5 \times 10^6$  and  $5.2 \times 10^6$  psi are reasonable representative experimental values of pore-free composites.

The Young's modulus values of well densified graphite-fiber, nickel-matrix composites which were fabricated over the course of this program from graphite yarn having  $50 \times 10^6$  psi modulus are shown in Figure 51. These earlier data were supplemented at this time with measurements on specimens containing approximately 35 and 65 v/o fibers. Experimental data are also shown for composites fabricated from yarn with a modulus of  $75 \times 10^6$  psi. All specimens represented in Figure 51 contained less than 3 v/o porosity.

According to Hill (32), the Young's modulus is bounded by:

$$\left( \frac{c_1}{E_1} + \frac{c_2}{E_2} \right)^{-1} = E_R \leq \left( \frac{E \text{ or } c_1 E_1 + c_2 E_2}{c_1 E_1 + c_2 E_2} \right) \leq E_V$$

if the constituents in a composite experience equivalent strain.  $E_V$  defines the upper bound of Young's modulus. The special case,  $E$  (or "rule of mixtures") is applicable when the two constituents have equivalent Poisson ratios and experience equivalent strain. The lower bound, noted as  $E_R$ , applies if both constituents experience equivalent stress. The constituents must be firmly bonded to experience equivalent strain, and, conversely, they must be poorly bonded to experience equivalent stress. The upper and lower bounds for two varieties of composites are noted in Figure 51. The upper bound in each instance concurs very closely with the rule-of-mixtures values. Empirical evidence depicting fiber-matrix debonding has been

viewed in a variety of microstructures, suggesting, perhaps, that one should not expect composite modulus values equivalent to those identified by the upper bounds. If the concept of poor bonding is assumed, results in Figure 51 show that agreement is good with the limited experimental data obtained on composites containing  $75 \times 10^6$  psi modulus fibers. The correlation, however, is not so good with data obtained on composites with  $50 \times 10^6$  psi modulus fibers.

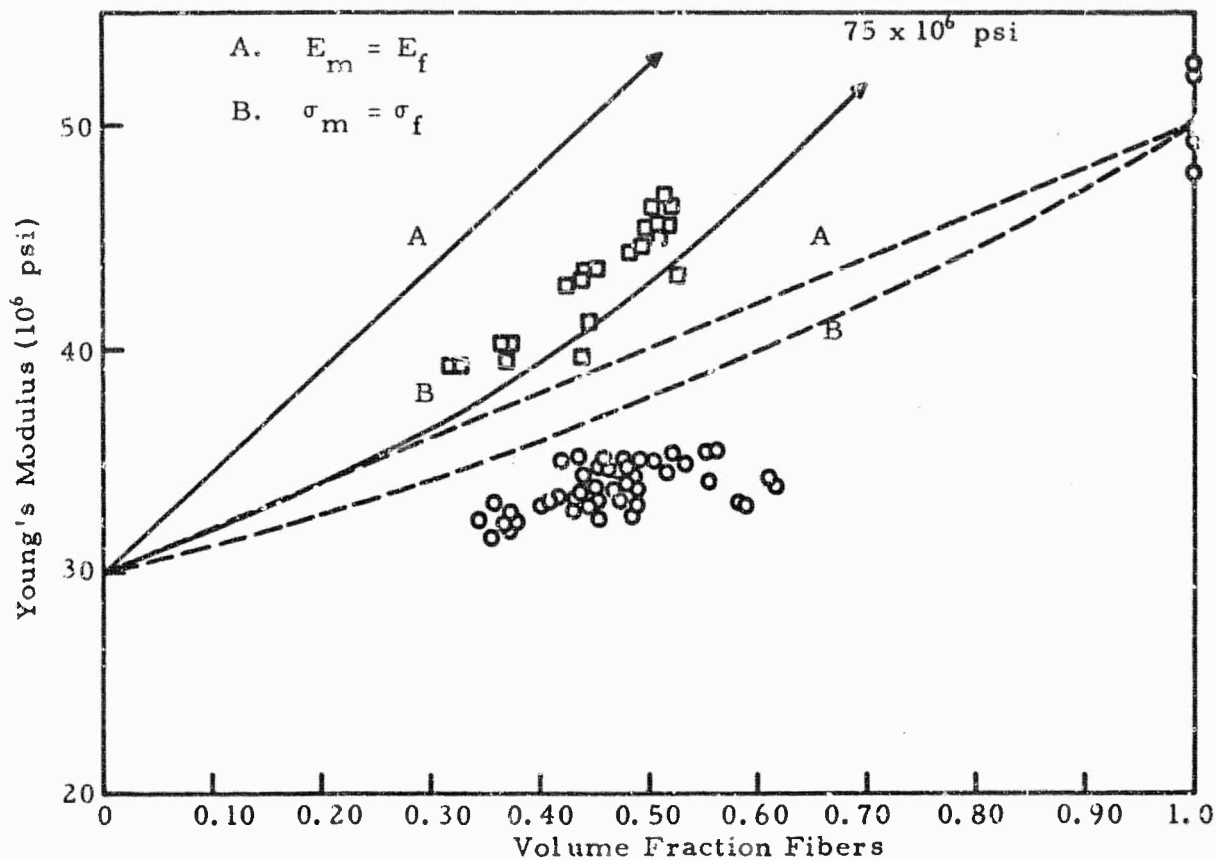


Figure 51. Comparison Between Experimental and Calculated Young's Modulus for Bands of Equivalent Strain and Equivalent Stress.

Nickel electrodeposition was attempted on five different types of carbon and graphite yarns. This effort was undertaken to extend the scope of the elastic measurements on composites. The various carbon/graphite yarns were considered as constituents in the composites because of an interest in the correspondence between experimental and analytical Young's modulus. The fibers considered for these studies included Union Carbide Corporation VYB carbon and WYD graphite yarns with  $E = 6 \times 10^6$  psi and "Thornel" 25, 50S, and 75 graphite yarns. The "Thornel" yarns had moduli of approximately 25, 50, and  $75 \times 10^6$  psi, respectively. "Thornel" 50S-fiber resin composites have improved interlaminar shear properties compared with those fabricated with "Thornel" 50 fibers, an improvement which is related to fiber surface differences.

Yarns having wide range of metal-coating thicknesses were prepared for use in the fabrication of Young's modulus specimens. These specimens were fabricated as one-inch long bars by hot-pressing at  $1050^\circ\text{C}$  for one hour under 3000 psi. The deposition of nickel on the two lowest modulus yarns (VYB and WYD) was not successful. The quantity of metal electroplated on the yarns was too low to fabricate suitable specimens, and the nickel distribution was particularly poor in the WYB material. The higher resistivity of this yarn is believed to be responsible for these results.

The measured Young's modulus values obtained on composites prepared from different "Thornel" fibers are presented in Figure 52. A portion of these data was presented previously in Figure 51 and discussed in conjunction with analytical bounds. Three of the six specimens fabricated from "Thornel" 50S had above average Young's modulus values, but two of the six are significantly below average. A remeasurement confirmed the two low values, but reasons are not known for this behavior. Because of the large scatter in data, no definite conclusions can be drawn at this time on the effect of different fiber surface characteristics on Young's modulus.

The measured values for "Thornel" 75 composites in Figure 52 conform to the lower bound proposed by Hill (see Figure 51), but moduli for the composites containing 50 and 25 million modulus fibers are significantly lower.

According to Greszczuk (31), the effect of unbonded fibers on the Young's modulus of a unidirectional composite can be estimated from the following equation:

$$E_{L*} = E_L - E_f k^*,$$

where

$E_{L*}$  = modulus of elasticity of a composite that contains unbonded fibers,

$E_L$  = modulus of elasticity of a composite in which all the fibers are bonded together,

$E_f$  = modulus of elasticity of the fiber, and

$k^*$  = volume fraction of the unbonded fibers.

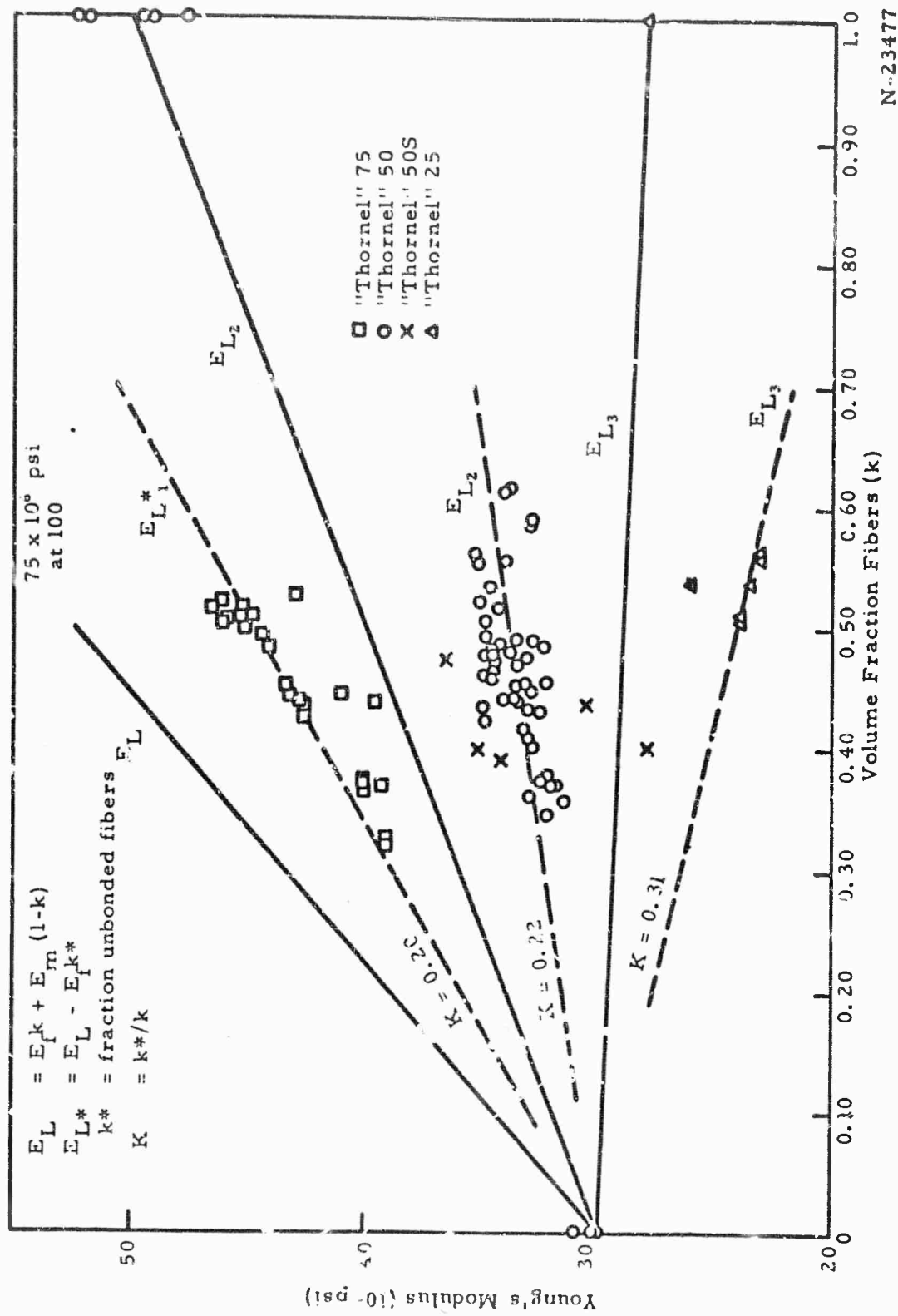


Figure 52. Agreement Between Experimental and Predicted Young's Modulus Values in Graphite-Fiber, Nickel-Matrix Composites Assuming Perfect and Partial Interfacial Bonding.

The curves  $E_{L_1}$ ,  $E_{L_2}$ , and  $E_{L_3}$  in Figure 52 were calculated with the familiar rule-of-mixture expression which applies to firmly bonded constituents. The curves identified by  $E_{L*1}$ ,  $E_{L*2}$ , and  $E_{L*3}$  were calculated by Greszczuk's equation shown above. The ratio of unbonded fibers to total fiber fraction in each of the three curves was assumed constant. The ratio, however, varies from curve to curve;  $k$  is 0.20 in composites containing the highest modulus fibers and 0.35 for the lowest modulus fibers. Although the spectrum of fiber contents is not as great as one would desire, the available data, nevertheless, appear to conform systematically with calculated values. An experimental confirmation of the fraction of unbonded fibers is obviously a difficult task. It has been suspected, on the basis of empirical evidence, that the interfacial bond in this composite system was not strong. The results in Figure 52 represent the first quantitative appraisal of this contention.

The shear modulus of unidirectional composites has been measured as a matter of practice over the course of this program. Various aspects of this property have been discussed in the past, i. e., effect of fabrication parameters on  $G_{12}$ , variation with porosity, variation with fiber content, and the agreement obtained with analytical results. The latter aspect was considered only for a fiber content of 45 percent. The curve depicted in Figure 53, however, was calculated for all fiber fractions from the expression used by Whitney.<sup>(33)</sup>

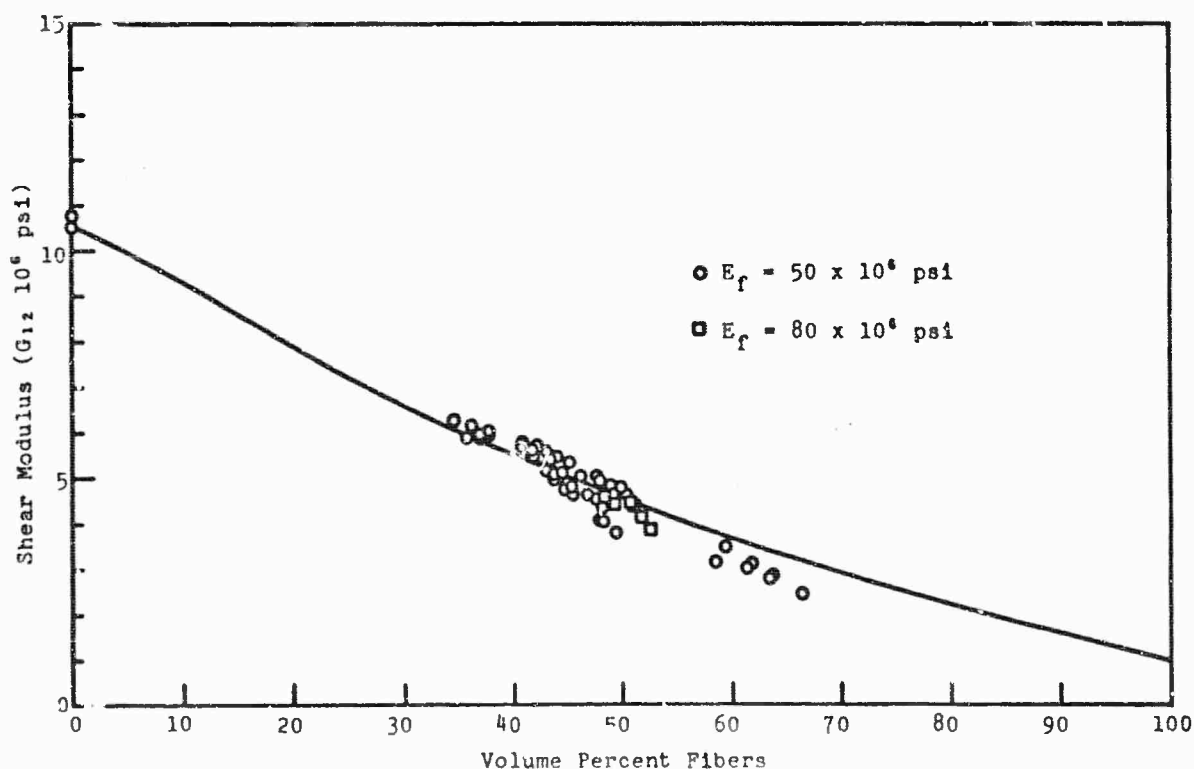


Figure 53. Experimental and Predicted Shear Modulus ( $G_{12}$ ) Values for Graphite-Fiber, Nickel-Matrix Composites.

N-22941



The experimental data are for specimens which contained no more than three percent porosity. Shear modulus values are included for composites fabricated with 50 and  $75 \times 10^6$  psi modulus graphite fibers. The value for  $G_{12}$  for the composite is obviously independent of the fiber modulus. An experimental value of  $G_{LT}$  for the fiber is not available. A "best fit" was obtained in graphite-fiber, resin-matrix composites (see Section VIII-B of Reference 2) with  $G_{LT} = 1.0 \times 10^6$  psi, a value that applies equally as well in this composite system. According to Hill (32), the bounding of shear modulus remains a difficult problem even though Hashin and Shtrikman (referred to by Hill) proposed a set of inequalities.

Two graphite-fiber, nickel-matrix composite specimens were tested in torsion by using the procedure outlined in Section V-B of the Third Annual Report.(3) The specimens were hot-pressed as bars, but they were subsequently ground into rods with a diameter of 0.130 inch. The results of one torsion test are shown in Figure 54. Similarly, the behavior of a resin composite containing the same graphite yarn employed in the metal matrix composite is also shown in Figure 54. Shear strengths of approximately 13,500 and 4200 psi were obtained for the metal and resin matrices, respectively. The angular displacement of nickel was measured up to maximum applied torque of 5000 inch-grams (shear stress of approximately 31,500 psi). The results are shown in Figure 54 to 3000 inch-grams; the behavior to 5000 inch-grams is essentially a linear continuation. Deviation from linearity occurs when the torque exceeds 500 and 250 inch-grams for nickel and for the nickel-matrix composite, respectively. Shear moduli approximately  $11 \times 10^6$  and  $5 \times 10^6$  psi for nickel and the metal matrix composite, respectively, were calculated from the elastic portions of the torsion curves.

#### D. Properties of Composites Fabricated From Tapes

The fabrication of a unidirectional and a 5-ply orthogonal plate from composite tapes was outlined in Section V A-2 of this report. The microstructure of a section cut perpendicular to the unidirectional fiber axis is shown in Figure 55. Spacing between the white metal-rich regions is approximately 0.010 inch, the equivalent of a tape thickness. The high degree of densification achieved at the low fabrication temperature of 700°C is reflected in the microstructure. Specimens of a comparable 1/16 inch thickness which were fabricated directly from the nickel-plated yarn were approximately 5 percent more porous. The average properties for 0° specimens were:  $E = 31.9 \times 10^6$  psi,  $G = 5.15 \times 10^6$  psi,  $\sigma_{ult.} = 70,000$  psi, and percent theoretical density = 97.8. The strength value is particularly disappointing in view of the low temperature used in fabrication and the precautions taken to curtail fiber breakage. Nine specimens cut in the 0°, 45°, and 90° orientations from a 5-ply orthogonal laminate were also studied. This laminate was also prepared from prefabricated tapes. Microstructural studies revealed some microcracks created by thermal expansion differences between the transverse and longitudinal orientations. Bonding between the tapes was not so good in the orthogonal specimen as that obtained for the unidirectional laminate. Property values, as noted in Table XIV, indicate that no obvious advantage exists when preformed tapes are used rather than hot-pressed pre-aligned yarns. The latter fabrication procedure was described in Section III-D of the Third Annual Report.(3)

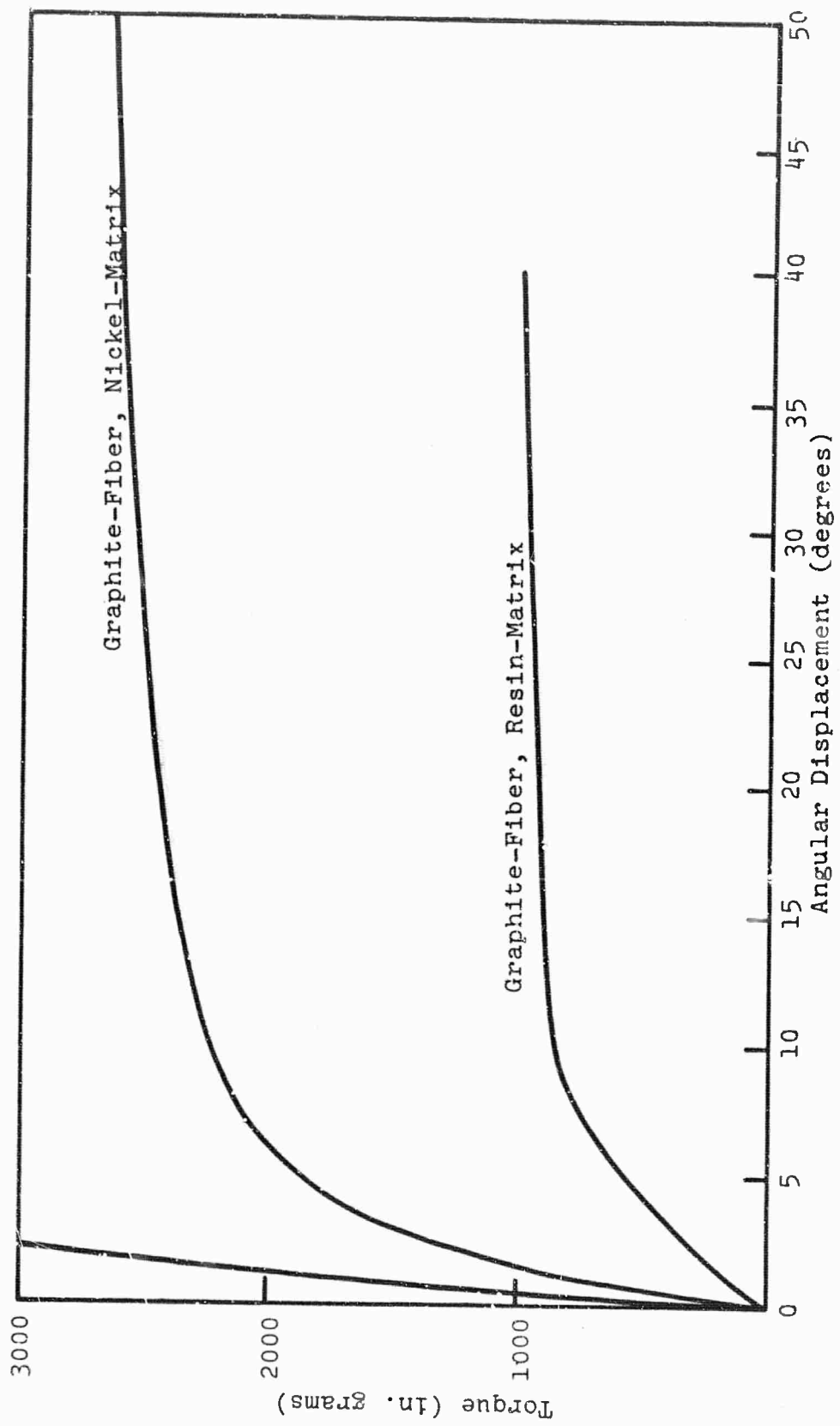


Figure 54. Torque vs. Angular Displacement Curves for Nickel, and Graphite-Fiber, Nickel and Resin-Matrix Composites.

N-22945

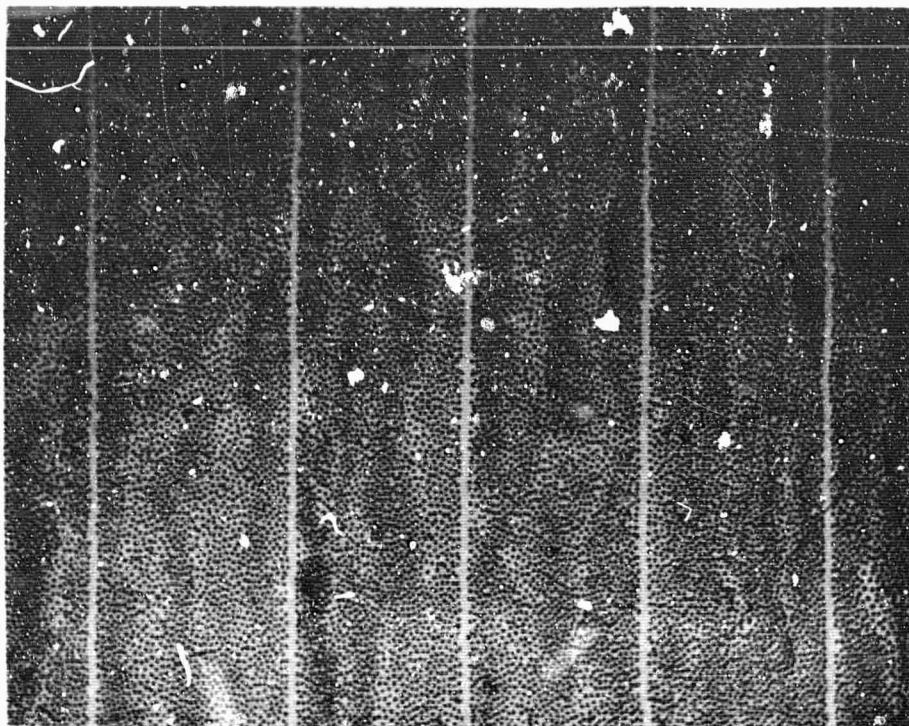


Figure 55. Microstructure of Graphite-Fiber Nickel-Matrix Composite Fabricated from Tapes. (Mag. 75X)

N-2300  
746-6-01

TABLE XIV  
PROPERTIES OF ORTHOGONAL LAMINATES FABRICATED  
BY DIFFERENT PROCEDURES

Fabrication Procedure	Property	Specimen Orientation		
		0°	45°	90°
Tapes	Young's Modulus ( $10^6$ psi)	21.0	10.7	10.1
Yarns	Young's Modulus ( $10^6$ psi)	21.4	11.9	17.2
Tapes	Tensile Strength ( $10^3$ psi)	41.2	13.0	23.7
Yarns	Tensile Strength ( $10^3$ psi)	28.1	16.3	33.2

## E. Composite Behavior - Elevated Temperature

### 1. Thermal Expansion Behavior

The expansion and contraction of both nickel metal and "Thornel" 50 graphite-fiber, nickel-matrix composite were remeasured in a fused quartz dilatometer. This effort is essentially a repetition of the work presented in the Fourth Annual Report (4) except that the specimen dilation is monitored differently in the two instances. The curves shown in Figure 56 indicate that a decrease in overall expansion occurs during the first two cycles. Cycles 3, 4, and 5 show little variation and are confined to the shaded regions of the figure. Permanent deformation observed after the second cycle in the earlier test (4) was not evident this time. The expansion coefficients and the hysteresis decrease with cycling observations (as shown in Figures 56 and 57) which represent additional differences from the earlier data. Permanent longitudinal deformation was not observed in the present study. Adequate explanation cannot be provided at this time for the differences in expansion behavior between the present and earlier work. The atmosphere is capable of being controlled more closely in the present dilatometer which might be a factor in these tests.

The expansion-contraction of nickel metal and of a composite (37 v/o<sub>f</sub>) in the transverse direction is shown in Figure 58. These data concur reasonably well with previously reported results (4). A discussion of the various coefficients of expansion and factors influencing those values was also discussed previously (4). The measurements were repeated at this time principally for increased accuracy and to clarify the cyclic behavior.

### 2. Thermal Cyclic Studies

The substantial mismatch in thermal expansion between the constituents of a graphite-fiber, nickel-matrix composite raises the question about degree of thermal fatigue resistance such a system might possess. In preliminary experiments, specimens were manually cycled ten times between room temperature and 500°, 750°, and 1000°C. Property changes in the composites resulting from the cycling were not great. Drastic changes, however, were observed when the work was extended to include additional test temperatures and to include a greater number of cycles (up to 1000 cycles) with test specimens containing "Thornel" 75 instead of "Thornel" 50.

Four 3-inch long x 9/16-inch wide specimens were hot-pressed at 1050°C under an applied pressure of 3000 psi. The four specimens were cut into smaller bars, each measuring 1/8-inch wide. Six of the bars cut from each large specimen were 1 1/2-inches long; one was retained in the original 3-inch length. The twenty eight small bars were mixed, and specimens were then picked at random to provide four groups, each containing one long bar and six short ones. One group was evaluated to determine the as-fabricated properties and the other three groups were cycled 100, 500, and 1000 times between 125° and 500°C. A similar procedure was followed for specimens that were cycled 500 times between 125°C and the following temperatures: 225°, 350°, 425°, 750°, and 1000°C. The density, Young's and shear modulus of the as-fabricated specimens are represented in Figure 59.

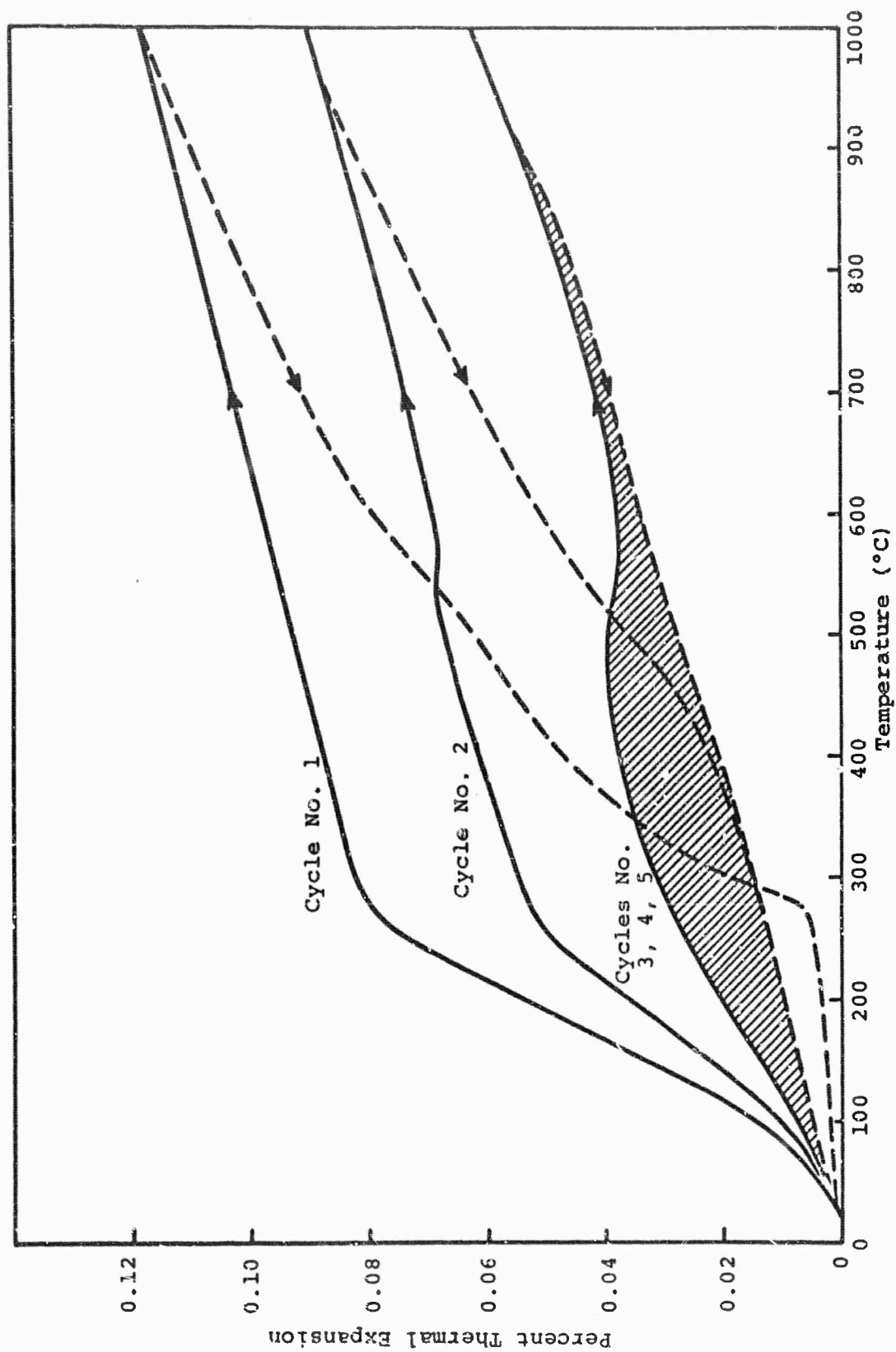


Figure 56. Longitudinal Thermal Expansion of Graphite-Fiber, Nickel-Matrix Composite.

N-23481

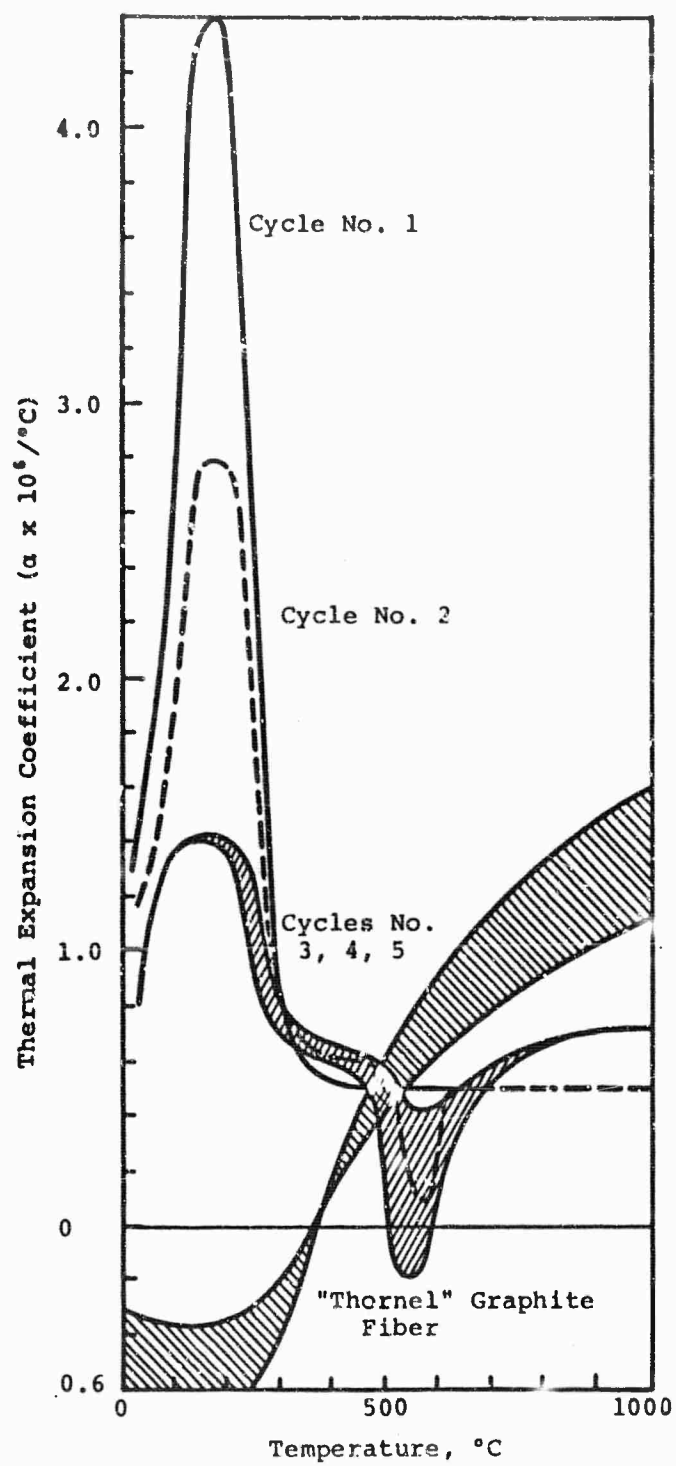


Figure 57. Thermal Expansion Coefficient of Graphite-Fiber, Nickel-Matrix Composite. N-23482

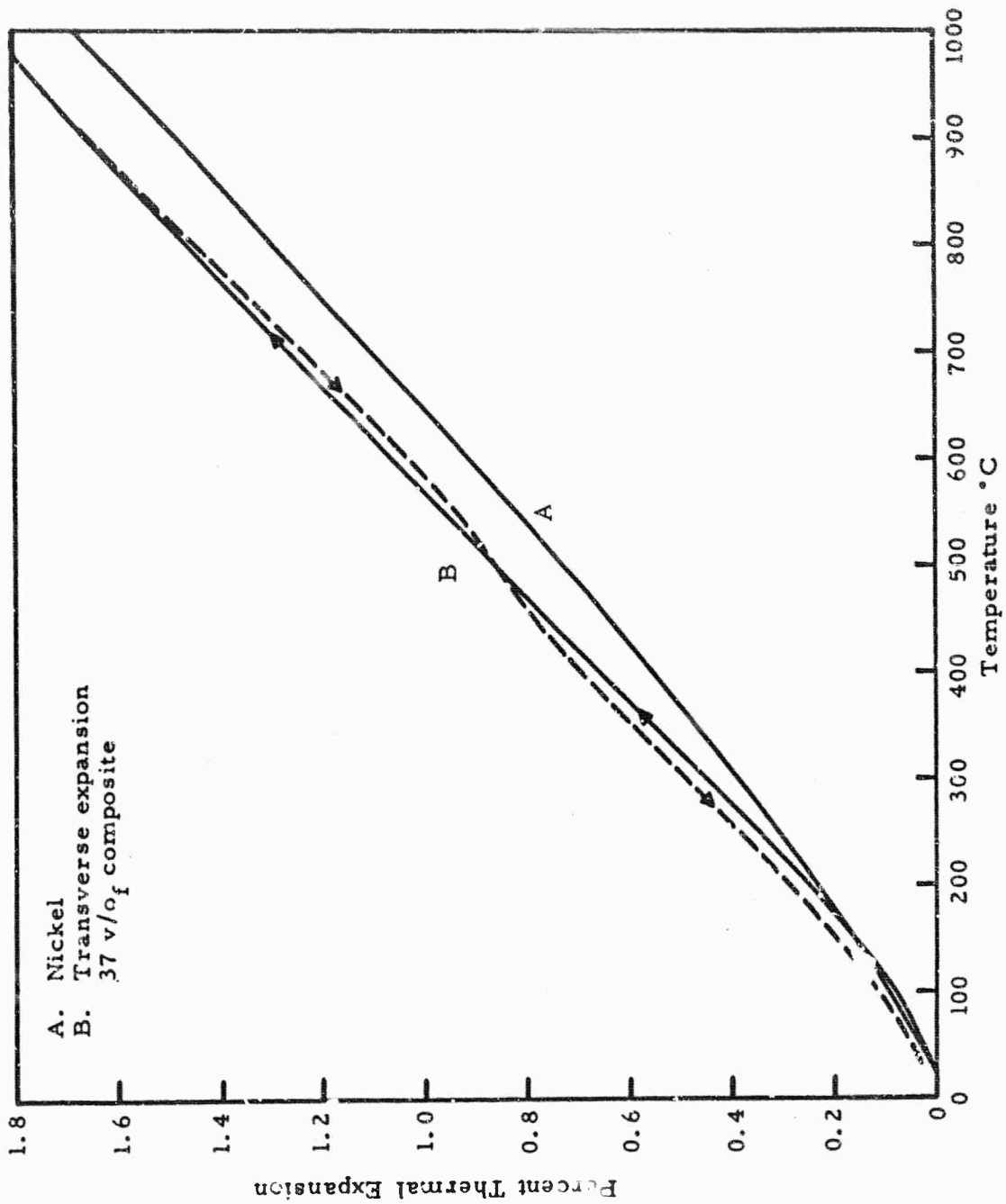


Figure 58. Linear Thermal Expansion of Nickel and of a Graphite-Fiber, Nickel-Matrix Composite in the Transverse Direction.



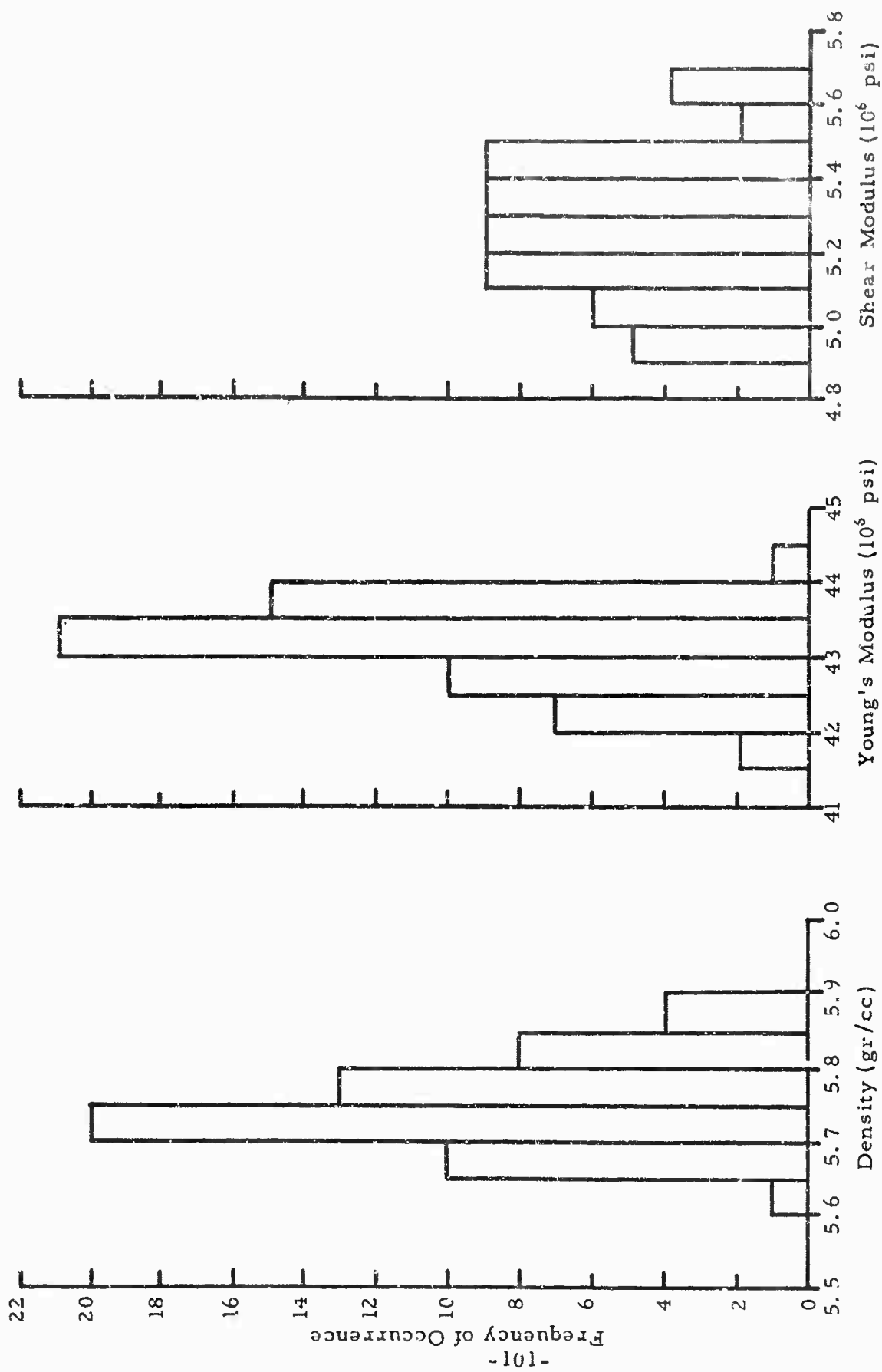


Figure 59. Properties of Composite Specimens Utilized in Thermal Cycle Experiments.

A schematic description of the equipment assembled for this study is shown in Figure 60. A variable speed motor (A) activates the microswitch (C) by means of a cam (B). When electric current passes to the damper motor (D), the horizontal arm is raised to a vertical position, tensioning the spring (E) and withdrawing the specimens from the furnace. The specimens are contained in a sealed fused quartz vial which is partially filled with argon. When the cam activated microswitch curtails flow of current to the damper motor, the tensioned spring causes the arm to return to a horizontal position, thereby lowering the specimen into the furnace.

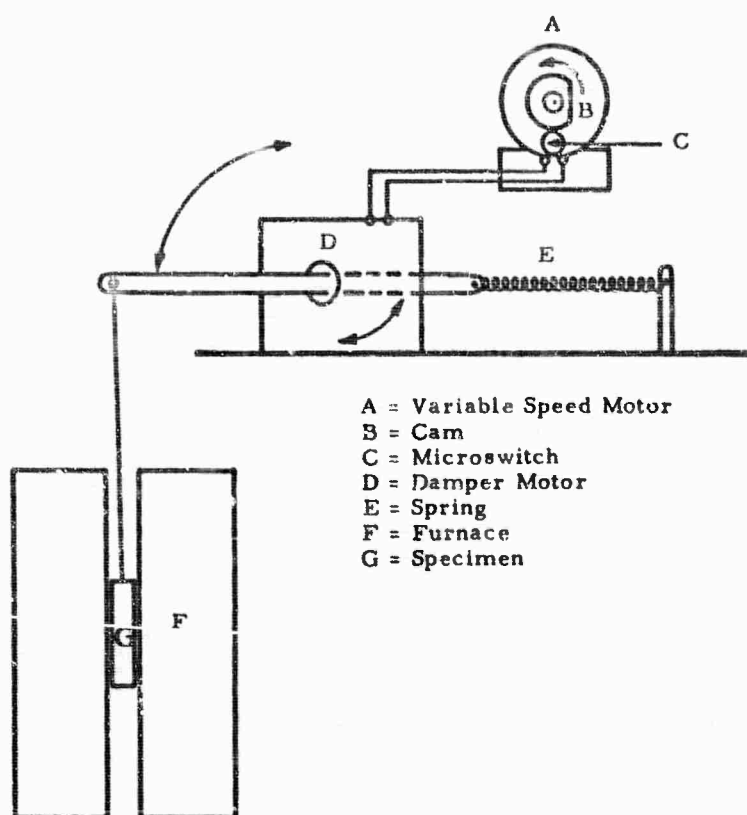


Figure 60. Schematic of Thermal Fatigue Apparatus.

N-23479

The type of cycle employed at 500°C is shown in Figure 61. It requires approximately 23 minutes to complete heating and cooling between 100° and 500°C. The on-off feature of the furnace controller is responsible for a temperature band depicted for the cycle. The heating rate and other features of the cycle are related to the furnace temperature, cam configuration, and its RPM.

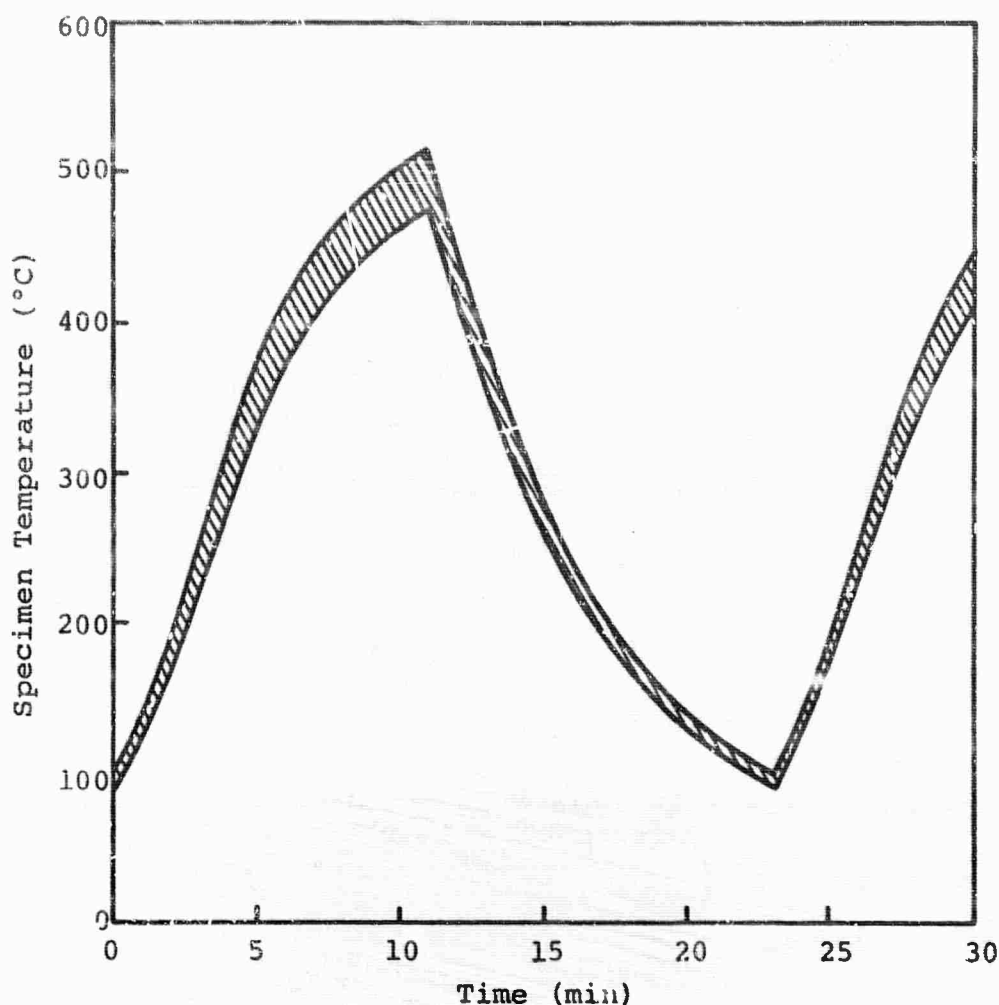
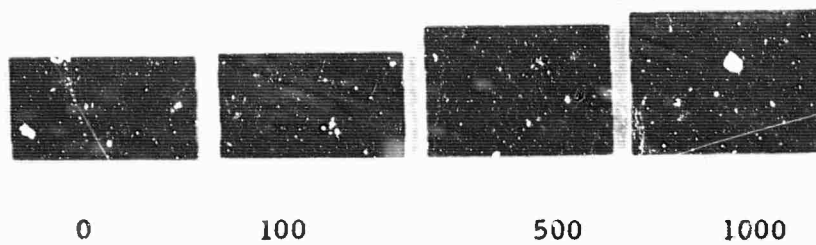


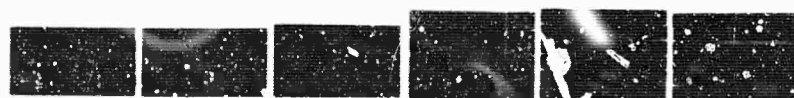
Figure 61. Thermal Fatigue Cycle Between 100° and 500°C. N-23476

The most astounding change in the specimens as a result of thermal cycling is the large increase in cross-sectional area. Photographs of the specimens are shown in Figures 62, 63, and 64. The increase in width can be judged by comparing with the first set of specimens in Figure 62 and 63. The photograph in Figure 64 is an enlargement of one specimen which was cycled 1000 times between 100° and 500°C. The dark areas are fibers which are devoid of nickel metal. This condition is illustrated very effectively by the photograph obtained with a scanning electron microscope and shown in Figure 65. The change in cross-sectional area evidently is the result of metal flow as depicted schematically in Figure 66. The effect depicted in this schematic is not thermal fatigue in the strictest sense but thermal "ratcheting"; a phrase which was appropriately used (34) to describe a similar phenomenon observed in zinc bicrystals. The ratcheting was attributed to a nonreversible distortion in certain grains created by grain boundary flow at elevated temperatures and transcrystalline slip at lower temperature. Material movement at the two temperature levels was the relaxation process in response to interfacial stress. Thermal cycling, therefore, produces a nonreversible distortion because the material flow is unbalanced.



N-23309

Figure 62. Change in Specimen Width as a Result of Elapsed Cycles Between 100° and 500° C.



230 350 425 500 750 1000

N-23646

Figure 63. Specimen Width After Cycling 500 Times Between 125° C and the Indicated Temperatures.

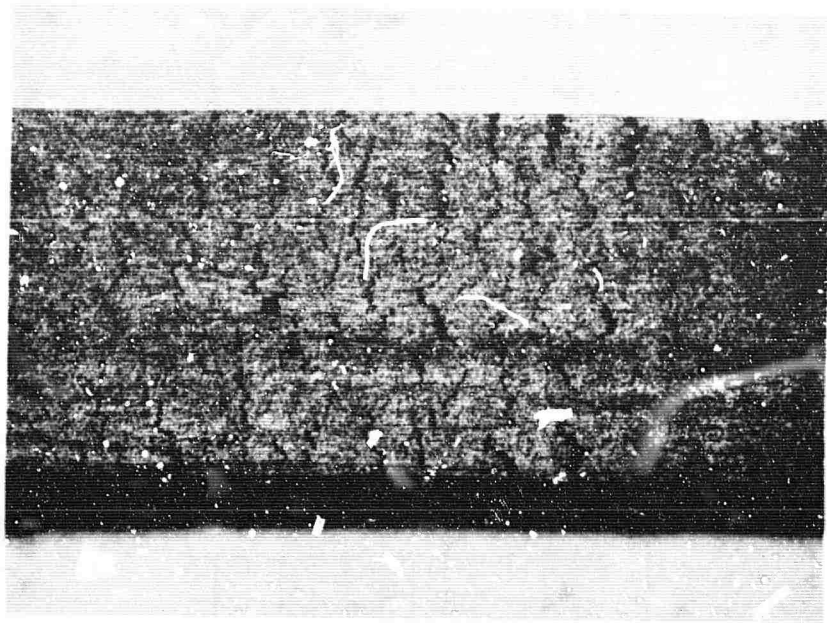


Figure 64. Surface Crazing in a Graphite-Fiber, Nickel-Matrix Composite After 1000 Cycles Between 100° and 500°C.

N-23310



Figure 65. Fibers Devoid of Nickel After Cycling 1000 Times Between 100° and 500°C. (500X Mag)

1080-1-S24

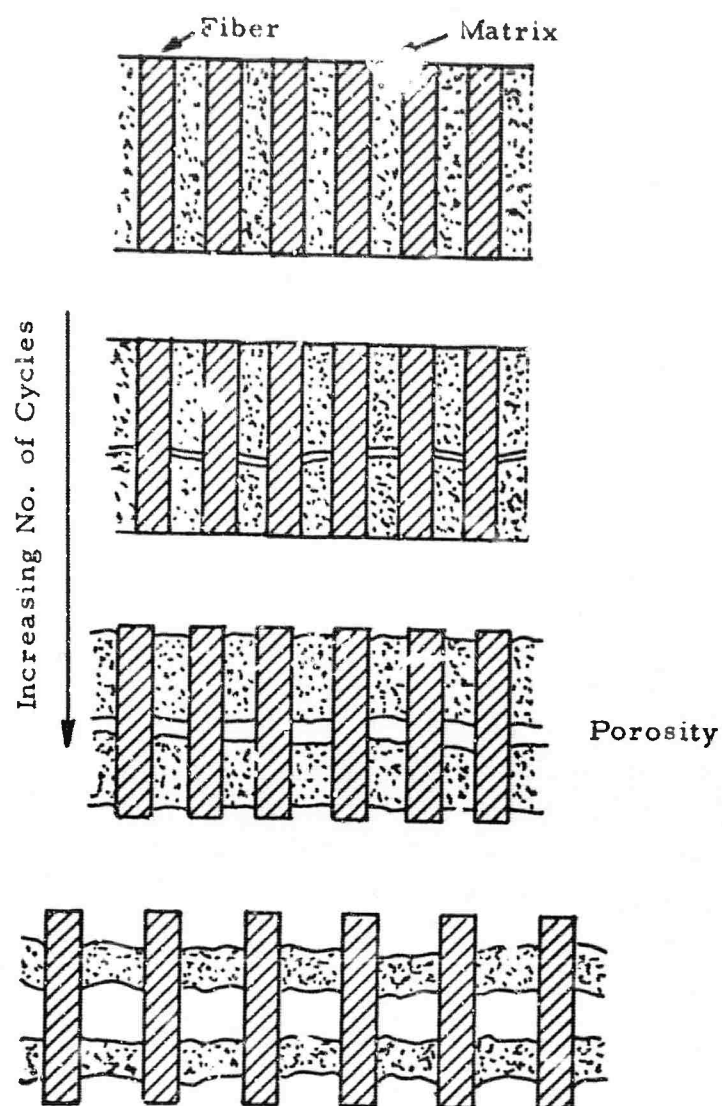


Figure 66. Redistribution of Matrix as a Result of Thermal Cycling.

Shear stresses are generated at the zinc bicrystal interface because the crystals have different thermal expansion coefficients. An analogous thermal expansion mismatch prevails at the graphite-fiber, nickel interface. The ratcheting, according to Figure 66, strives to minimize the contact area between fiber and metal. Each thermal cycle, presumably causes a slight increase in the fiber-fiber spacing as the metal flows into the region between the fibers. No change has been noted in the length of thermally cycled specimens because that dimension is controlled by the non-deformable graphite fiber. The low axial expansion of the graphite fiber and the high expansion coefficient of nickel places the latter in compression as the composite temperature is increased. The thermal expansion data in Figures 56 and 57 signify that plastic deformation probably occurs at temperatures above 200°C. Aiding the axial constraint quite possibly is hoop tension in the matrix as a result of slightly greater radial expansion of the fiber compared to the matrix. To complete the ratcheting process it is necessary that the metal contract along the fiber axis during the cooling process. This might occur in one of two ways. A poor interfacial bond coupled to the condition of a fiber contracting radially at a faster rate than the matrix would probably allow unhampered thermal contraction of nickel along the fiber axis. If, on the other hand, tensile stresses are generated in the matrix because constraints impede the thermal contraction, slippage is feasible if the tensile stress exceeds the interfacial shear strength. Exceeding the shear strength in tension but not in compression might arise because of different yield strengths; the yield strength decreases with increasing temperature. In principle, the distortion of nickel at the elevated temperature is consistent with grain boundary movement in the zinc bicrystal system but relaxation of the stress by slip at low temperatures is probably replaced by a different mechanism in graphite-fiber, nickel composites. The possibility cited above was simple slippage because the shear strength is exceeded by tensile forces. If this is the case, ratcheting might be curtailed in the graphite-fiber, nickel-matrix system by improving the interfacial bond.

The changes in specimen cross-section as a result of cycling are shown in Figures 67 and 68. It can be seen from Figure 67 that ratcheting does not occur unless the cycle band exceeds a particular  $\Delta T$  value; this is discussed subsequently. Increase in cross-section appears to be a maximum when the peak temperature in the cycle is 700°C. According to Figure 68, the specimen area increases with the number of cycles and has not approached an asymptotic value at 1000 cycles. The increase in area is accompanied by a porosity increase. Consequently, all properties are adversely affected (see Figures 69 to 74). The longitudinal expansion-contraction of specimens previously cycled to 500°C for varying times is shown in Figure 75. The total expansion decreases with increased cycling which is typical of behavior cited previously in Figure 56 for specimens heated and cooled from 1000°C. The fiber almost completely controls the composite expansion after 500-1000 cycles to 500°C; this behavior is reasonable since the nickel has no continuity in the axial direction.

The axial thermal expansion behavior of a graphite-fiber, nickel-matrix composite is shown in Figure 76. The specimen was heated to 350°C, cooled to 125°C, and reheated to 425°C. It is apparent that contraction-expansion in the interval 125° to 350°C is retraced without evidence of hysteresis.



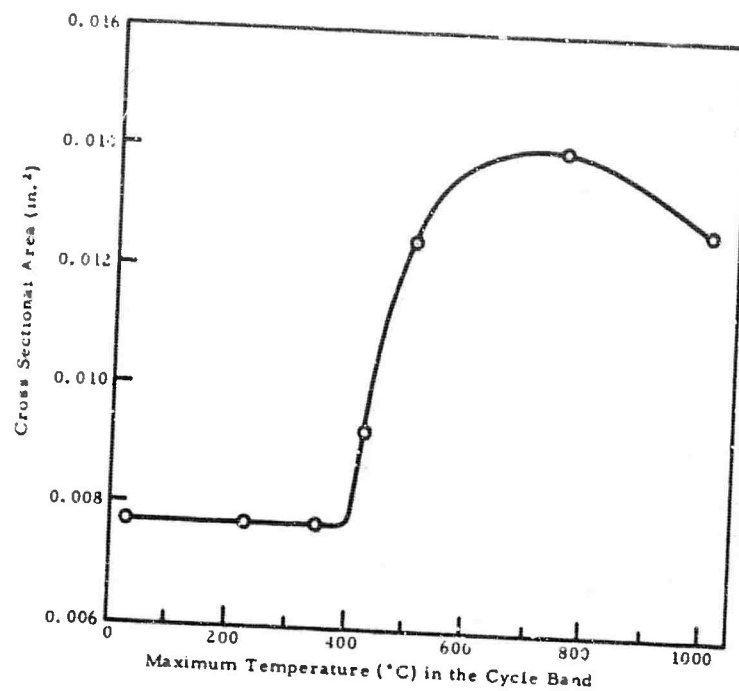


Figure 67. Specimen Cross-Sectional Area After Cycling 500 Times to Various Peak Temperatures

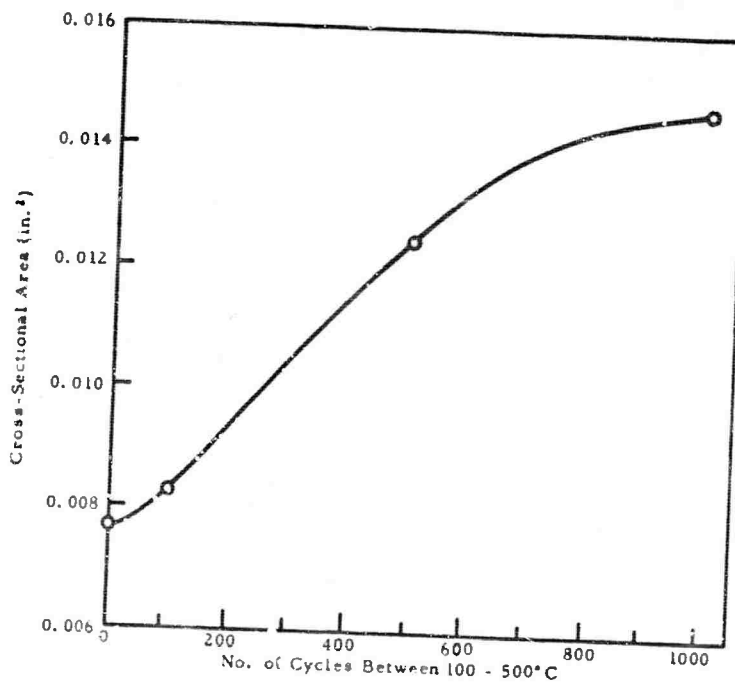


Figure 68. Specimen Cross-Sectional Area in Relation to Elapsed Cycles Between 100° and 500°C.

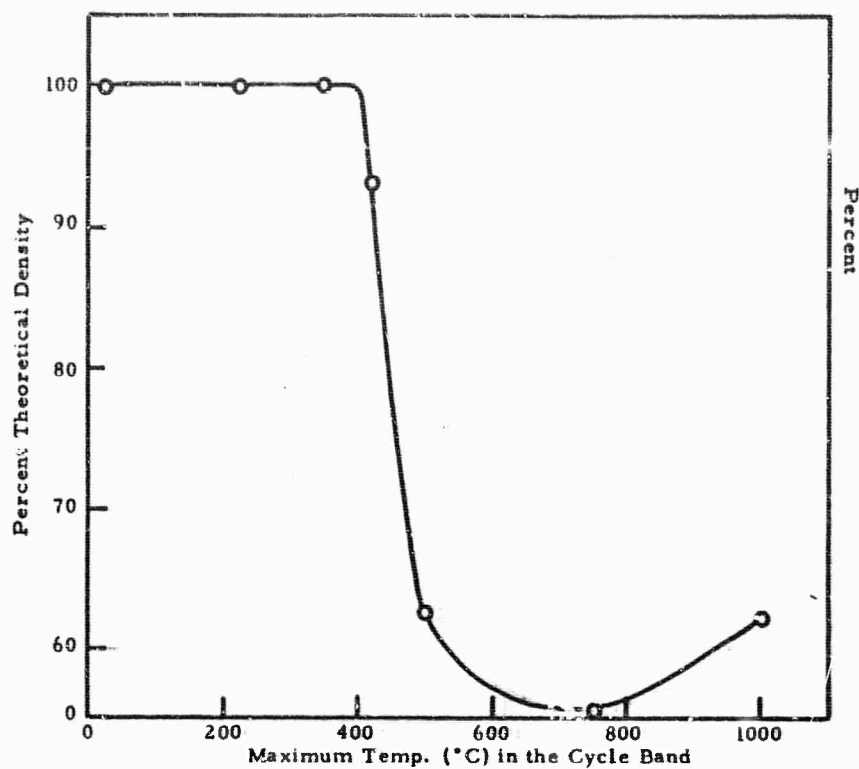


Figure 69. Effect of Peak Temperature in Cycle Band on Composite Density.

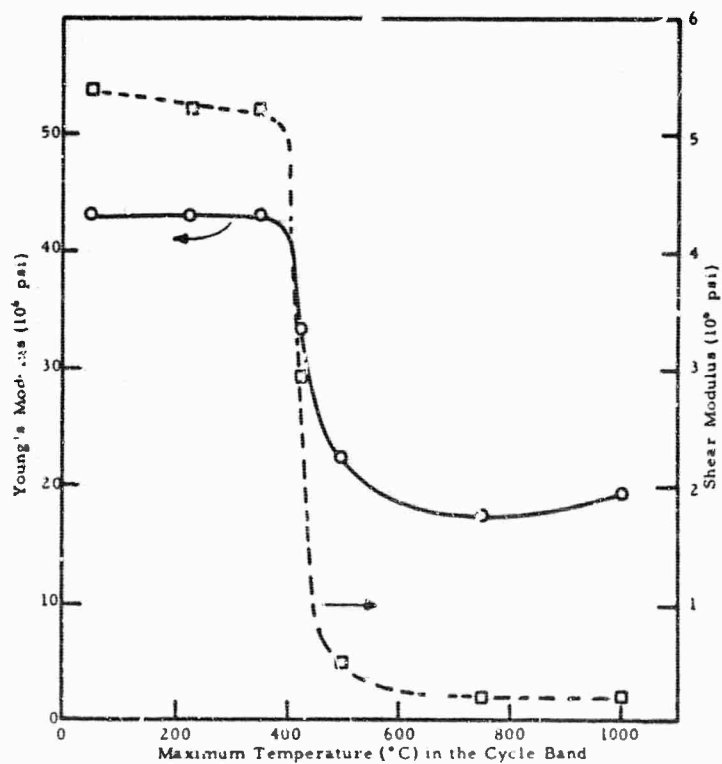


Figure 70. Effect of Peak Temperature in Cycle Band on Composite Young's and Shear Modulus.

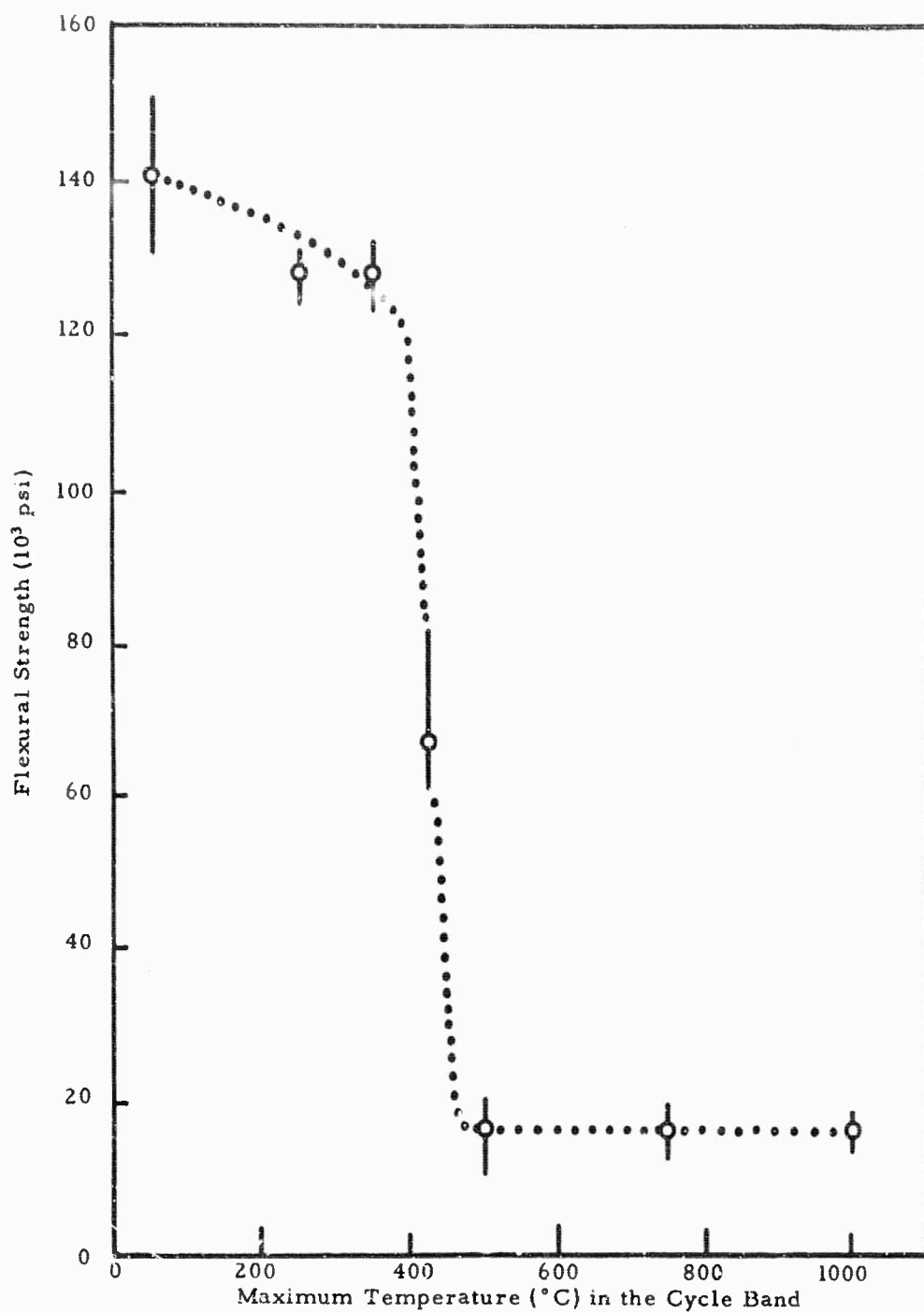


Figure 71. Effect of Peak Temperature in Cycle Band on Composite Flexural Strength.

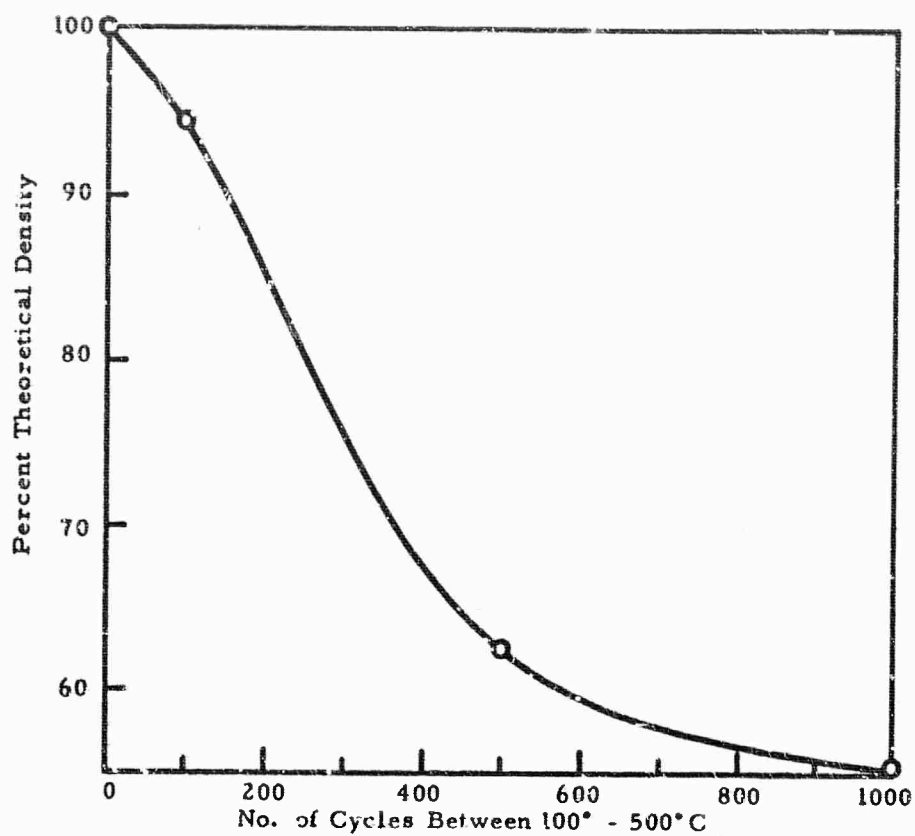


Figure 72. Effect of Elapsed Cycles on Composite Density

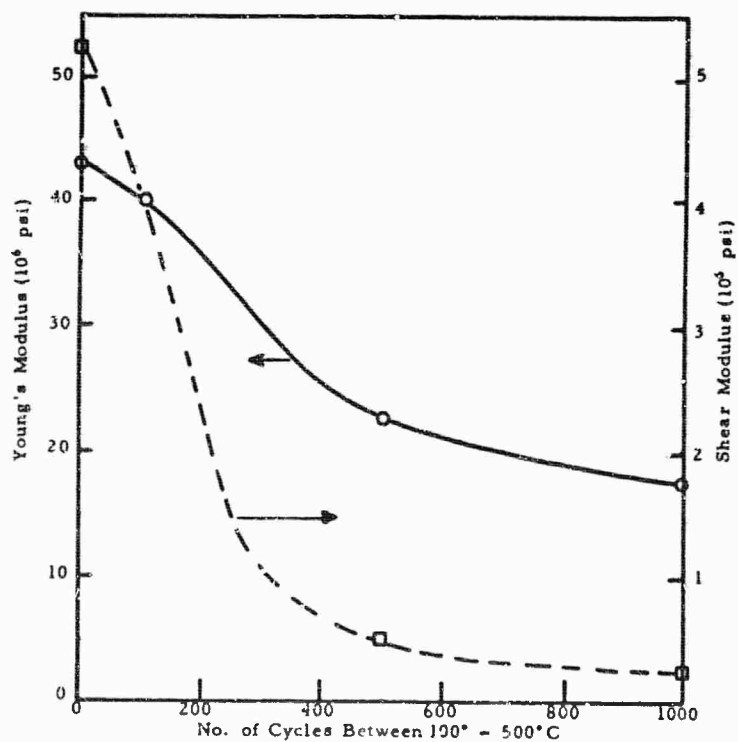


Figure 73. Effect of Elapsed Cycles on Composite Young's and Shear Modulus.

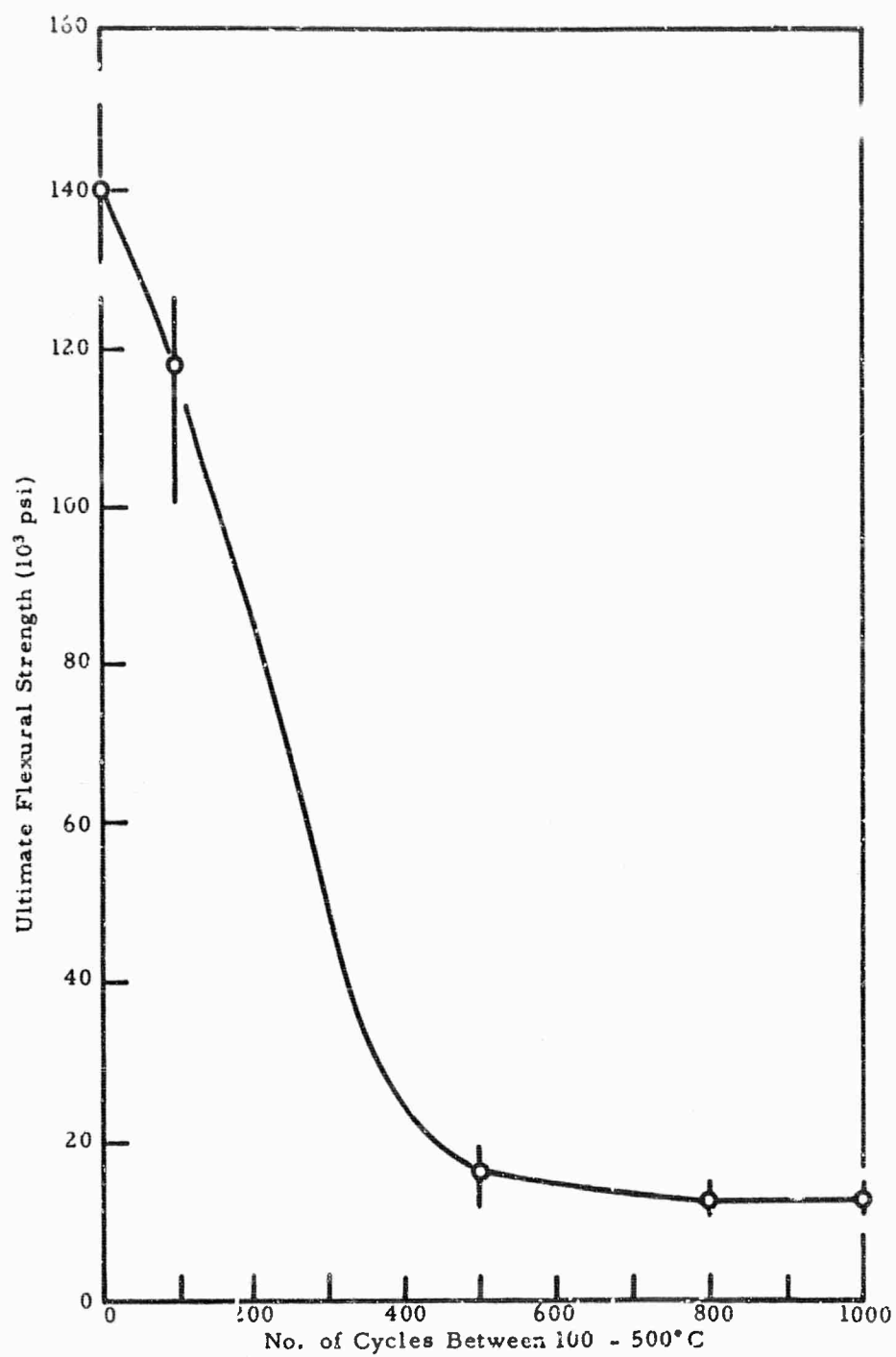


Figure 74. Effect of Elapsed Cycles on Composite Flexural Strength.

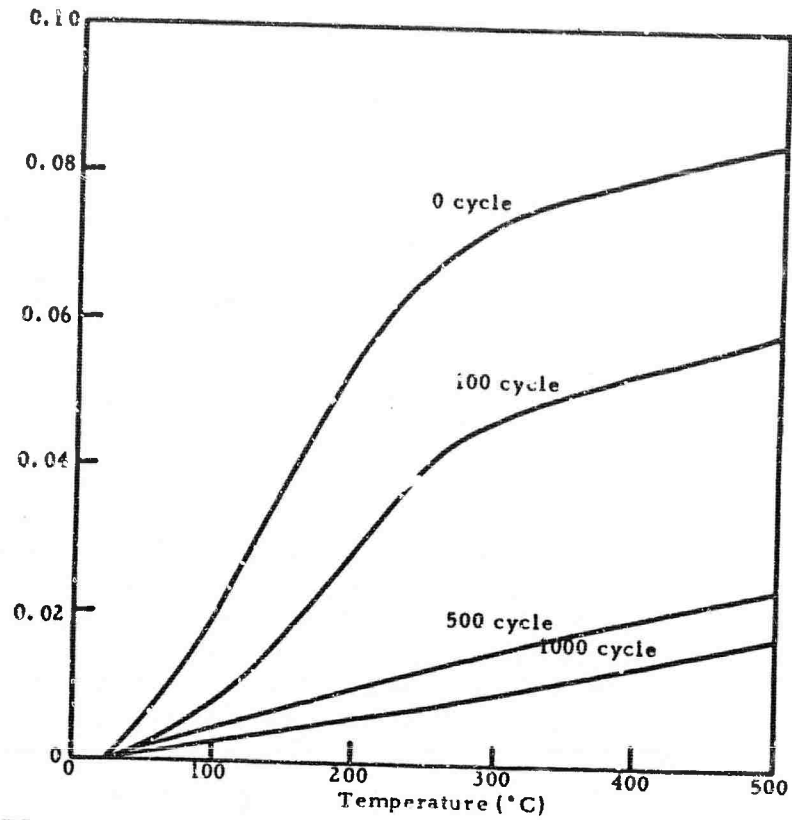


Figure 75. Effect of Elapsed Cycles on Composite Thermal Expansion.

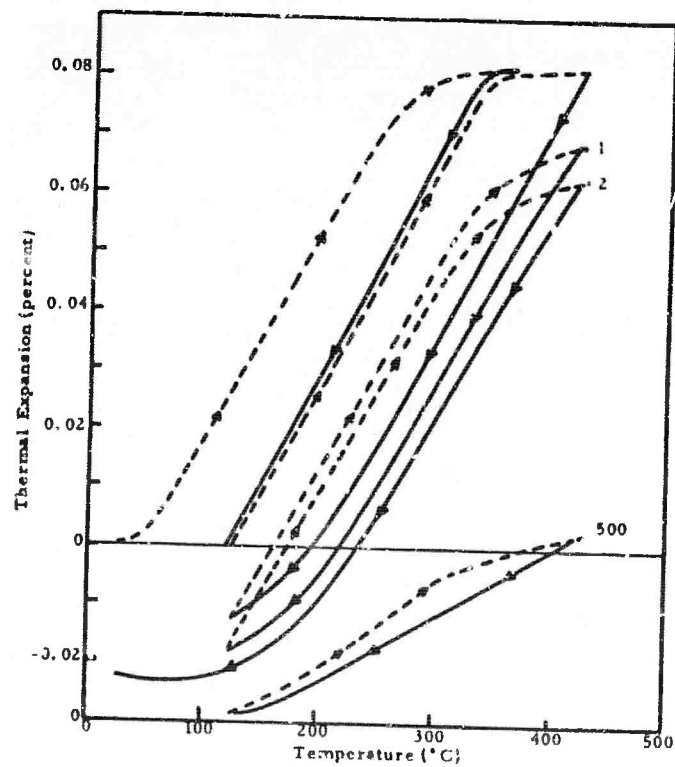


Figure 76. Effect of Cycle Band on Thermal Expansion Hysteresis in a Unidirectional Composite.

The same figure indicates that cycling between 425°C and 125°C, on the other hand, generates a hysteresis loop. The loop results from elastic-plastic deformation in the matrix which is a requirement for ratcheting. Thus, expansion-contraction between 125° and 350°C is elastic; a behavior which causes no permanent deformation in the specimen or property changes (see Figures 67, 69, 70, 71). When elastic-plastic behavior is encountered as was evidenced between 125° and 425°C, ratcheting is evident and composite properties deteriorate. Figure 76 also includes expansion-contraction of a specimen previously cycled 500 times over the interval 125°-425°C. The hysteresis loop is now asymmetric and a familiar change is evident; i.e., reduced total expansion. These results infer that it is possible to ascertain from thermal expansion measurements the possibility of a composite undergoing permanent deformation and the cycle bond required for such a change.

In an additional study relevant to ratcheting the changes in a transversely oriented composite specimen after cycling were observed by microscopic techniques. The specimen was polished and etched before heating and cooling was resumed. Figure 77a shows the composite before cycling and Figure 77b depicts essentially the same specimen area after 200 cycles between 125° and 500°C. The most obvious change in the microstructure after the 200 cycles are cracks consisting of fiber-matrix separations.

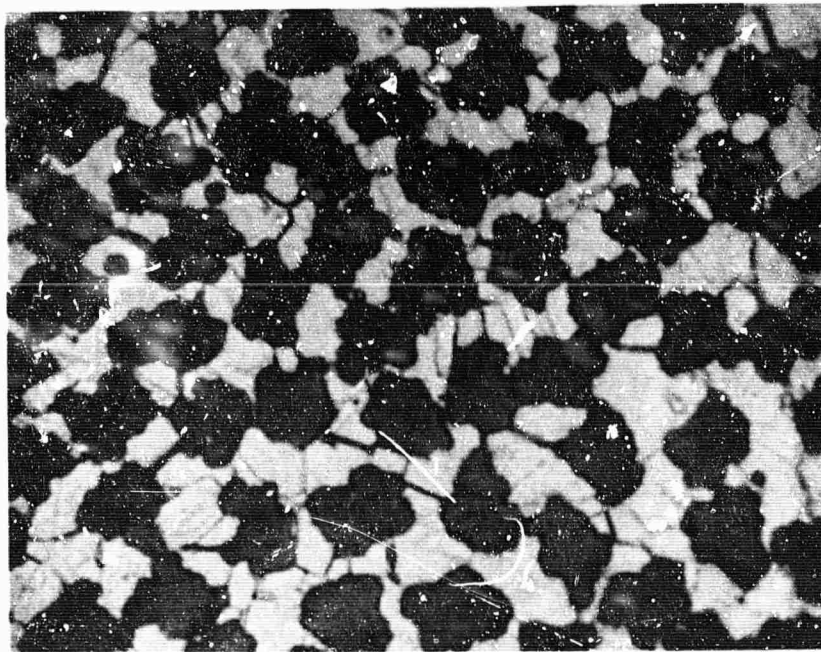


Figure 77a. Graphite-Fiber, Nickel-Matrix Composite Prior to Cycling.  
(1500X Mag)



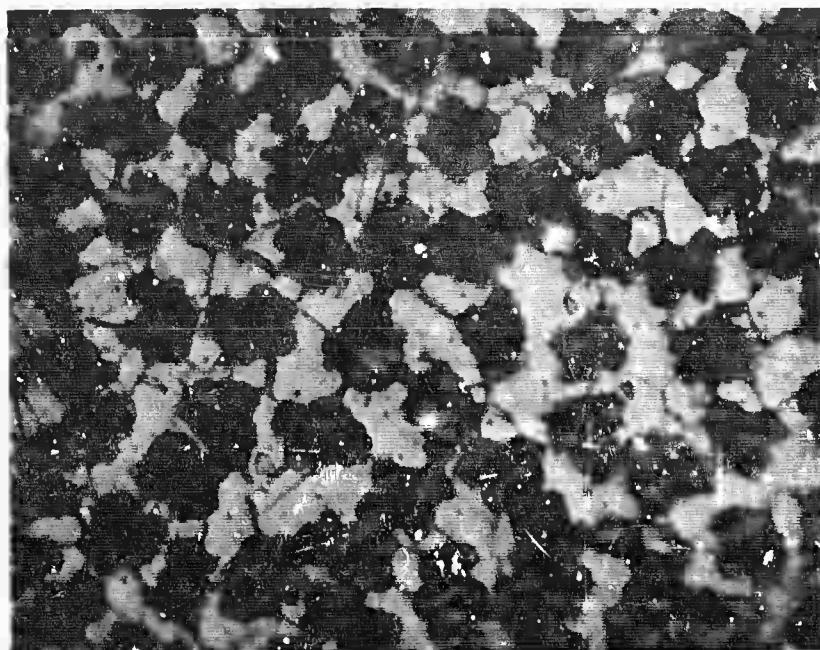


Figure 77b. Graphite-Fiber, Nickel-Matrix Composite After 200 Cycles Between 125° and 500°C. (1500X Mag)

This feature was prevalent over the entire specimen area. In general, the fiber ends are on the same plane as the matrix metal. After 350 cycles, however, the fiber ends and matrix metal are on different planes according to the SEM photographs in Figures 78 and 79; after 1000 cycles, the metal is substantially removed from the fiber ends (see Figure 80). An estimate of metal recessing along the fiber axis in relation to the number of cycles is shown in Figure 81. It can be seen that the recession rate increases with cycling but at this time the rate controlling factor is questionable; the interfacial bond is a prime suspect.

Ratcheting also occurs in as-plated graphite-fiber bundles. The single nickel-coated filament in Figure 82 shows separation in the deposit during the early stages of cycling. Several nickel granules remain on the fiber surface as the two sections of nickel recede from each other. After 1000 cycles, the yarn bundle has numerous separations in the nickel coating (see Figure 83); it appears that the coating thickness increases the further removed it is from the separation. This is probably due to metal pile up as resistance to flow increases.



Figure 78. Graphite-Fiber, Nickel-Matrix Composite After 350 Cycles  
Between 125° and 500° C. (1000X Mag) 1223-5-S1



Figure 79. Graphite-Fiber, Nickel-Matrix Composite After 350 Cycles  
Between 125° and 500° C. (5000X Mag) 1223-5-S2

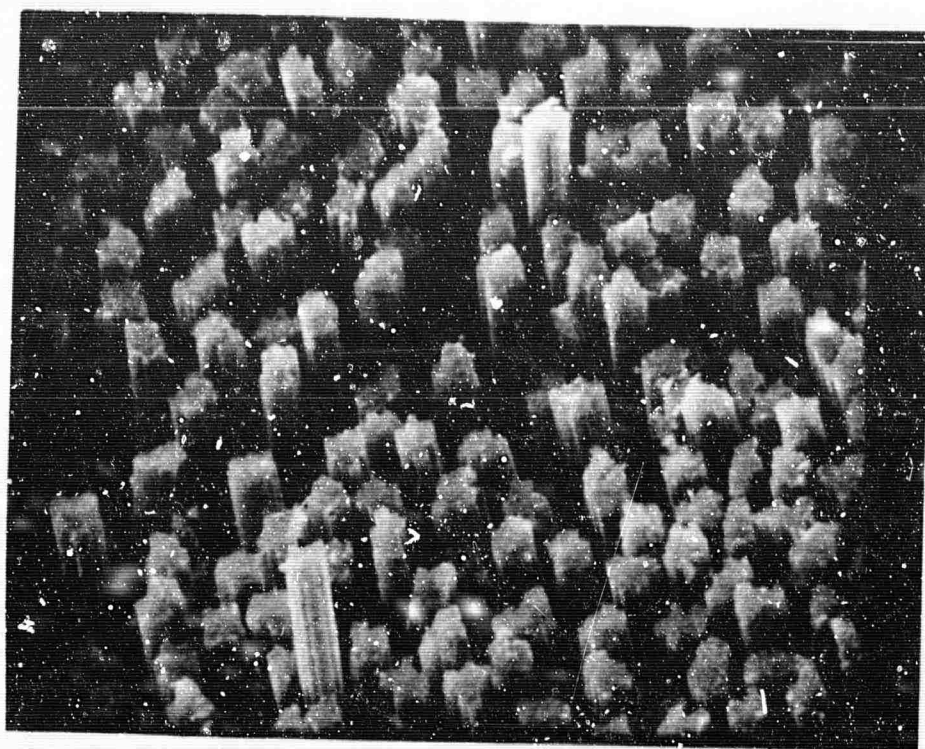


Figure 80. Graphite-Fiber, Nickel-Matrix Composite After 1000 Cycles  
Between 125° and 500° C. (1000X Mag)

1418-1-S1

Deformation by a ratcheting process is not a universal behavior for composite systems containing constituents with markedly different thermal expansion coefficients. In a fused quartz-fiber, aluminum-matrix composite, the fiber has an expansion coefficient similar to the longitudinal expansion of a graphite fiber and the aluminum metal expands almost twice as much as nickel over the same temperature interval. It would appear that ratcheting might occur in the  $\text{SiO}_2/\text{Al}$  system because plastic deformation is a distinct possibility. Surprisingly, after 750 cycles between 125° and 350° C, no change was discernible in the dimensions of a 50 v/o  $\text{SiO}_2$ -fiber, aluminum-matrix composite. Longitudinal expansion and contraction of the unidirectional composite in Figure 84 depicts a well-defined hysteresis loop for the temperature interval considered in the cycling experiment. The  $\text{SiO}_2$  fiber is thermally isotropic and has elastic properties which differ appreciably from "Thornei" high modulus fibers. These factors appear to be secondary, however, to the interfacial bond differences in the two systems. There is reason to believe that if bonding could be developed between graphite fiber and matrix to the degree which prevails in the  $\text{SiO}_2$ -fiber, aluminum system, ratcheting would become secondary to fatigue in cyclic operations.

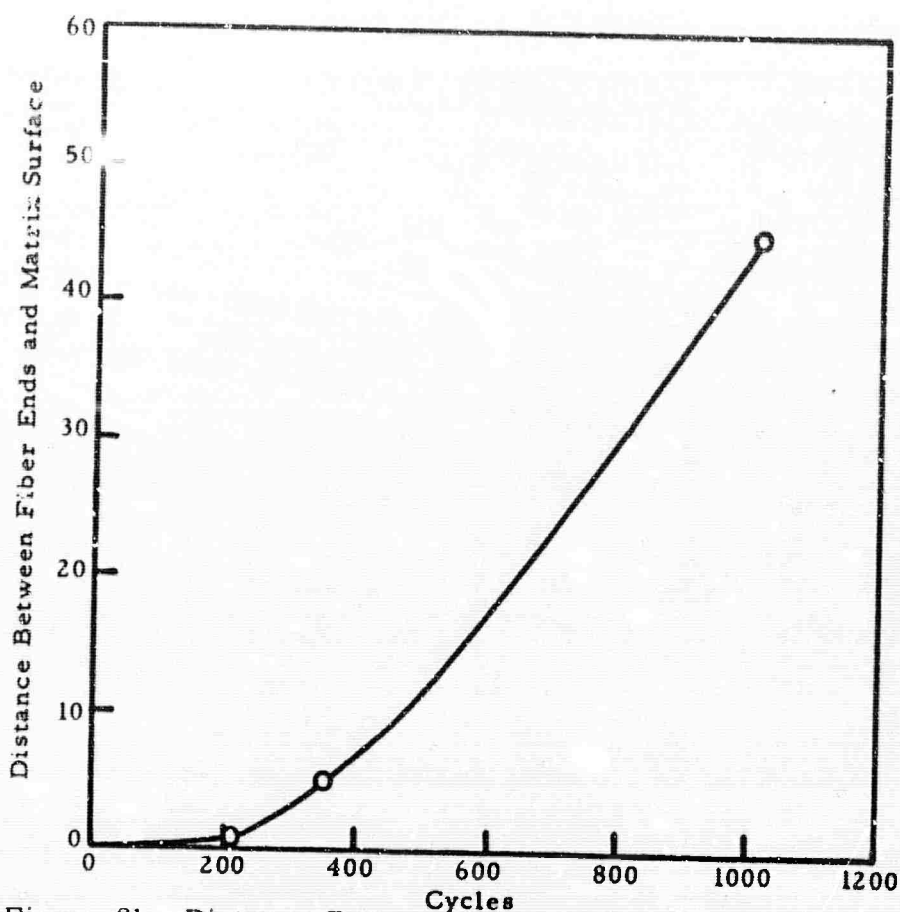


Figure 81. Distance Between Fiber Ends and Matrix Surface After Cycling in the Interval 125° - 500°C.

Attempts to constrain ratcheting by using orthogonal lay-up patterns in graphite-fiber, nickel-matrix test specimens were unsuccessful. The photograph in Figure 85 reveals separated layers of the five-ply orthogonal specimen which was thermally cycled 500 times between 125° and 500°C. Separations in this instance occurred at the ply interfaces.

### 3. Young's Modulus at Elevated Temperatures

The Young's modulus of nickel-metal and nickel-matrix composites containing "Thornel" 50 and "Thornel" 75 graphite fibers was measured sonically while the specimens were heated to 1000°C and then cooled to room temperature. The composite specimens contained approximately 45 v/o fibers. These results are shown graphically in Figure 86. Included with current experimental data are published (35) Young's modulus values for nickel up to 650°C. The two independent sets of data for nickel are generally in good agreement. The Young's modulus of composites containing "Thornel" 50 graphite fibers is approximately 15 percent lower at 1000°C than at room temperature. The "Thornel" 75 composite modulus shows little change with temperature.



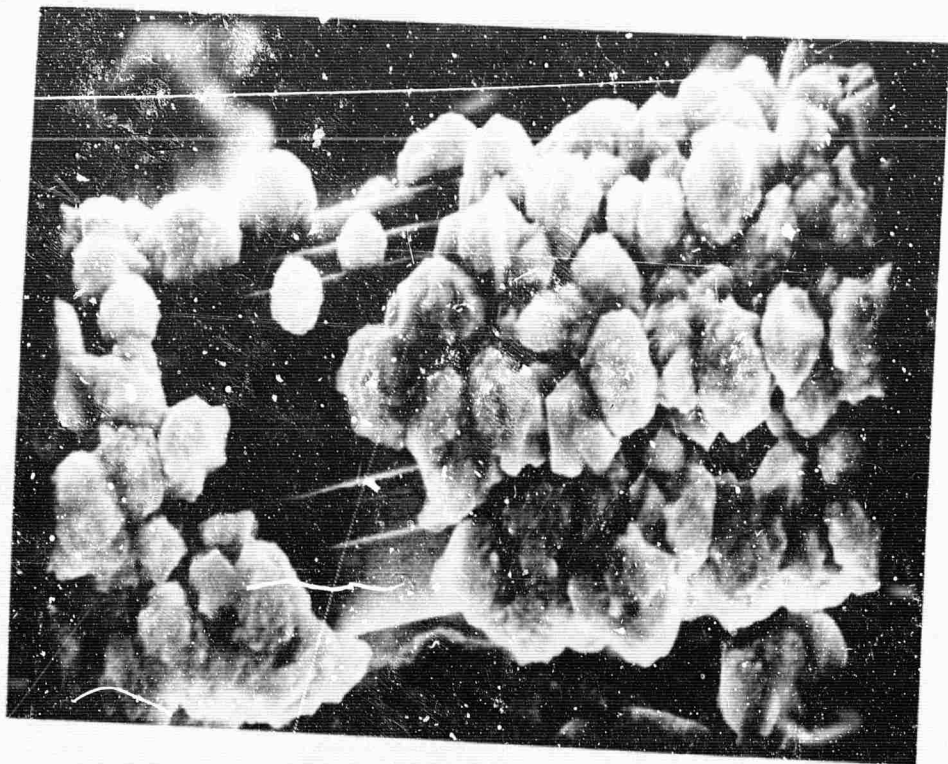


Figure 82. Initial Stage of a Discontinuity in the Nickel Coating After Cycling Between 125° and 500° C. (5000X Mag)

1223-1-S6

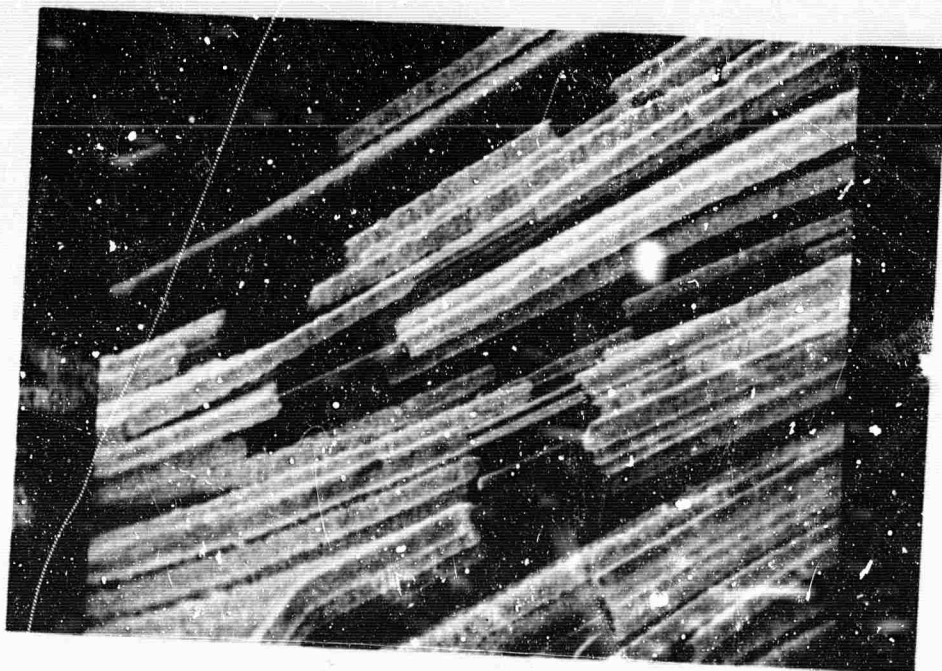


Figure 83. Multiple Discontinuities in the Nickel Coating on "Thornel" Yarn After 500 Cycles Between 125° and 500° C. (200X Mag)

1223-4-S4

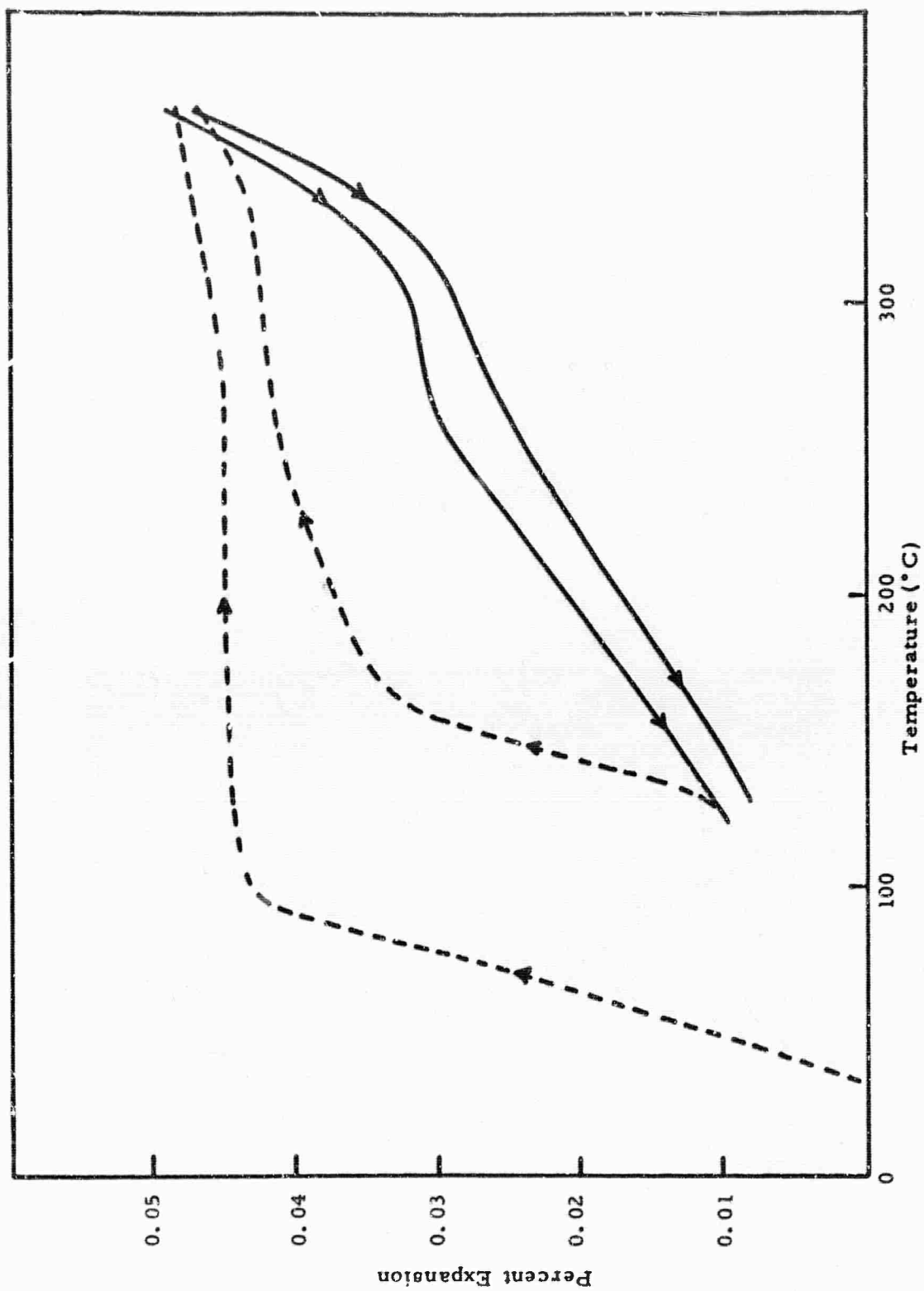


Figure 84. Longitudinal Thermal Expansion Behavior of SiO<sub>2</sub>-Fiber, Aluminum-Matrix Composite.

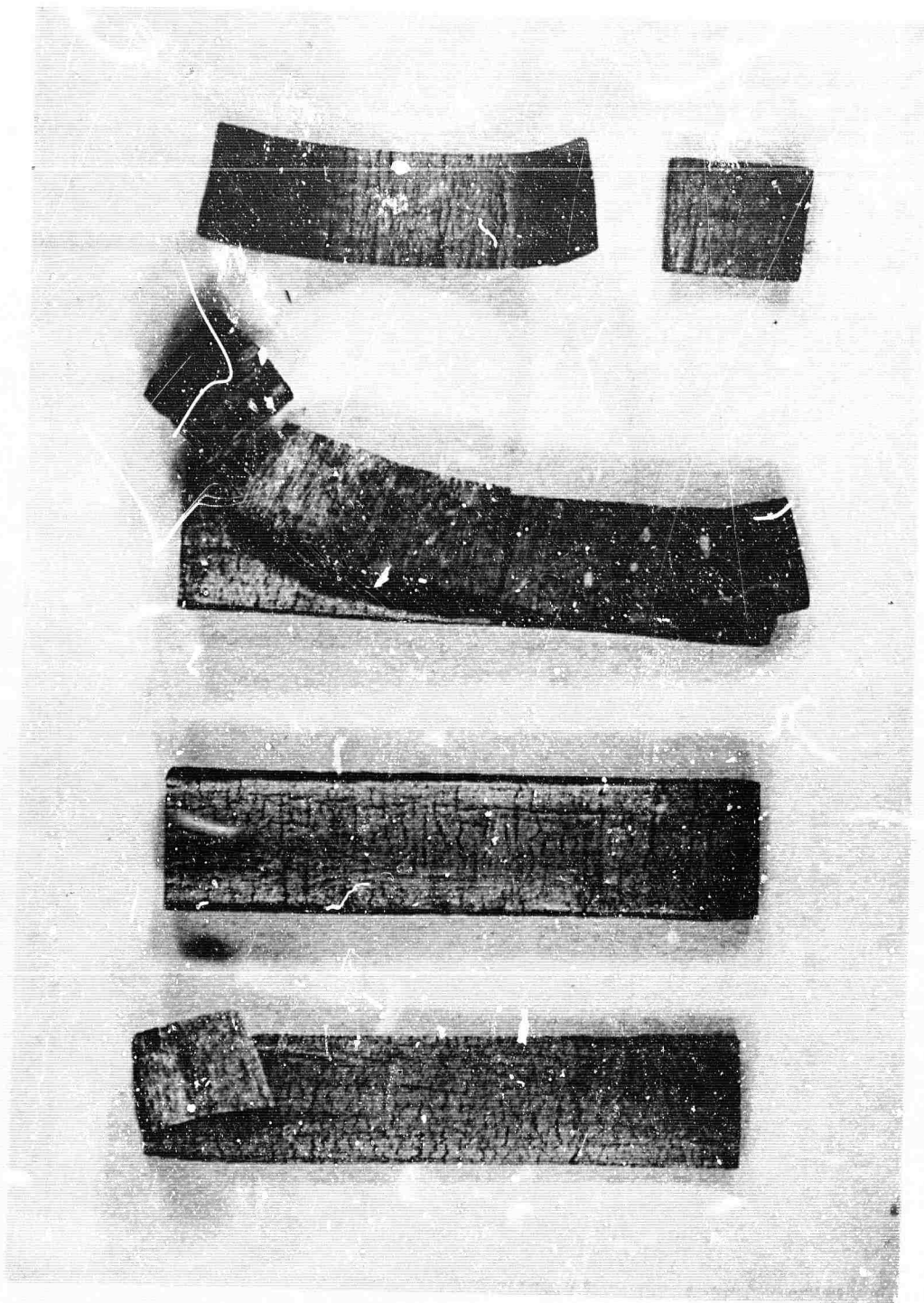


Figure 85. Delamination of a 5-Ply Orthogonal Specimen  
After 525 Cycles Between 125° and 500° C. N-23644

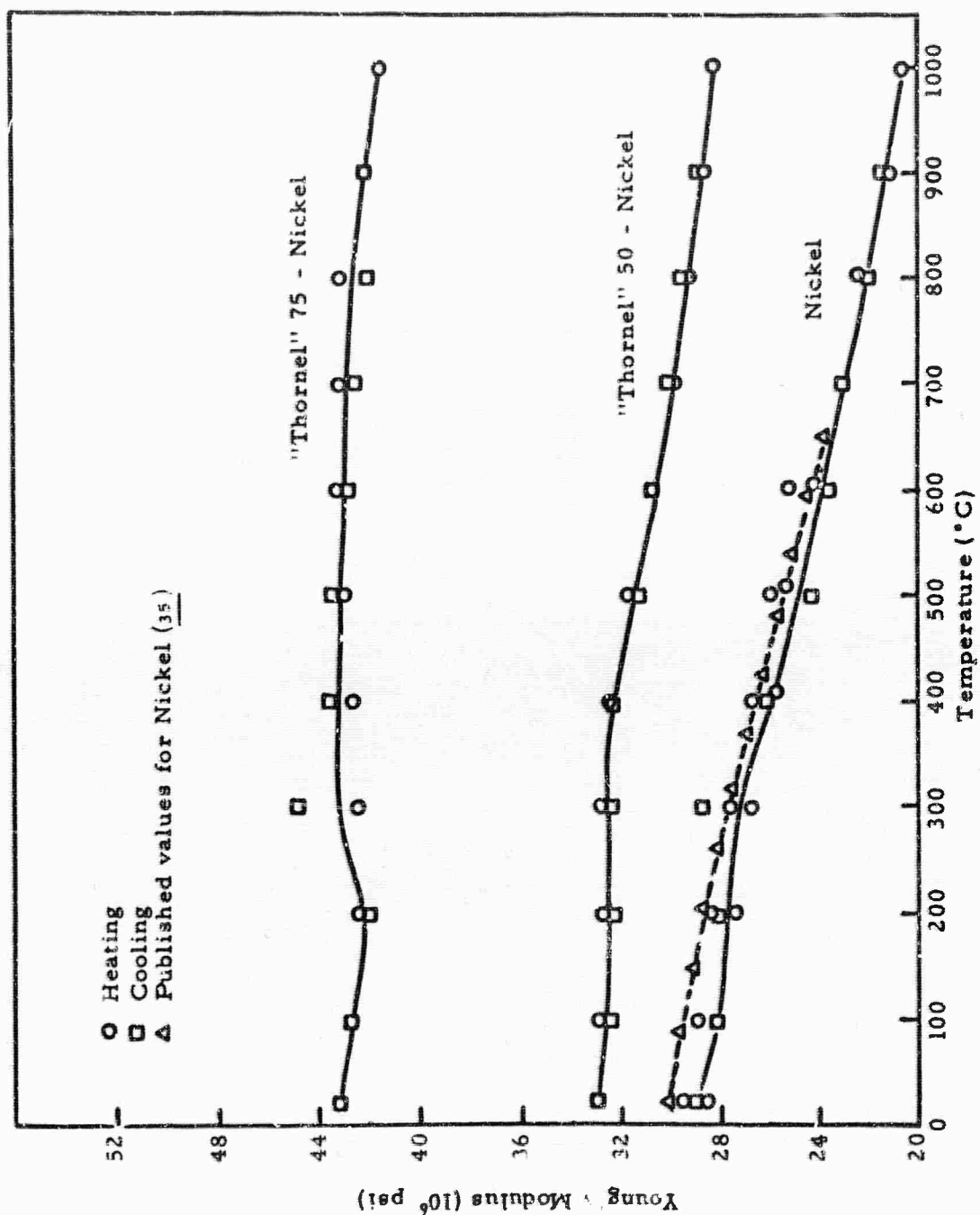


Figure 86. Young's Modulus of Nickel-Metal and "Thornel" 50 and "Thornel" 75 Graphite-Fiber, Nickel-Matrix Composites.



No anomalies are evident in the composite modulus values in the 200°-300°C region which can be ascribed to plastic deformation of the matrix in compression. The temperature region between room temperature and 500°C was studied in greater detail than is shown in Figure 86 with the intent of detecting an elastic-plastic transition in the matrix. The Young's modulus for both composites at 1000°C is also higher than expected if one assumes that the matrix is compressed beyond its elastic limit. On the basis of tensile stress-strain measurements shown in Figure 40, secondary moduli for "Thornel" 50 and 75 composites, for example, correspond to  $19 \times 10^6$  psi and  $31 \times 10^6$  psi, respectively. Reasons are presently unknown for the inconsistency between these data and rationale contrived from thermal expansion measurements.

#### 4. High Temperature Tensile Strength

Specimens fabricated to contain 45 v/o "Thornel" 75 fibers in a nickel matrix were tested in tension using essentially the same test procedures which were outlined in the Second Annual Report (2). The grips were modified at this time so that approximately twice the specimen area was under the compression plate; a factor which retarded slippage and shear failure to a great extent. The compression plate, formed from "Hastelloy"-C, had a slot equivalent to the specimen width but the depth was 0.005-inch less than the specimen thickness. Molybdenum screws were used to draw the compression plates containing the specimen against the main body of the holder. The close-fitting slot prevented lateral flow of the specimen at high temperatures. The molybdenum screws had a lower expansion coefficient than the Hastelloy so the specimen was compressed as temperature was raised. Three specimens were stressed to failure at each temperature. The scatter band and average results are shown in Figure 87; values reported previously in the Third Annual Report (3) for "Thornel" 50 composites are also shown. The composites containing "Thornel" 75 fibers have higher tensile strengths than composites containing the lower modulus fibers. Both series are similar, however, in that fiber pull-out is appreciable at 700°C and higher. It is believed that short fibers and poor interfacial shear strength are major factors contributing to the decrease in strength with temperature.

#### 5. High Temperature Flexural Strength

Four specimens were broken in three-point bending at each of five different temperatures which extended to 1000°C. The specimens were fabricated to contain 45 v/o "Thornel" 75 in nickel. The trend in breaking strength is shown in Figure 88 as a smooth curve drawn through the average values. The flexural strength at room temperature is higher than the tensile strength for similar type specimens. The compression strength was not measured on specimens containing "Thornel" 75 graphite fibers; specimens with "Thornel" 50 fibers, however, failed at approximately 100,000 psi.

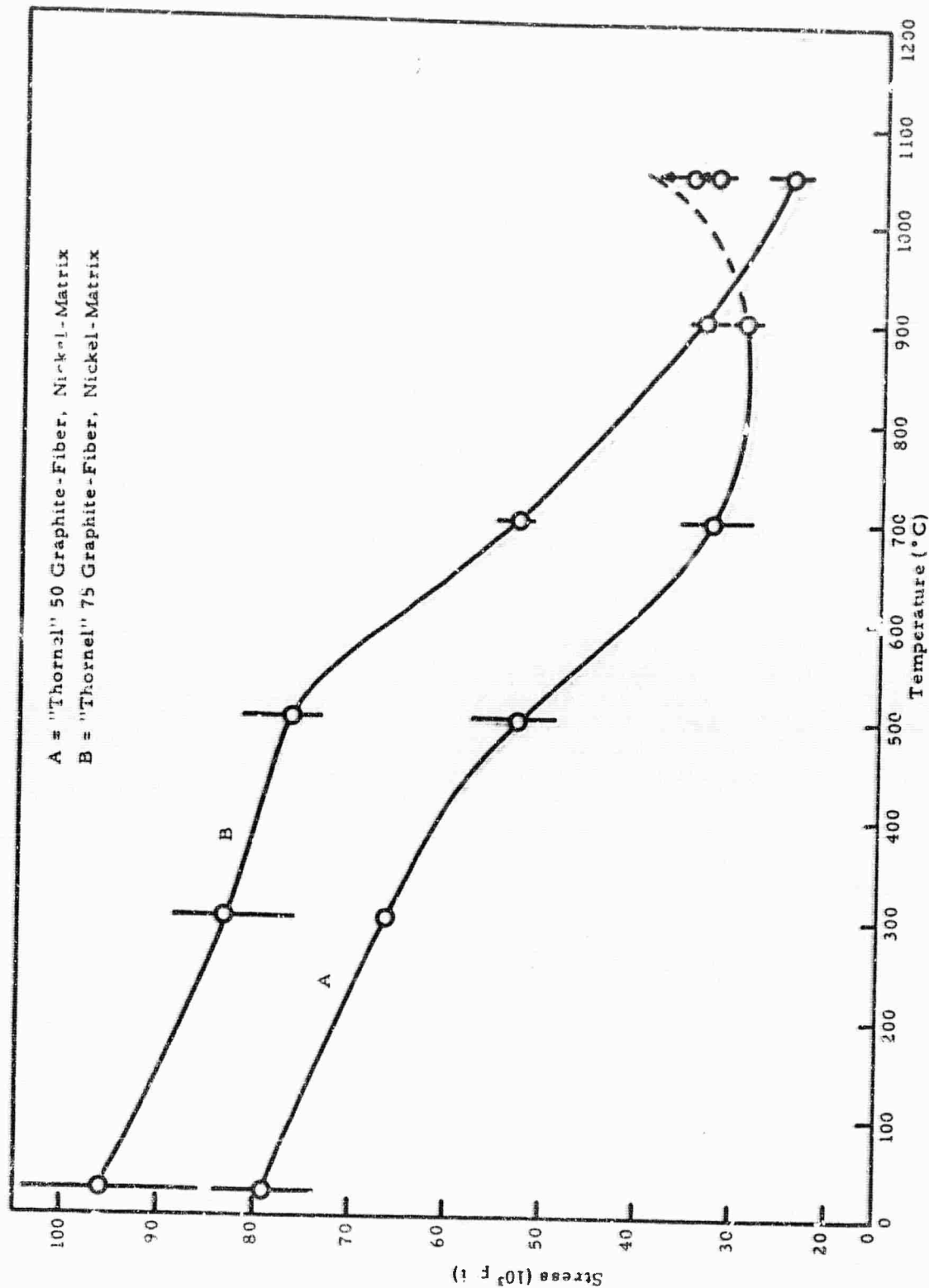


Figure 87. Tensile Strength of "Thornel" 50 and "Thornel" 75 Graphite-Fiber, Nickel-Matrix Composites.

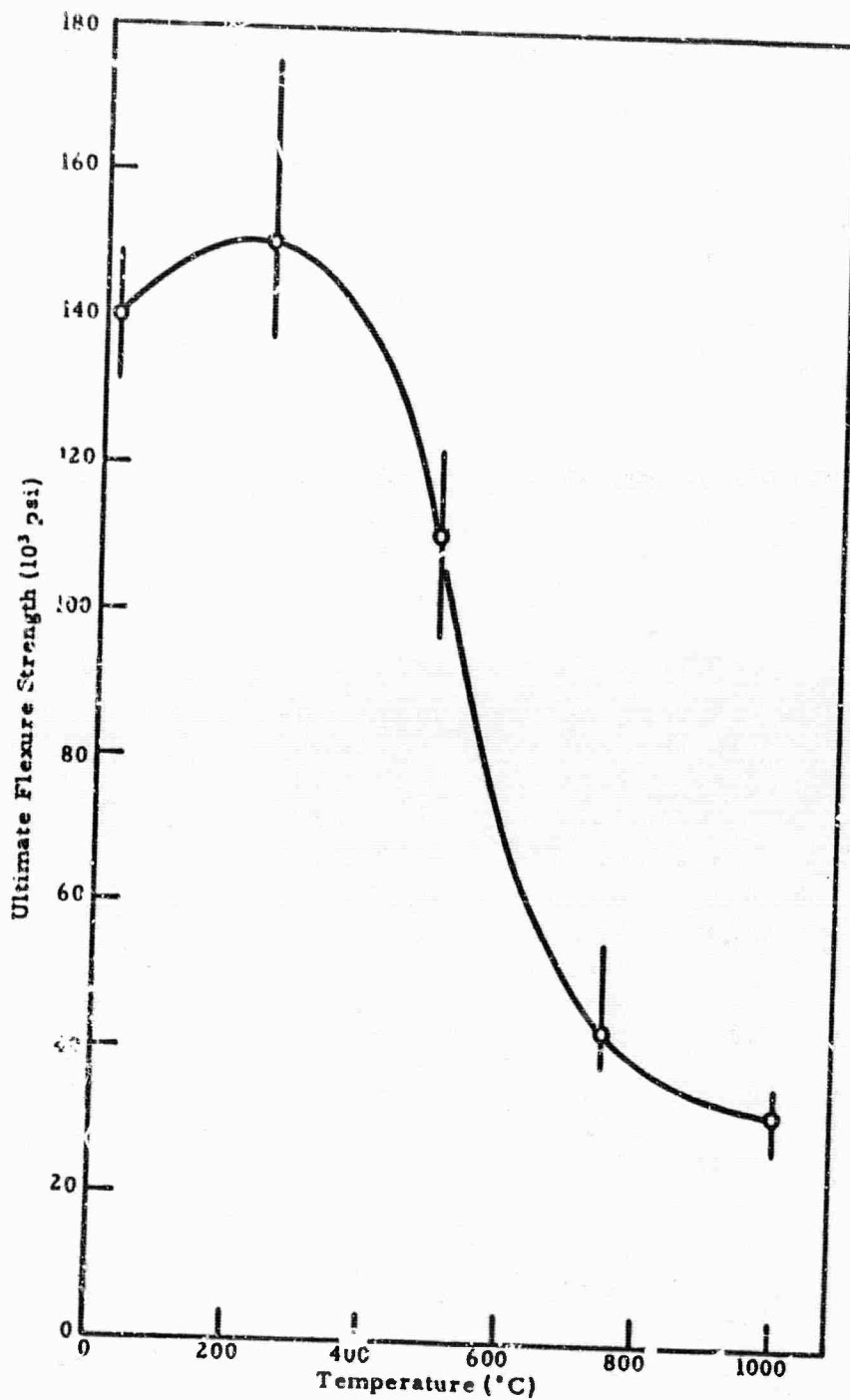


Figure 88. Ultimate Flexure Strength of "Thornel" 75 Graphite-Fiber, Nickel-Matrix Composite.

Interestingly, the flexure strength is even higher at 250° C than at room temperature. Some flexure strength values extended to approximately 180,000 psi at 250° C. The composite specimens show increasing deformation tendencies above 500° C (see Figure 89) which tends to obscure the significance of the strength values in those instances. It is apparent that the matrix has an important contribution to the composite behavior at the higher temperatures; probably because the poor interfacial bond is not complemented by a large fiber aspect ratio.

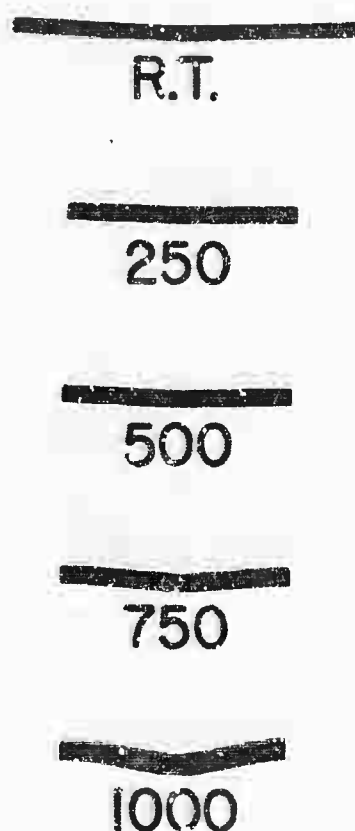


Figure 89. Flexure Specimens After Testing at the Indicated Temperatures.

N-23645

## 6. Stress Rupture

The time required to rupture "Thornel" 75 graphite-fiber, nickel-matrix composites at 500°C in vacuum was measured using the same test facility and gripping procedure described previously in conjunction with high temperature tensile testing. The stresses employed in this study varied between 40,000 and 62,000 psi. Four specimens were stressed to failure and testing was curtailed on one specimen which survived in excess of 100 hours without failure under 40,000 psi. These data are represented in Figure 90 from which it might be inferred that rupture strength at 500°C for long stress periods is approximately 40,000 psi.

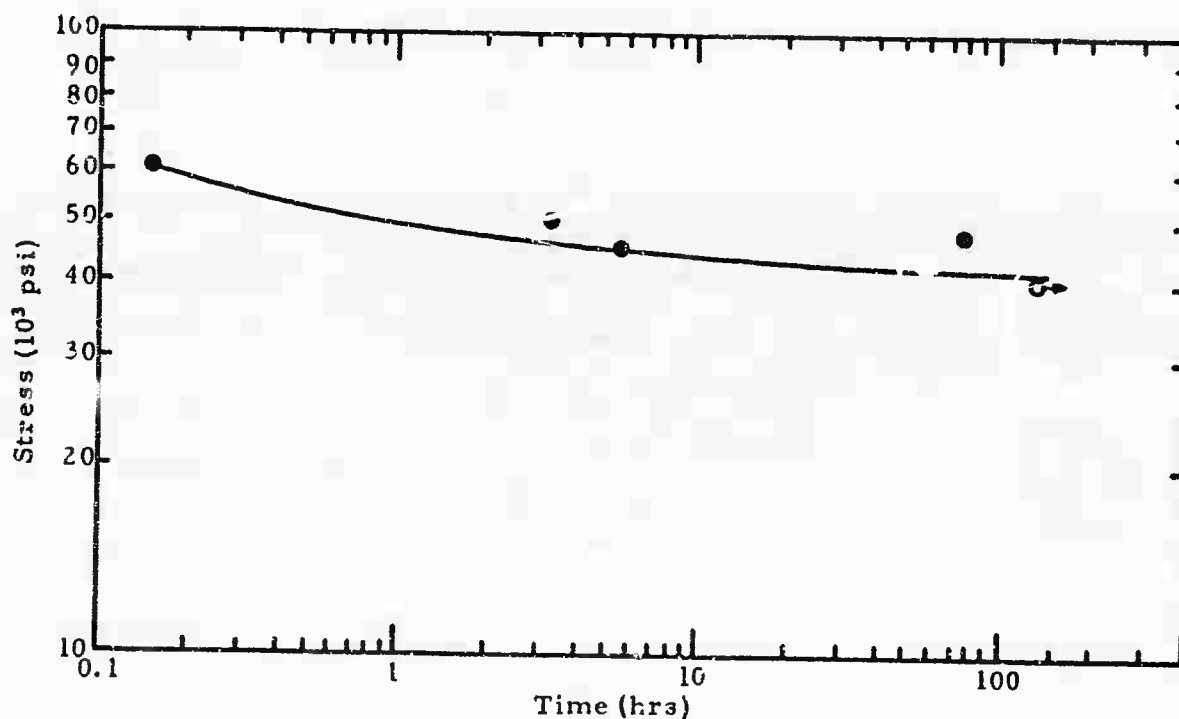


Figure 90. Stress-Rupture at 500°C for "Thornel" 75 Graphite-Fiber, Nickel-Matrix Composites.

## REFERENCES

1. Union Carbide Corporation, Carbon Products Division, in Association with Case Western Reserve University and Bell Aerospace Company, a Division of Textron, Integrated Research on Carbon Composite Materials, AFML-TR-66-310, Part I (October 1966) (AF 33(615)-3110, Air Force Materials Laboratory, Wright-Patterson Air Force Base, Ohio).
2. Union Carbide Corporation, Carbon Products Division, in Association with Case Western Reserve University and Bell Aerospace Company, a Division of Textron, Integrated Research on Carbon Composite Materials, AFML-TR-66-310, Part II (December 1967) (AF 33(615)-3110, Air Force Materials Laboratory, Wright-Patterson Air Force Base, Ohio).
3. Union Carbide Corporation, Carbon Products Division, in Association with Case Western Reserve University and Bell Aerospace Company, a Division of Textron, Integrated Research on Carbon Composite Materials, AFML-TR-66-310 Part III (January 1969) (AF 33(615)-3110, Air Force Materials Laboratory, Wright-Patterson Air Force Base, Ohio).
4. Union Carbide Corporation, Carbon Products Division, in Association with Case Western Reserve University and Bell Aerospace Company, a Division of Textron, Integrated Research on Carbon Composite Materials, AFML-TR-66-310 Part IV Volume I (September 1969) (AF 33(615)-3110, Air Force Materials Laboratory, Wright-Patterson Air Force Base, Ohio).
5. Union Carbide Corporation, Carbon Products Division, in Association with Case Western Reserve University and Bell Aerospace Company, a Division of Textron, Integrated Research on Carbon Composite Materials, AFML-TR-66-310 Part IV Volume II (October 1969) (AF 33(615)-3110, Air Force Materials Laboratory, Wright-Patterson Air Force Base, Ohio).
6. Union Carbide Corporation, Carbon Products Division, in Association with Case Western Reserve University and Bell Aerospace Company, a Division of Textron, Integrated Research on Carbon Composite Materials, AFML-TR-66-310 Part IV Volume III (December 1969) (AF 33(615)-3110, Air Force Materials Laboratory, Wright-Patterson Air Force Base, Ohio).
7. J. J. Kipling and E. H. M. Wright, J. Chem. Soc. (London) 855 (1962).
8. A. V. Kiselev and I. V. Shikalova, Colloid J. (USSR) 24, 585 (1962).

#### REFERENCES (Cont'd.)

9. F. Tuinstra and J. L. Koenig, J. Chem. Phys., 53, 1126 (1970).
10. G. M. Arnold, Carbon 5, 33 (1967).
11. W. Johnson and W. Watt, Nature 215, 384 (1967).
12. D. J. Johnson and C. N. Tyson, Brit. J. Appl. Phys. 2, 787 (1969).
13. J. C. Goan and S. P. Prosen, "Interfaces in Composites", ASTM STP 452, American Society for Testing and Materials, 1969, pp.3-26.
14. R. J. Dauksys and J. D. Ray, J. Composite Materials 3, 684 (1969).
15. J. W. Herrick, SPI Reinf. Plast. Compos. Div. ann. Techn. Conf. Proc., 23rd 1968, 15A-1.
16. F. Tuinstra and Eric Paer, Polymer Letters 8:861 (1970).
17. J. W. Herrick, "Advances in Structural Composites," Soc. of Aerospace Material and Process Engineers, Vol. 12, 1967, Section ACS.
18. G. Hennig, Physics of Graphite and Carbon, P. E. Walker, Ed. Vol. 5, Page 113 (1964).
19. F. Tuinstra and J. L. Koenig, J. Composite Materials 4, 492 (1970).
20. P. D. Frayer and J. B. Lando, Molecular Crystals and Liquid Crystals, 9, 465 (1969).
21. K. Jesch, J. E. Bloor, and P. L. Kronick, J. Polymer Sci., A-1, 4, 1487 (1966).
22. A. J. G. Allan, J. Polymer Sci., 38, 297 (1959).
23. R. A. Hines, Am. Chem. Soc. Meeting, 17, 69, NPN (1957).
24. Amoco Bulletin, HT 6a.
25. Amoco Bulletin, HT 9a.
26. Union Carbide Product Data - Bakelite Polysulfone.
27. Union Carbide Product Data - ERLA-4617.
28. Plastics Technology 14 No. 11, 296 (1968).
29. Loc. cit., Reference 3, page 63.

#### REFERENCES (Cont'd.)

30. P. W. Jackson, J. P. Marjoram, "Compatibility Studies of Carbon Fibers with Nickel and Cobalt," *J. Mat. Sci.* 5, 9-23 (1970).
31. Interfaces in Composites, ASTM Special Technical Publication 452, American Society for Testing and Materials, Philadelphia, Pennsylvania, pp. 45-57.
32. R. Hill, "Elastic Properties of Reinforced Solids: Some Theoretical Principles," *J. Mech. Phys. Solids*, 11, 357-372 (1963).
33. J. M. Whitney, "Elastic Moduli of Composite Materials Reinforced with Orthotropic Filaments," Technical Report AFML-TR-654 January 1966.
34. J. E. Burke and A. M. Turkulo, "Deformation of Zinc Bicrystals by Thermal Ratcheting," *J. Metals*, 651, June 1952.
35. International Nickel Company, Inc., Engineering Properties of Nickel, Technical Bulletin T-15, (New York, New York, October 1957).



UNCLASSIFIED

Security Classification

## DOCUMENT CONTROL DATA - R &amp; D

(Security classification of title, body of abstract and indexing annotation must be entered when the overall report is classified)

1. ORIGINATING ACTIVITY (Corporate author) Union Carbide Corporation Case Western Reserve University Bell Aerospace Company		24. REPORT SECURITY CLASSIFICATION Unclassified	
3. REPORT TITLE INTEGRATED RESEARCH ON CARBON COMPOSITE MATERIALS Part V Volume I - Materials Research		25. GROUP	
4. DESCRIPTIVE NOTES (Type of report and, inclusive dates) Summary Technical Report July 1969 to September 1970			
5. AUTHOR(S) (First name, middle initial, last name) Union Carbide Corporation, Carbon Products Division, in Association with Case Western Reserve University and Bell Aerospace Company, a Division of Textron			
6. REPORT DATE January 1971		7a. TOTAL NO. OF PAGES 130	7b. NO. OF REFS 35
8a. CONTRACT OR GRANT NO. F33615-68-C-1077		9a. ORIGINATOR'S REPORT NUMBER(S)	
b. PROJECT NO. ARPA Order No. 719			
c. Program Code 7D10		9b. OTHER REPORT NO(S) (Any other numbers that may be assigned this report) AFML-TR-66-310, Part V, Volume I	
10. DISTRIBUTION STATEMENT This document is subject to special export controls and each transmittal to foreign governments or foreign nationals may be made only with prior approval of the Nonmetallic Materials Division, AFML/LN, Air Force Materials Laboratory, Wright-Patterson Air Force Base, Ohio 45433			
11. SUPPLEMENTARY NOTES		12. SPONSORING MILITARY ACTIVITY Air Force Materials Laboratory Wright-Patterson AFB, Ohio	
13. ABSTRACT The work presented in Volume I is concerned with materials research on graphite fiber reinforced composites. Graphite fiber surfaces were characterized by gas phase and solution adsorption experiments and by Raman spectroscopy. The latter technique allows a differentiation between fibers of different origins and heat-treatment temperatures. The fabrication of "Thornel" fiber, polyamide- imide and polysulfone composites was investigated. Fabrication of polyamide- imide composites was very tedious and evaluation was limited to determinations of torsion shear strength. Several plates of polysulfone matrix composites were fabricated; the evaluation of these plates is presented in Volume II of this report. "Thornel" fiber composites were further prepared by <u>in situ</u> polymerization of nylon. The epitaxial crystallization of nylon monomer on graphite fiber surfaces has been investigated. Graphite-fiber, nickel-matrix composites were further characterized at room and at elevated temperatures. Measurements of Young's moduli, tensile strength, stress rupture, thermal expansion, and thermal fatigue are presented. Graphite filament degradation resulting from fabrication (hot-pressing) of nickel-matrix composites was also determined.			

UNCLASSIFIED

Security Classification

A-81408

KEY WORDS	LINK A		LINK B		LINK C	
	ROLE	WT	ROLE	WT	ROLE	WT
Carbon						
Graphite						
Fibers						
Graphite Fibers						
Composites						
Plastic Matrix						
Metal Matrix						
Properties						
Analysis						
Synthesis						
Mechanical Properties						